Computer Aided Design of components for energy transfer

MODELLING OF DEVICES FOR ENERGY TRANSFER AND CONVERSION

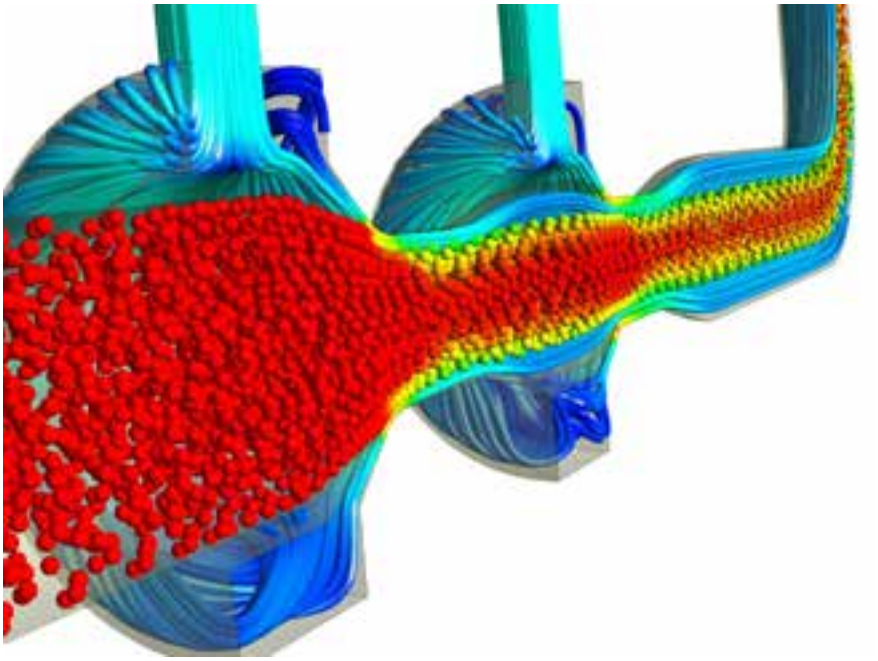

Mariusz Domagała, Hassan Momeni,
Jolanta Stacharska-Targosz

Bergen University College, 2013

Skriftserien, nr. 4/2014

Boken kan bestilles hos:
Høgskolen i Bergen
www.hib.no/nettbutikk/

ISBN 978-82-77-09120-4

Denne fagrapporten er vurdert av Thomas Impelluso

Opplag:
45 eksemplarer

Grafisk produksjon:
BODONI

Computer Aided Design of components for energy transfer

MODELLING OF DEVICES FOR ENERGY TRANSFER AND CONVERSION

Scientific Committee:

Prof. Mons Erik Monstad
Prof. Edward Lisowski
Ragnar Gjengedal, PhD
Mariusz Domagała, PhD
Wojciech Czyżycki, PhD
Grzegorz Filo, PhD

Bergen University College, 18th April 2012

Table of contents

1 INTRUDUCTION

Devices for energy transfer and conversion play a key issue in lot of industry branches such as energy, oil and gas, chemical and HVAC. They are sophisticated equipment which make difficulties during modeling and simulation. It is due to the phenomena which appears at energy transfer/conversion are complex and coupled such us fluid flow and heat transfer, phase changes, etc. Therefore, modeling such components requires powerful simulation tools. A new possibilities and quality of simulation, particularly for such complex phenomena, offer CAD/CAE systems. Combining both systems allows to prepare not only geometry of investigated components, which sometimes is very complex, but also allows to simulate mass and energy transfer as well as strength analysis and lots more. In particularity, numerical simulation tool which is Computational Fluid Dynamics (CFD) offers wide capabilities in area of energy transfer and conversion. CFD capabilities are very wide and allow to investigate flow of compressible and incompressible fluids, at high Reynolds number coupled with heat transfer, including phase changes and even with interaction with solids. Besides these design tools very helpful is relatively new technology which is a Rapid Prototyping that allows preparing prototypes in reliable time, good quality and cost, much lower than final manufacturing process. Prepared prototype might be tested and verified before goes to a the final production.

Capabilities of modern simulation systems in modeling of components for energy transfer and conversion were presented in this work. On example of jet pumps and cross flow fans there is shown an application of using CAD/CAE tools. Both component were virtually tested at operational conditions with the use of CFD codes. There is also presented a method of visualization of flow at the cross flow fan as well as a test stand for testing

jet pumps. In case of jet pump was also presented a way for preparing prototype by the use of FDM Rapid Prototyping technology.

2 JET PUMPS

2.1 JET PUMP DESCRIPTION

Jet pumps, depending on theirs application are called eductors, ejectors, elevators or gas compressors, and are devices that transfer energy from one fluid that is called motive or primary to another one (called driven or secondary). Motive fluid might be liquid or a gas as well, while secondary might be liquid, gas or a mixture. The biggest advantageous of jet pumps is no moving parts, and in a consequence high rate of reliability and needs of very little maintenance. Other advantages of jet pumps are low production costs in comparison to other type of pumps and they can be made in many sorts of materials. These advantages give jet pumps a very wide area of application, for example in chemical and oil industry for nuclear engineering. The disadvantageous of jet pumps are low efficiency and height of pumping. All types of jet pumps consist of the same basic components: nozzle, a mixing chamber, throat and a diffuser.

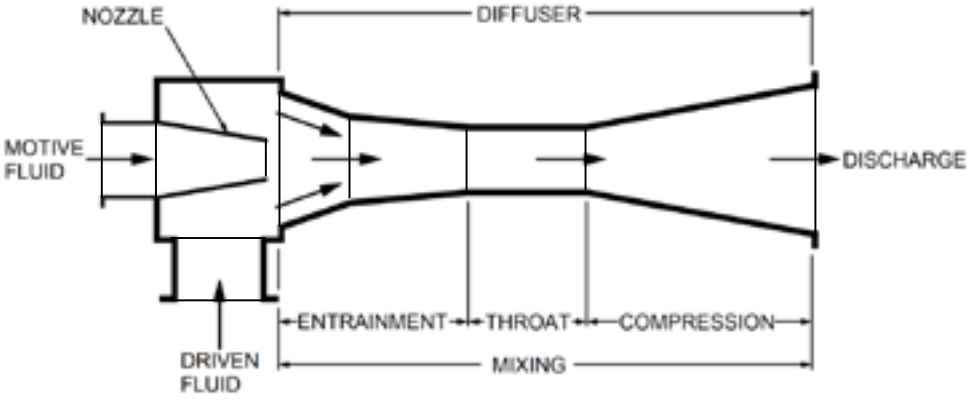

Fig. 2.1. Jet pump schema [1]

The motive fluid accelerates to a high velocity at motive nozzle at the cost of pressure energy. In the mixing chamber a low pressure zone is created which drawn other fluid. The mixed fluids then go to the mixing chamber where both fluids are mixed, and later after throat expanded where velocity energy is converting back into the pressure energy. There are two main types of jet pumps where the difference is the nozzle of the motive fluid which can be axial or annular.

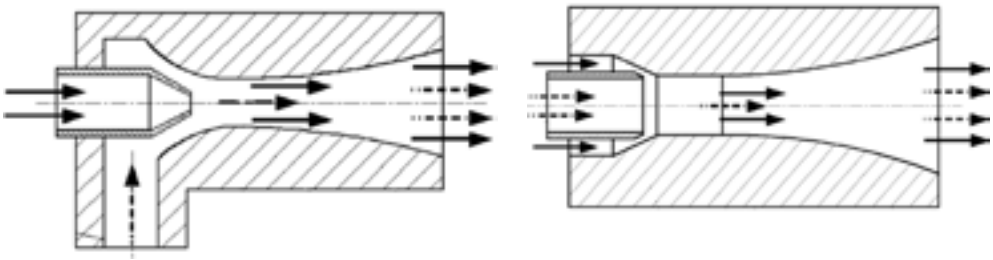

Fig. 2.2. Jet pump with central and circumferential nozzle

The main advantageous of the circumferential nozzle is the ability to transport non liquid objects with significant dimensions.

The jet pumps might be also distinguished by the number of working nozzles, it can be found solution with single and multiple nozzle for both solutions (with central and annular nozzle). Figure below shows multi central nozzle pump.

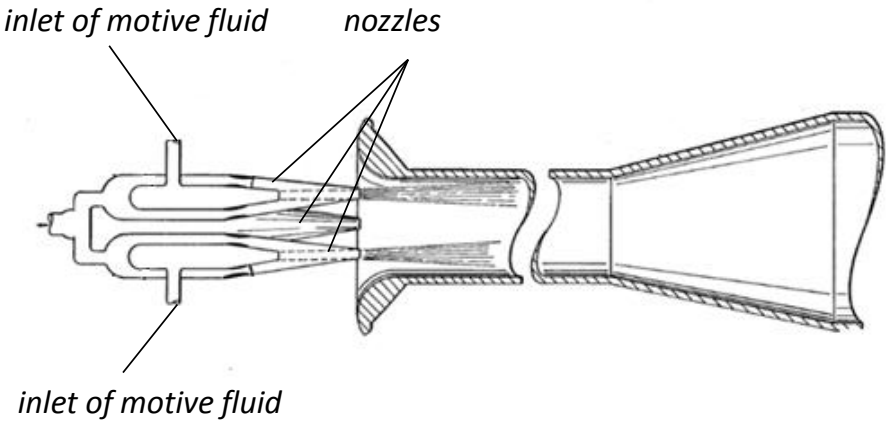

Fig. 2.3. Jet pump with three central nozzle [2]

There is also known modification of annular nozzle shape as it is presented in patent" US2008/0310970". It is an annular motive nozzle with shape that allows to create shock wave in correct position. Presented in fig. 2.4 and fig. 2.5 solution allows the motive steam to mix with secondary fluid and form the shock wave in correct position.

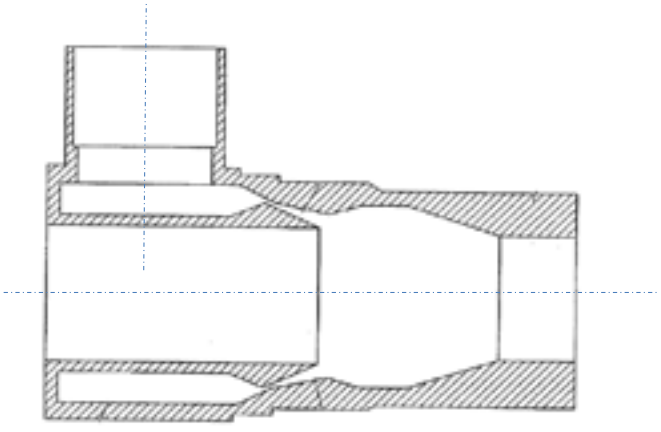

Fig. 2.4. Jet pump according to patent US2008/0310970

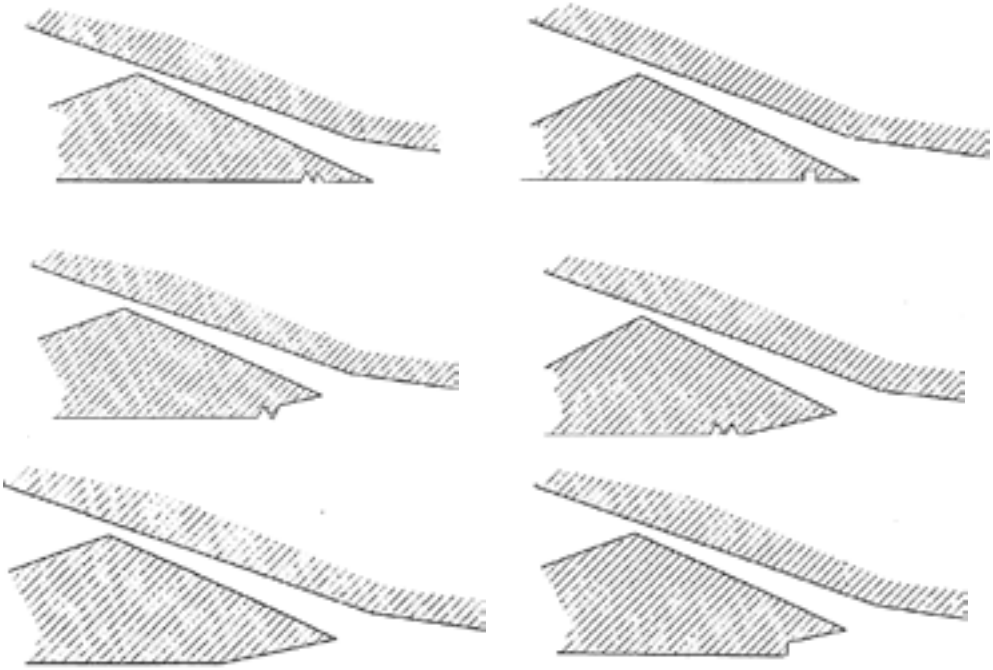

Fig. 2.5. Jet pump motive nozzle according to patent US2008/0310970

Presented in fig 2.5 shape of annular nozzle allows to form shock wave in the most convenient position at throat and avoid unfavorable phenomenon during pump work.

The example of multi annular nozzle pump is presented in fig. 2.6.

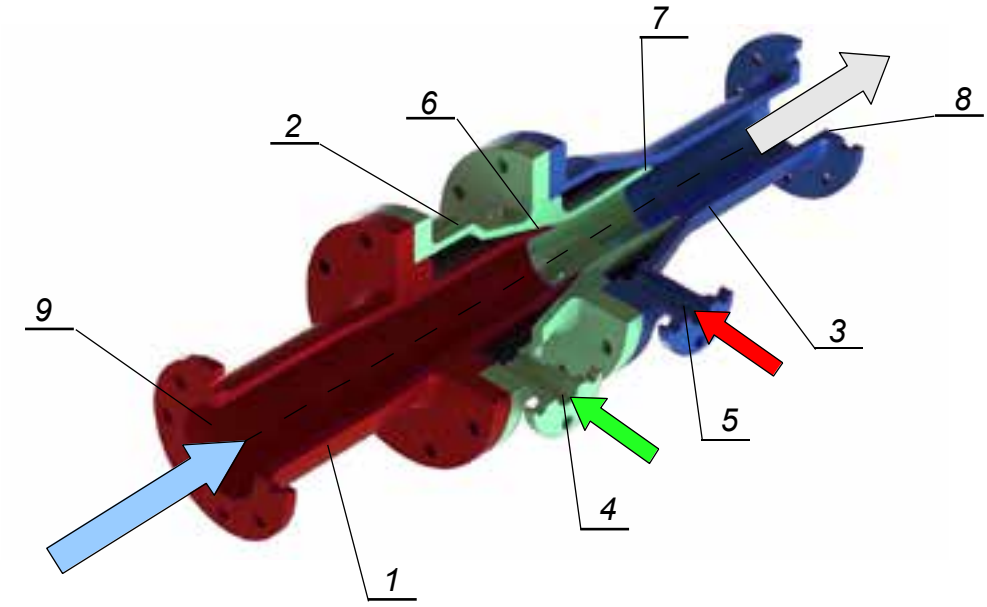

Fig. 2.6. Jet pump with two annular nozzle, 1,2,3 – pump component, 4 – inlet of motive liquid for 1st stage, 5 – inlet of motive liquid for 2nd stage, 6 – annular motive nozzle for 1st stage, 7 – annular motive nozzle for 2nd stage, 8 outlet of jet pump, 9 – inlet of jet pump

Usually jet pumps motive stream is generated by another mechanical pumps driven either by electric motor or combustion engine or in some cases motive fluid is a part of gas from oil or gas well. Typical way of using jet pump is presented in fig. 2.7. In this case jet pump is supplied by mechanical pump with electric motor.

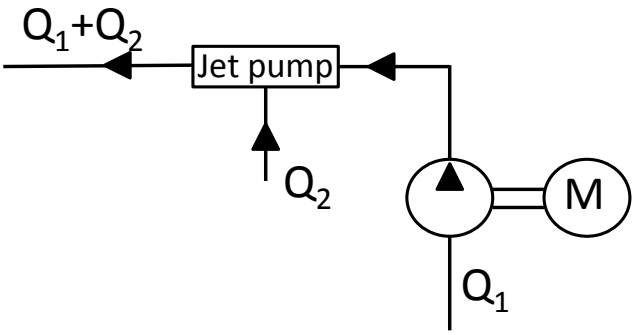

Fig. 2.7. Typical jet pump installation

Jet pumps might be also distinguished by the medium for motive and driven fluids. Therefore the following jet pumps might be found:

- Liquid Jet Gas pumps (LJG) use liquid as motive fluid and a gas as driven fluid. The principle of operation is the same as the liquid jet liquid pump, but the difference in density between the fluids has to be taken in consideration in the design of the jet pump. This principle is utilized to generate vacuum in the suction chamber. The low pressure generated in the mixing chamber will then entrain the gas into the liquid stream.
- Gas Jet Gas pumps (GJG) pumps use gas as motive and driven fluid. These jet pumps are often used in processing or chemical industries. Which gas is being used as motive fluid depends on the jet pump's range of use. Steam or some other chemical gas is often used.
- liquid Jet Liquid (LJL) use liquid as a motive and driven fluid.

The low efficiency of jet pumps have traditionally been their biggest disadvantage. Fall in efficiency due to friction and pressure losses are

unavoidable. But efficiency as high as 30-40% can be achieved with correct design.

2.2 APPLICATION OF JET PUMPS

Because of simple design with no moving parts, low production cost and no material limitations, jet pumps are ideal for use in a wide range of industries and environments. Theirs dimensions can diversify from few millimeters to few meters. The jet pumps are commonly used in the following industries:

– Oil and gas.

Jet pumps are used to boost low pressure wells. A gas jet gas pump can create higher pressure in the well by using highly compressed gas form newer wells with a higher natural pressure. By taking advantage of the pressure in newer wells it is possible to utilize energy that otherwise would be lost. The suction side of the pump is then connected to the low pressure well. By using this method it is possible to extract higher quantities of gas or oil from the well.

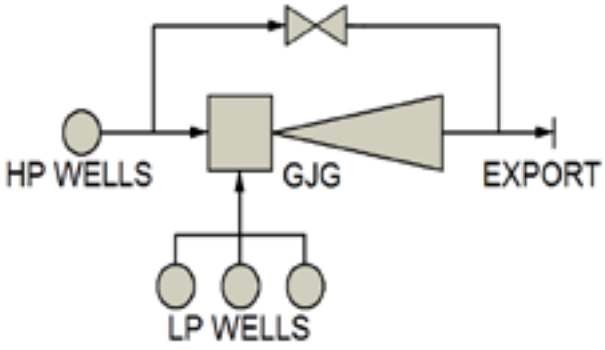

Fig. 2.8. Boosting of low pressure wells
(LP-Low Pressure, HP-High Pressure)

– Processing and chemical.

Jet pumps can be used for filtration, distillation, vacuum packaging and degassing of sealed volumes or generate vacuum. In the last case the degree of vacuum that the pump is able to generate depends on the number of pressure stages the pump consists of.

– Energy.

Jet pumps are used as an efficient way of transferring energy from one fluid to another. This is because of direct contact between the two fluids. The jet pumps can be used for cooling and heating fluids in-line. The most common use is for the cooling of superheated steam. Cold water is sprayed into the superheated steam flow and the energy from the steam is used to vaporize the water. This results in a cool-down of the steam. This method is often combined with power turbines to cool down the used superheated steam before its being recycled.

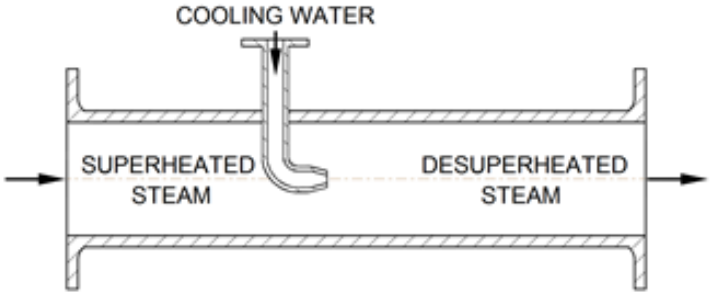

Fig. 2.9. Steam cooling.

Thanks to high reliability jet pumps are used in power plants in cooling system of nuclear reactors.

– Environmental protection.

Jet pumps found a wide application in engineering protection, there are used for example for removing extremely dangerous fluids or waste (for example: radioactive or extremely aggressive fluids).

– Food.

Jet pumps are used as a transportation systems for food or even live animal like a fish or shellfish.

There is a lot of available references dealt with jet pumps, which describes jet pump applications and main futures. These dated before 1975 were gathered and described by Bonnington, S. T., and King, A. L. [3]. A new applications of using jet pumps still appears what may be found in new patent applications.

2.3 LIQUID JET LIQUID PUMP

Liquid Jet Liquid pumps use water for both, motive and driven streams. They are commonly used in oil industry, for removing contamination and to transport fish. Presented in fig. 2.10 pump is two stage LJL pump with annular nozzles manufactured by Fijel Industry, Norway. It is a pump with throat diameter 140 mm with overall length 1000 mm. It is made of stainless steel and to increase pumping height includes second motive stage. The main application of this pump is transport objects with big dimensions thanks to use the annular motive nozzles. The pump consists of few parts which are assembled by bolt connections what allows for fast disassembly and removing motive nozzle if necessary.

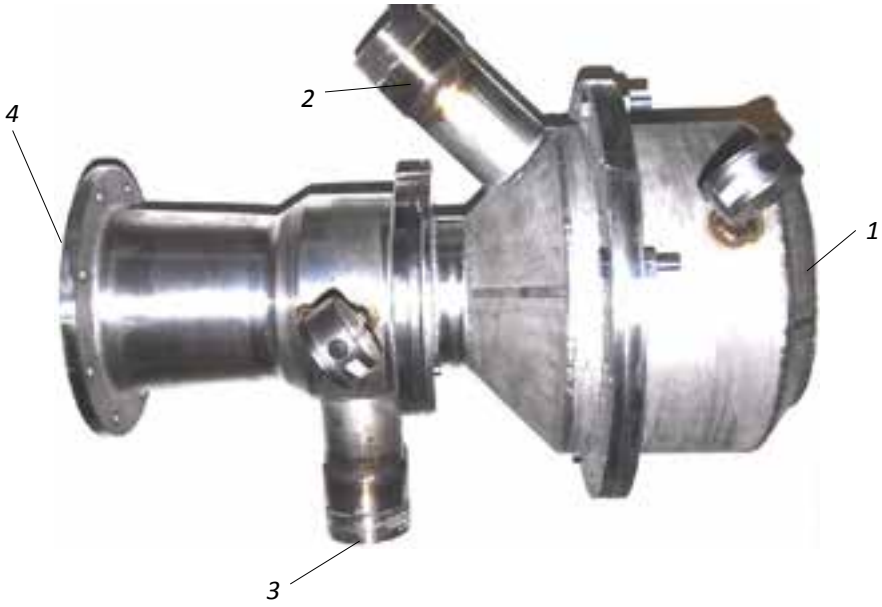

Fig. 2.10. LJL pump by Fijel Industry, Norway: 1 pump body, 2 – inlet to 1st motive nozzle, 3 – inlet to 2nd motive nozzle, 4 – pump outlet

2.4 MODELLING OF JET PUMP

2.4.1 MATHEMATICAL MODEL

Mathematical model of typical jet pump consist of mass, momentum and energy conservation equations. When we assume a fixed in space volume Ω, bounded by close surface S, the mass conservation equation in general form is the following [6].

Conservation of mass:

$$\frac{\partial}{\partial t}\int_{CV}^{\cdot}\rho dV + \oint_{CS}^{\cdot}\rho\vec{v}\cdot d\vec{A} = 0. \tag{2.1}$$

where: t – time, ρ – fluid density, $\vec{v}$ – fluid velocity, CV – control volume, CS – control surface.

Conservation of momentum:

$$\frac{\partial}{\partial t}\int_{CV}\rho\vec{v}dV + \oint_{CS}\rho\vec{v}\left(\vec{v}\cdot d\vec{A}\right) = -\oint_{CS}p\cdot d\vec{A} + \oint_{CS}\vec{\tau}\cdot d\vec{A} + \int_{CV}\rho\vec{f}_e dV \quad (2.2)$$

where: p– pressure, $\vec{\tau}$ – shear stress tensor, $\vec{f_e}$ – external force.

Conservation of energy:

$$\frac{\partial}{\partial t}\int_{CV}\rho e dV + \oint_{CS}\left(\rho\vec{v}h - k\vec{\nabla} - \vec{\tau}\cdot\vec{v}\right)d\vec{A} = \int_{CV}\left(\rho\vec{f}_e\cdot\vec{v} + q_H\right)dV \quad (2.3)$$

where: h –total enthalpy, e – total energy, T – temperature, k – thermal conductivity coefficient, q_H – external heat sources.

Above listed equations is very difficult to solve even with a lots of assumptions. During flow at the jet pumps a part of energy is lost due to sudden contractions at nozzle jet and sudden expansions at the throat and gradual expansion at diffusor. There are also appear energy losses which are caused by flow at ducts with uniform diameter but theirs value are not comparably with losses caused by changes in pump geometry. All of these losses are well known and widely described in literature, for example in work [8]. However, it is not easy estimate loss coefficient for jet pump due to the fact that available coefficient were estimated either for ideal conditions on relatively simple geometry. At jet pumps, an influence of one factor (for example sudden contractions) may have influence on another pump parameter. Furthermore, it is always assumed that velocity profile is

uniform which may not be true at the jet pumps which has complex geometry.

For LJL pump the following assumptions might be made:

- motive and driven fluid are both incompressible and has the same properties,
- flow is steady,
- uniform velocity profile at each section,
- no heat exchange between the fluids or with the environment.

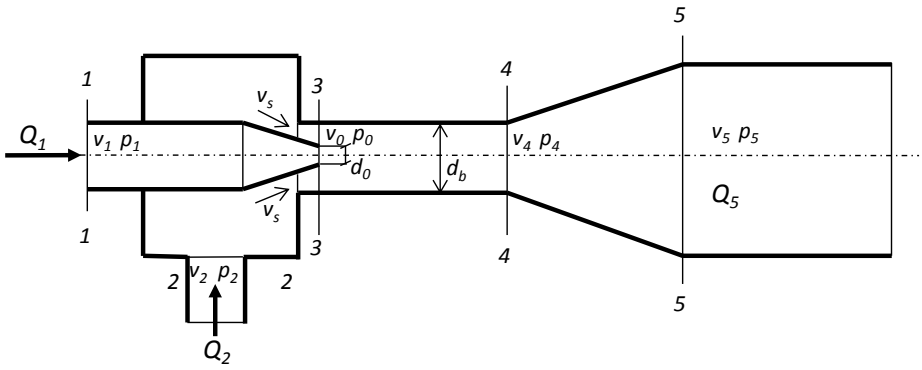

Fig. 2.11. Typical jet pump with center nozzle

When considering above assumptions the mathematical model for jet pump presented in Fig. 2.11 will be as follows (distinguishing various part of jet pump):

Nozzle:

- continuity equation:

$$Q_0 = Q_1. \tag{2.4}$$

- Bernoulli equation:

$$p_1 + \rho \frac{v_1^2}{2} = p_0 + \rho \frac{v_0^2}{2} + K_n \frac{v_0^2}{2}. \tag{2.5}$$

Throat entry:

- continuity equation:

$$Q_2 = Q_s. \tag{2.6}$$

- Bernoulli equation:

$$p_2 + \rho\frac{v_2^2}{2} = p_s + \rho\frac{v_s^2}{2} + K_t\frac{v_s^2}{2}. \tag{2.7}$$

Throat:

- continuity equation:

$$Q_4 = Q_1 + Q_2. \tag{2.8}$$

- momentum equation:

$$p_0A_3 + \rho Q_1 v_0 + \rho Q_2 v_s = p_4A_4 + \rho(Q_1 + Q_2)v_4. \tag{2.9}$$

Diffuser:

- continuity equation:

$$Q_4 = Q_5. \tag{2.10}$$

- Bernoulli equation:

$$p_4 + \rho\frac{v_4^2}{2} = p_5 + \rho\frac{v_5^2}{2} + K_d\frac{v_5^2}{2}. \tag{2.11}$$

where: ρ – liquid density, v_i– liquid velocity, Q_i – volumetric flow rate, p_i– pressure, K_j– loss coefficient, subscript i corresponds to adequate section, subscript j corresponds to adequate part of jet pump.

Above equations might be complemented with geometrical and flow relations at adequate sections of jet pumps. Volumetric flow ratio:

$$q = \frac{Q_2}{Q_1}. \tag{2.12}$$

Spatial ratio:

$$a = \frac{A_0}{A_b}, \tag{2.13}$$

$$b = \frac{A_4}{A_5}. \tag{2.14}$$

where: A_0 – area of jet nozzle, $A_b = A_4$ – area of throat, A_5 – area of diffusor outlet.

Than, fluid velocity at the entry to the throat will have following form:

$$v_s = \frac{q \cdot a}{1-a} \cdot v_0. \tag{2.15}$$

Fluid velocity at throat will have form:

$$v_b = v_4 = a(1+q)v_0. \tag{2.16}$$

And at diffuser outlet:

$$v_u = ab(1+q)v_0. \tag{2.17}$$

Ideal jet pump efficiency might be expressed as ration between energy extracted from the jet pump to energy delivered to the pump:

$$\eta = \frac{Q_2(p_5 - p_s)}{Q_1(p_0 - p_5)}. \tag{2.18}$$

During flow at the jet pumps a part of energy is lost due to sudden contractions at nozzle jet and sudden expansions at the throat and gradual expansion at diffusor. There are also appear energy losses which are caused by flow at ducts with uniform diameter but theirs value are not comparably with losses caused by changes in pump geometry.

2.4.2 CFD METHODS

CFD (Computational Fluid Dynamics) is a numerical method that allows to transform governing equation of fluid motion (called Navier-Stokes equations, set of Eq. 2.1, Eq. 2.2, Eq. 2.3) which are partial differential equations to set of algebraic equations. It might be distinguished three, the most common ways of transferring PDE (partial differential equations) to algebraic equations. The oldest one is Finite Difference Method (FDM) which main feature is that the differential equations are approximated by difference formulas The computational domain is divided into series on

computational nodes which are usually uniformly distributed over the domain. At these nodes flow governing equations are approximated. The biggest disadvantageous of FDM is limited use to domain that allows to create regular grid (with computational nodes). There is a lot of references that describes this methods in details, for example [4], [9], [10]. Due to its bid limitations was not applied to general purpose of commercial CFD codes.

The other way of transforming Navier-Stokes equation to algebraic equations is FEM method (Finite Element Method). At this method flow domain is also divided into smaller domains (finite elements) and solution is created in each element using basis function (called shape function) and integrated over each element. In comparison to FDM this method can be used for any domain even with very complex geometry. But even this advantageous using this method in commercial code is limited. Nowadays, CFD method based on FEM are used to combine flow simulation with structural analysis which gives the best benefits for FSI simulations (for example ABAQUS code with CFD modules, LSDyna, or MSC Dytran).

The most popular method available at the market is FVM method (Finite Volume Method) which also inherits from both mentioned above discretization of domain, but in this case into small domain (finite volumes). In this method Navier-Stokes equations are solved in integral form and solved for each finite volume. A sum of set of equations for finite volumes is a global N-S equation. This method is developed very fast last years, and most of CFD codes use it (Ansys CFX, FLUENT, Star CCM+).

CFD methods is a very wide subject which will be not presented in details in this work. More information about CFD method might be found in the work [11].

The common thing for all mentioned above methods is flow domain discretization (dividing into small domain). FEM and FVM have no limitation in generating discrete models, however, there are some differences. Both of this method may use in case of 2D domain quadrilateral or triangular shape of elements (in FEM) or cell (in FVM) that creates computational domain. Both shape might also be mixed. In case of 3D domain a common for both is hexahedral, tetrahedral, wedge shape (elements and cells). But there is only available at FVM grid which is called polyhedral grid (available at Star CCM+ and FLUENT code). This branch of CFD methods still evolves and new ways of domain discretization appears. More details about discretization methods are available at work [11].

2.4.3 CFD MODEL OF TWO STAGE LJL PUMP

2.4.4 BASIC ASSUMPTIONS

The following assumptions were set during CFD simulation:

- flow is incompressible, homogenous and single phase,
- no heat exchange between both streams (driven and motive) and with the environment,
- wall roughness was neglected,
- standard wall functions was applied,
- analysis is conducted for steady state conditions,
- fluid properties are constant (typical for water at 25°C): density ρ=1000 kg⁄m^3 , viscosity μ=1.003·e^{-3} Pa·s,
- flow is three dimensional and turbulent, a Reynolds Stress Model is applied,

- elastic deformations of pump components are neglected,
- there is no slip of liquid on walls,
- symmetry flow along the longitudinal axis.

2.4.5 GEOMETRICAL MODEL OF LJL PUMP

For CFD simulations a geometrical model of LJL pump was prepared. For presented in fig. 2.6 pump was prepared geometrical model in Creo Parametric CAD system, formelly known as a Pro/Engineer. 3D model of pump is presented in fig. 2.12 and its cross section in fig. 2.13. These models were later used to create domain of fluid flow. The model, which was used in CFD simulation is presented in fig. 2.14. As it was assumed aerlier only a half of fluid domain was used, at the symmetry plane an apropriate boundary conditions were set.

Fig. 2.12. Geometrical model of LJL pump body

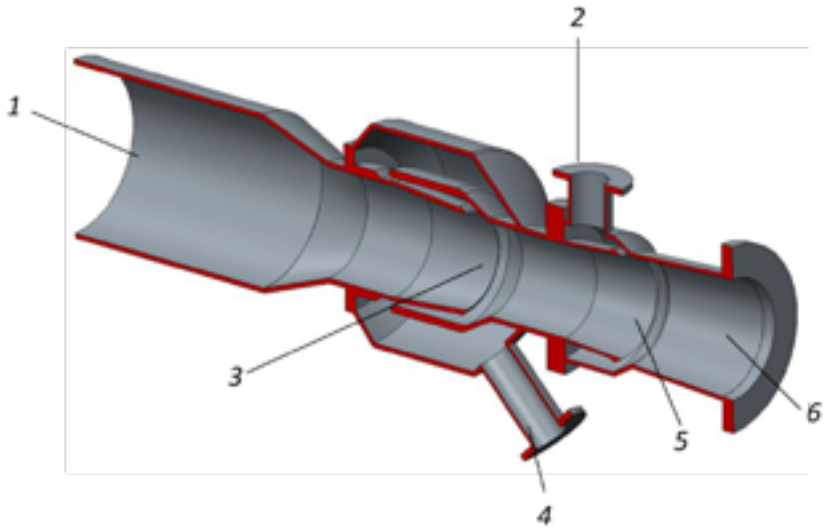

Fig. 2.13. Cross section of geometrical model of LJL pump body, 1 – pump inlet, 2 – inlet to 1st motive nozzle, 3 – 1st motive nozzle, 4 – inlet 2nd motive nozzle, 5 – 2nd motive nozzle, 6 – pump outlet

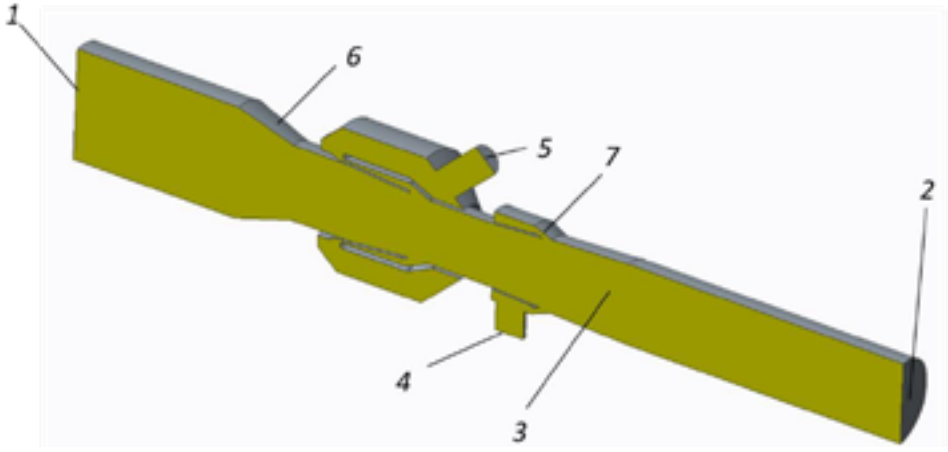

Fig. 2.14. Model of flow domain: 1 – inlet, 2 – outlet,
3 – symmetry, 4 – inlet to motive nozzle, 5 – inlet to motive nozzle,
6 - wall

2.4.6 DISCRETE MODEL

Discrete model of investigated object plays essential role in CFD simulations. It strongly influences on further results and solution convergence. The grid of jet pump was created in Ansys Mesh (a part of Ansys Workbench simulation environment), which offers a various grid types. Therefore, two different grid was tested, from tetrahedral with prism layers on pump walls to hexahedral with hybrid grid (see fig. 2.15, fig. 2.16, fig. 2.17, fig. 2.18). Each of them has advantageous and disadvantageous and allowed to obtain similar results, but tetrahedral/prism cells grid consumed more computational time. At both cases grid was refined in area of motive nozzles, what is presented in fig. 2.16 and fig. 2.18. There are also available other grid type such as polyhedral grid, but it was not available in Ansys CFX code, in which numerical simulations were conducted.

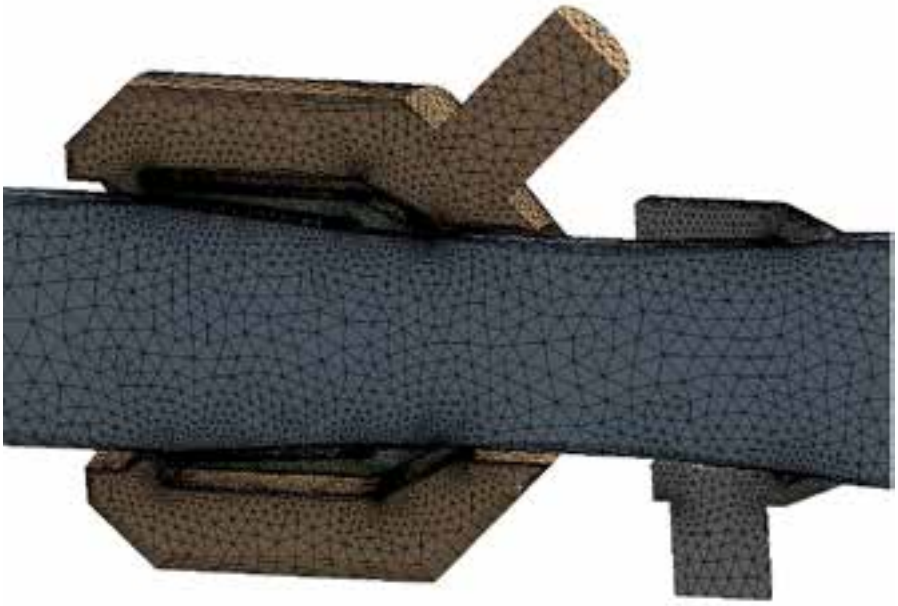

Fig. 2.15. Grid of LJL pump, tetrahedral/prism layer

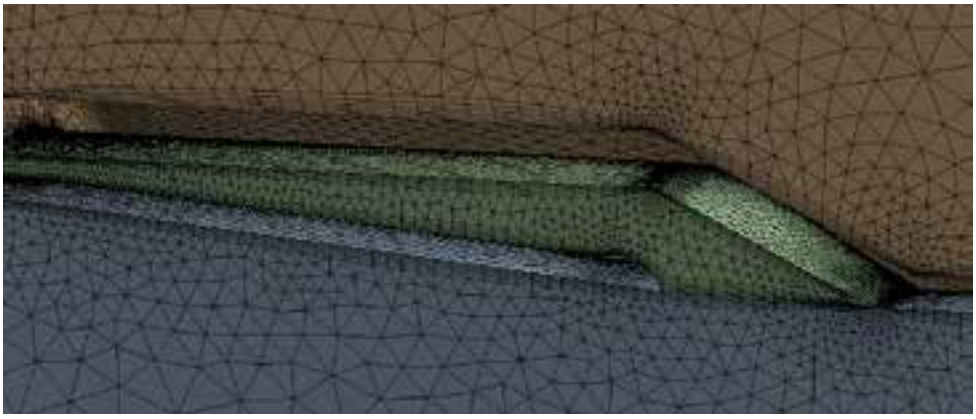

Fig. 2.16. Refined grid at motive nozzle, tetrahedral/prism layer

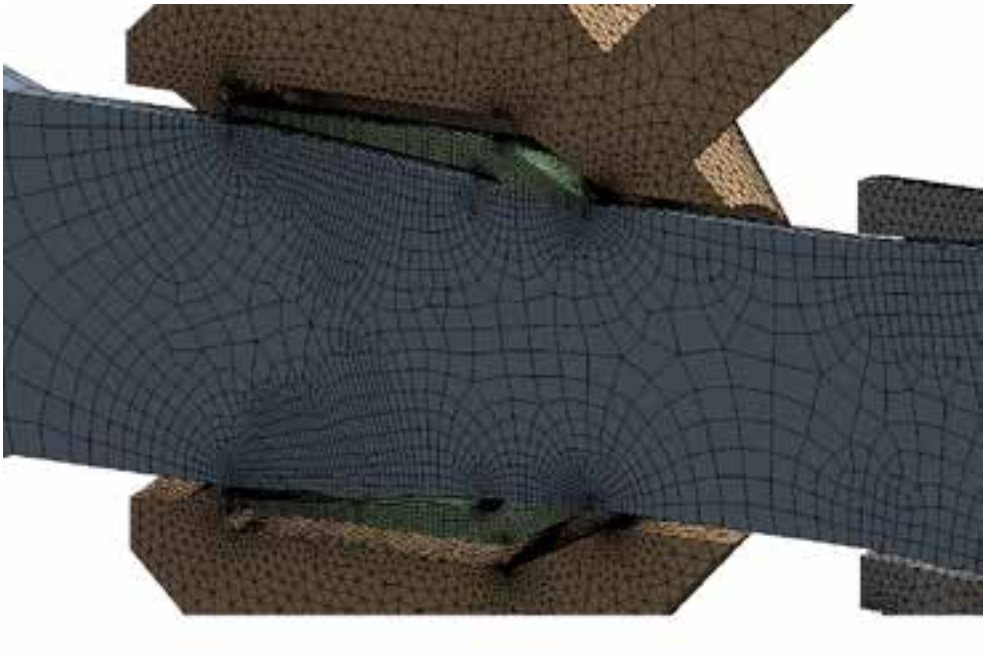

Fig. 2.17. Grid of LJL pump, hybrid grid hexahedral/tetrahedral

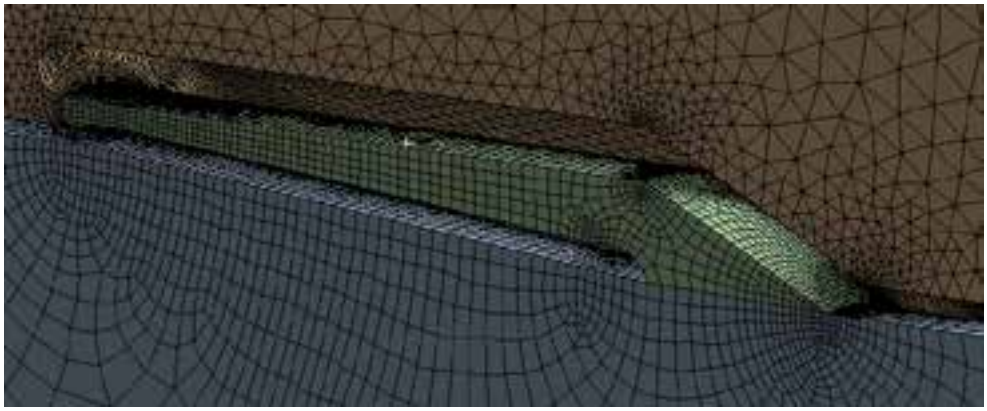

Fig. 2.18. Refined grid at motive nozzle, hybrid grid hexahedral/tetrahedral

2.4.7 CFD RESULTS

CFD analysis were conducted for steady state conditions for various flow parameters (from minimal to maximal flow rate) on inlet port to motive nozzle. There was also investigated operation scenario, in which either one or both motive nozzles are supplied with liquid. Conducted simulations allowed to investigate flow phenomena that appears inside jet pump, investigate velocity and pressure distribution and trajectory of motive and drive streams. Exemplary results of CFD simulation are presented in fig. 2.19 to fig. 2.22 for selected flow conditions (160 dm^3/min at motive inlet for 1^{st} stage).

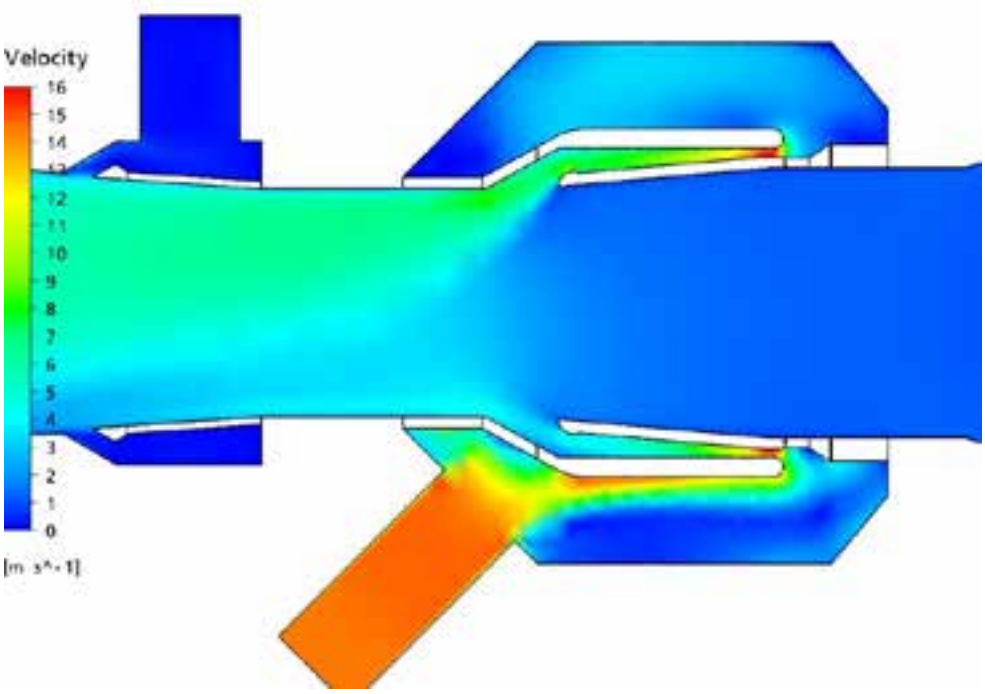

Fig. 2.19. Velocity distribution at symmetry plane (in m/s)

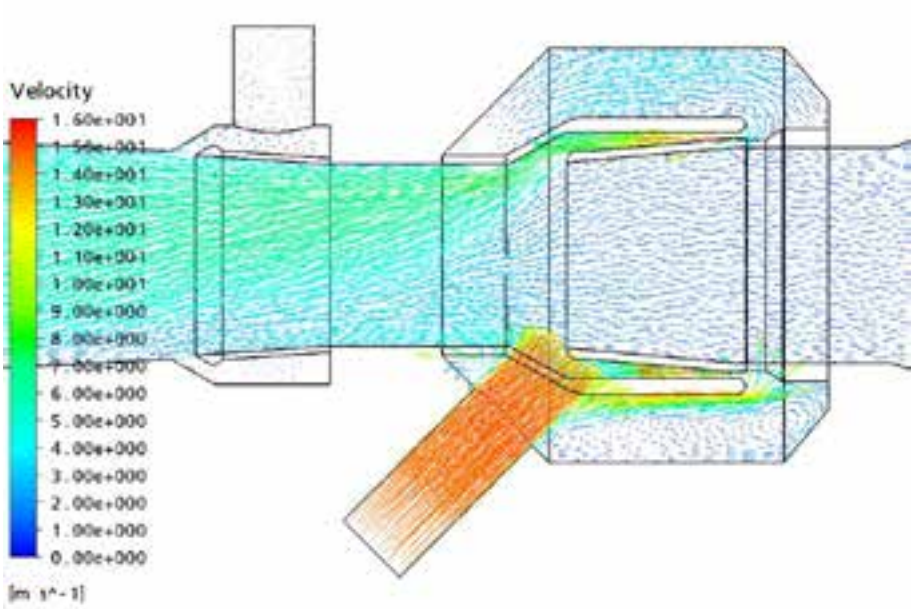

Fig. 2.20. Vectors of velocity at symmetry plane

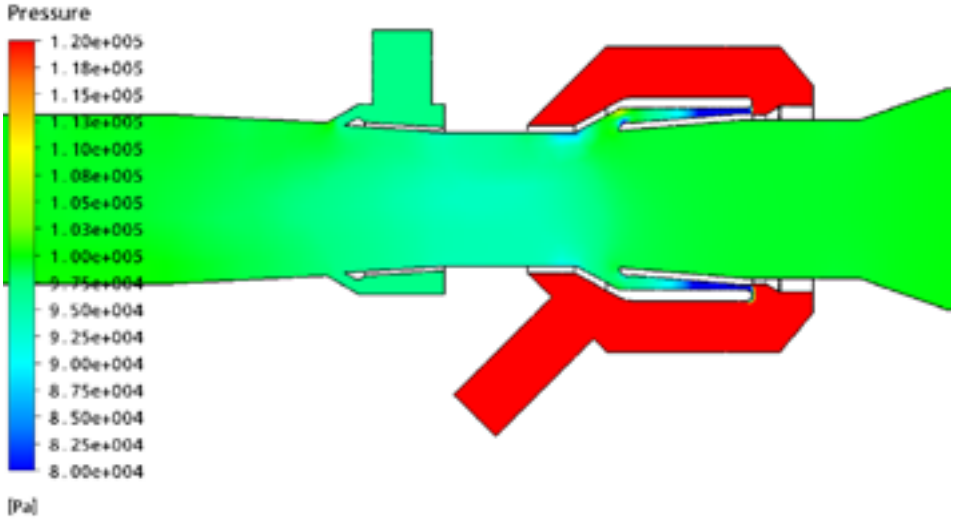

Fig. 2.21. Static pressure distribution at symmetry plane

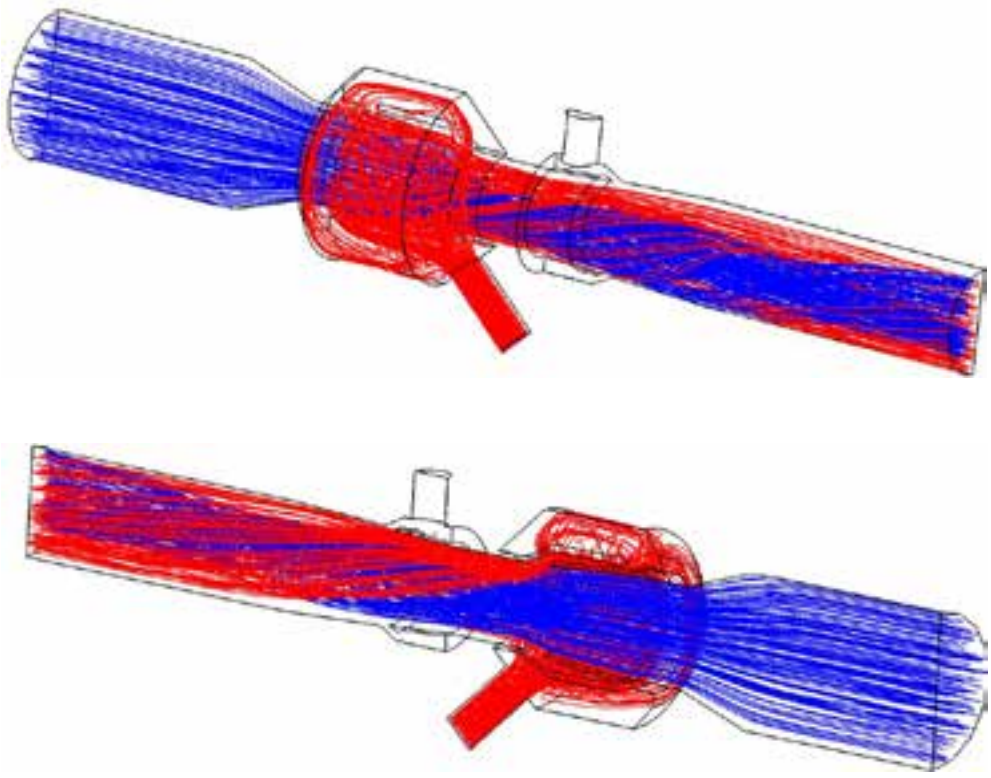

Fig. 2.22. Path lines: red is motive fluid, blue secondary

Presented results allowed to investigate flow phenomena during water flow inside the pump when 1st motive nozzle operates. It allowed to indicate area with highest velocity and evaluate pressure drop at the throat. What is worth of mention is that the maximal liquid velocity is not at the nozzle outlet to throat but at the entrance to the nozzle (see fig. 2.19 and fig. 2.20). At the next stage the simulation of pump operation was performed when both motive nozzle are feed with the same volumetric flow rate. Results of this simulations are presented on below figures (fig. 2.23-2.26).

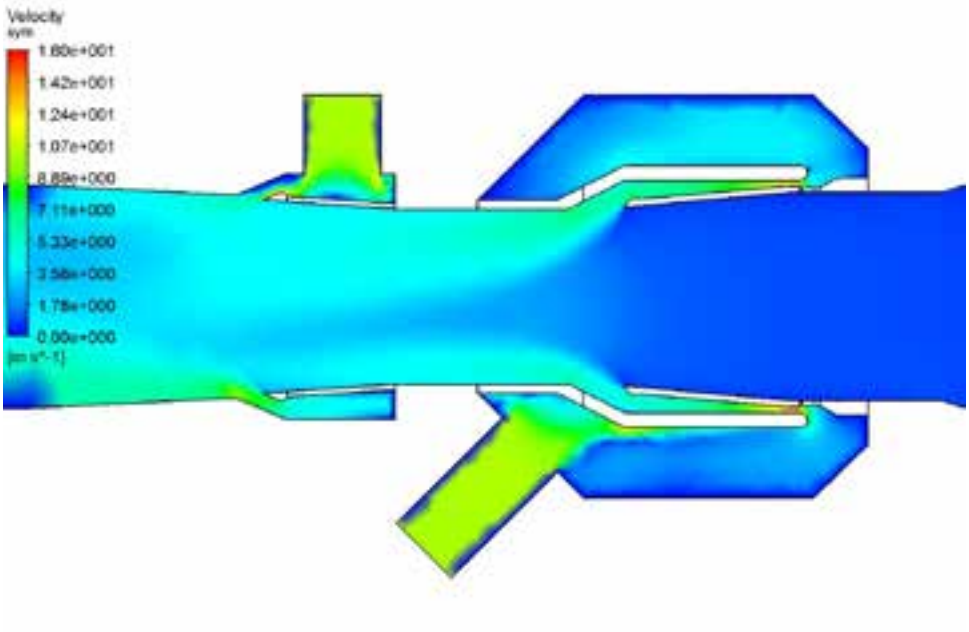

Fig. 2.23. Velocity of liquid in symmetry plane

After comparing with fig. 2.19 it can be found that maximal velocity is in more or less at the same level and appears at the same area. The difference is that much higher liquid velocity is at the throat. It resulting with different pressure distribution, what can be observed in fig. 2.23. Using both nozzles has also influence of stream of secondary liquid what shows path lines presented in fig. 2.25.

As it was already mentioned pressure distribution inside the pump for case when two nozzles are supplied with water with the same flow rate is a little different than in case when only one motive nozzle operates.

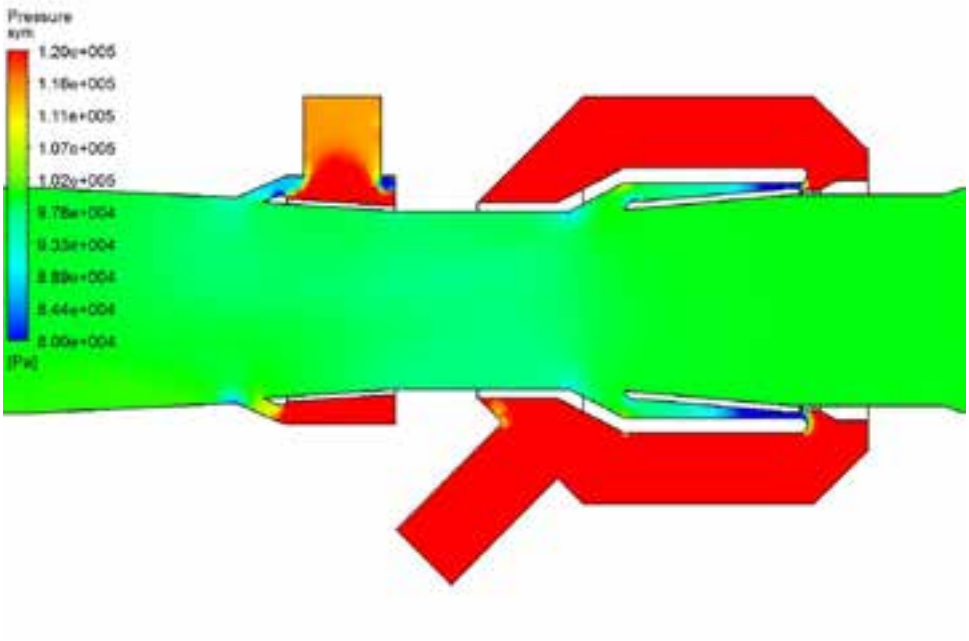

Fig. 2.24. Static pressure distribution

Presented below results in form of path lines allowed to indicated area where swirl may occur and in a consequences energy is lost. It may lead to conclusions in what way pump design may be improved to increase its efficiency and performance. Investigation of path lines allows also to investigate process of mixing both streams which may be important in some application of jet pups.

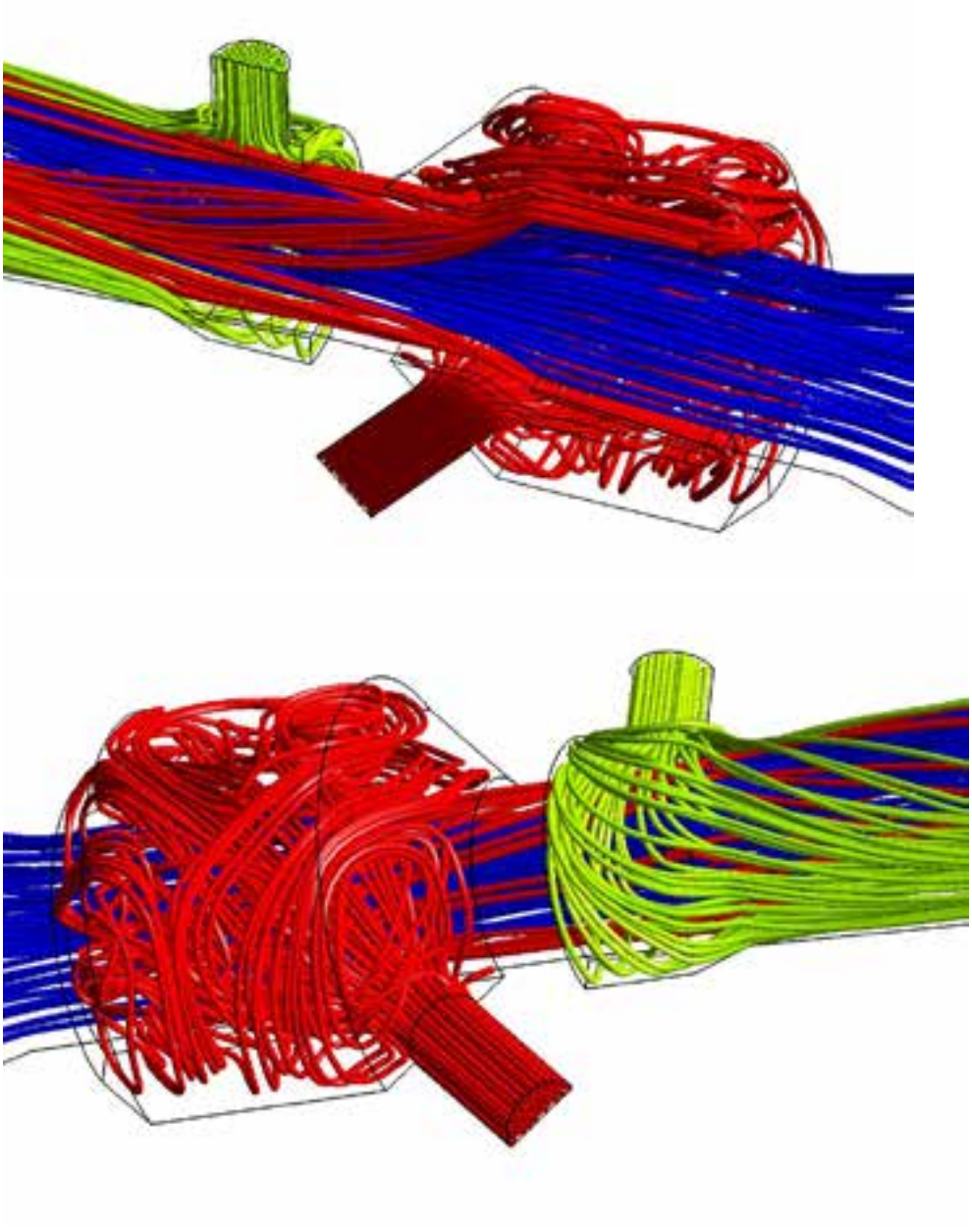

Fig. 2.25. Path lines when both nozzle operates, red is 1st nozzle, yellow is the 2nd while blue is secondary fluid

One of the most important issue of jet pumps is the pressure distribution inside pump. Sudden pressure drop to low value may lead to incorrect pump operation or may damage objects which are transported. One of method to avoid too low pressure is using additional discharging holes on motive nozzle as it is presented in fig. 2.26.

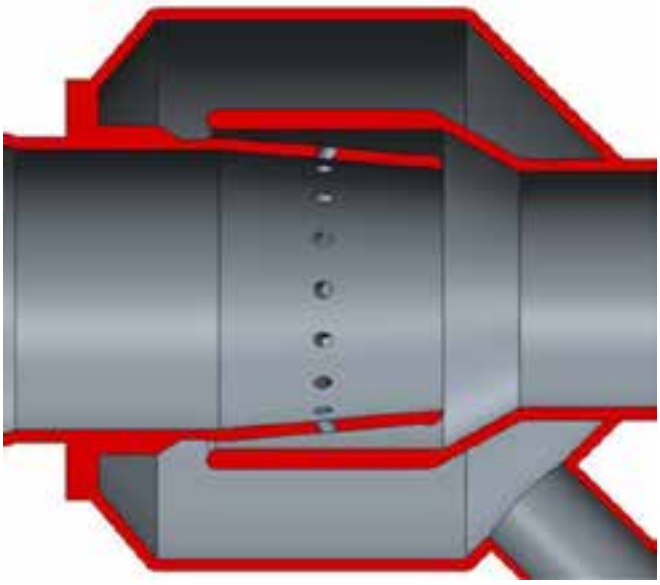

Fig. 2.26. Discharged holes on motive nozzle

The influence of such solution was verified by CFD simulation for the same conditions like presented before. Results of case, when only one nozzle is supplied are presented in fig. 2.27 and fig. 2.28.

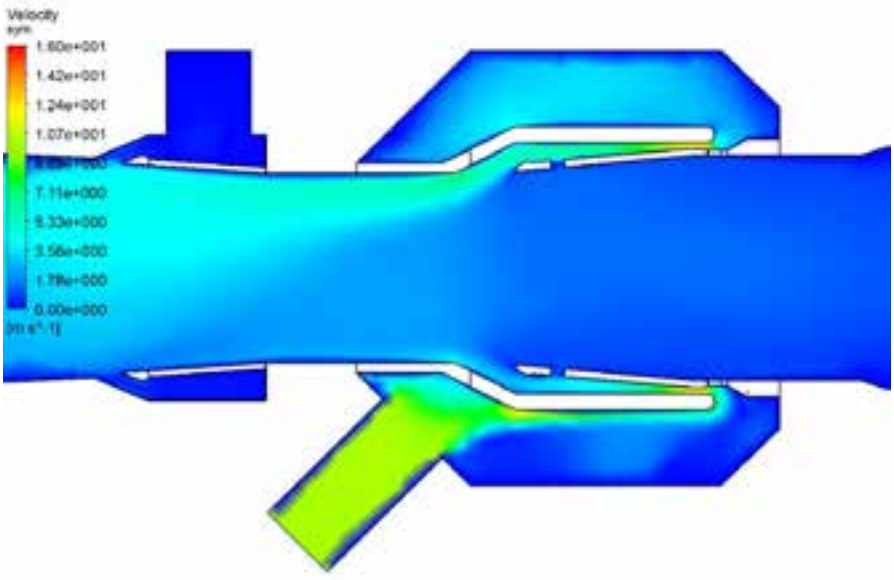

Fig. 2.27. Velocity distribution at symmetry plane

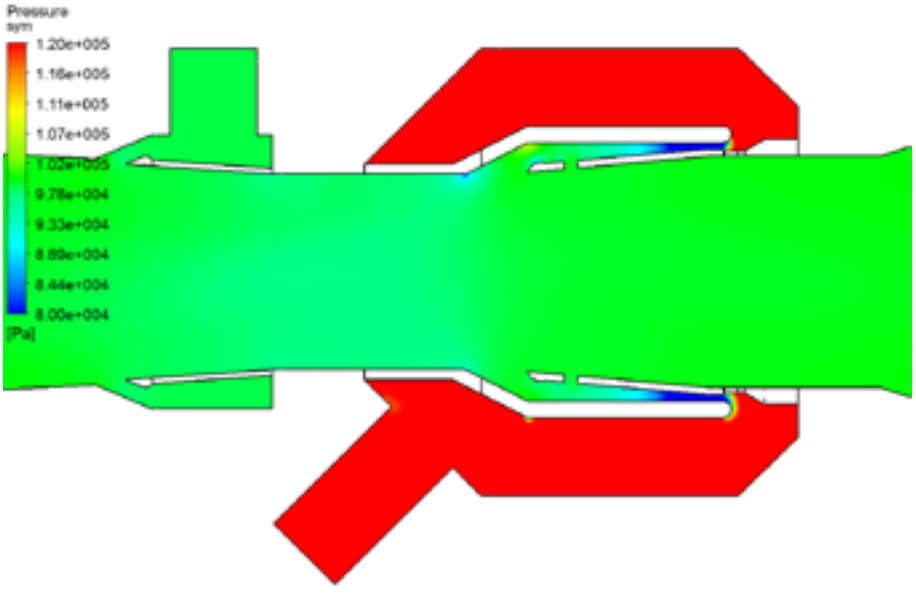

Fig. 2.28. Static pressure distribution at symmetry plane

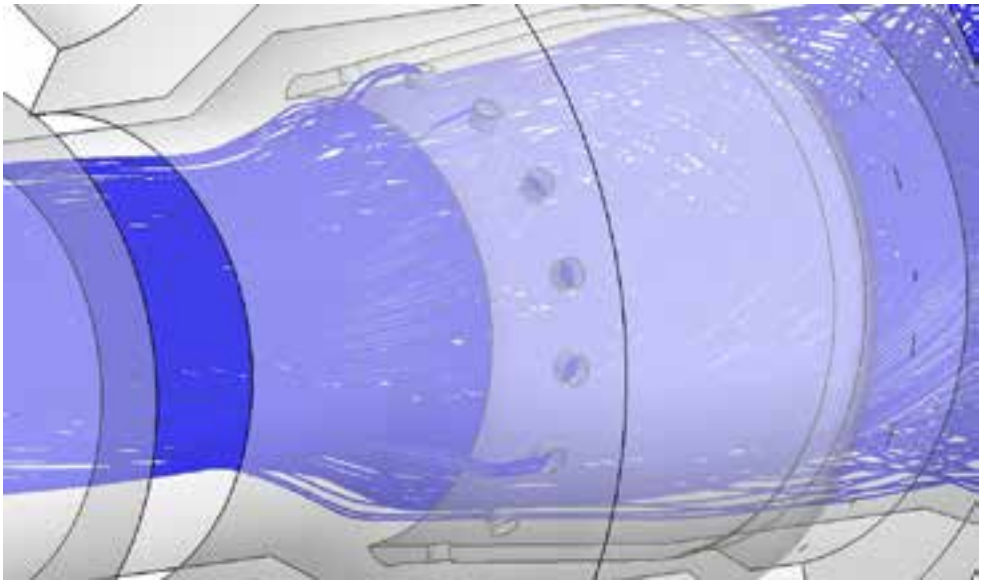

Fig. 2.29. Path lines in vicinity additional discharging holes

After comparison of results it is difficult to find significant difference between solution with and without discharging holes.

2.4.8 INFLUENCE OF NOZZLE PARAMETERS ON PUMP FLOW CHARACTERISTIC

In the next step was performed analysis of influence of discharge holes position and shape of nozzle on pump operational feature: the head pressure, which is the biggest weakness of jet pump besides low efficiency. There was investigated the following nozzle parameters: nozzle inclination angle (α), discharge hole inclination angle (β), number of holes (n), set of rows (r) and position of holes in relation to nozzle length (a) (see fig. 2.30).

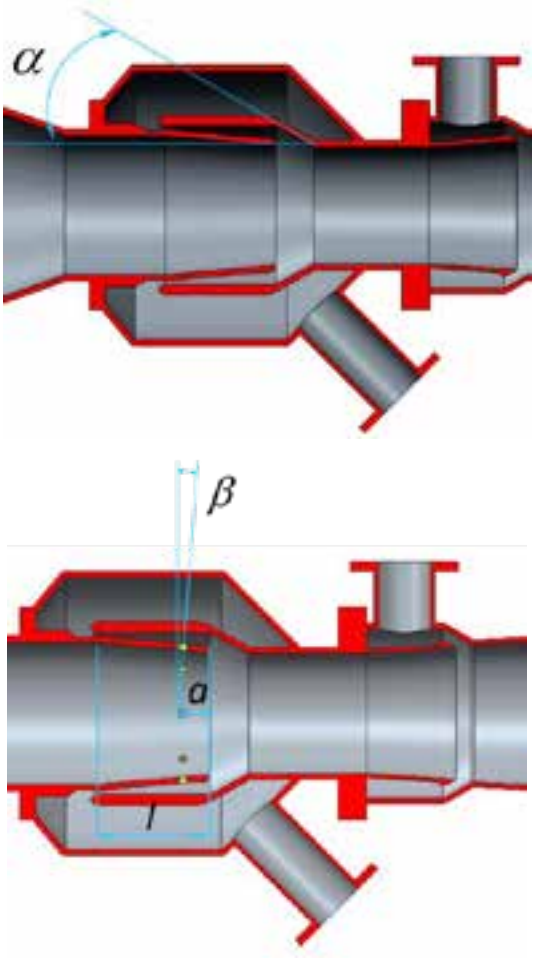

Fig. 2.30. Investigated nozzle parameters, nozzle inclination angle (α), discharge hole inclination angle (β), number of holes (n), set of rows (r) and position of holes in relation to nozzle length (a)

A number of simulations was performed what allowed to obtain flow characteristic of jet pump for various solution of nozzle design. These characteristic are presented in the following figures.

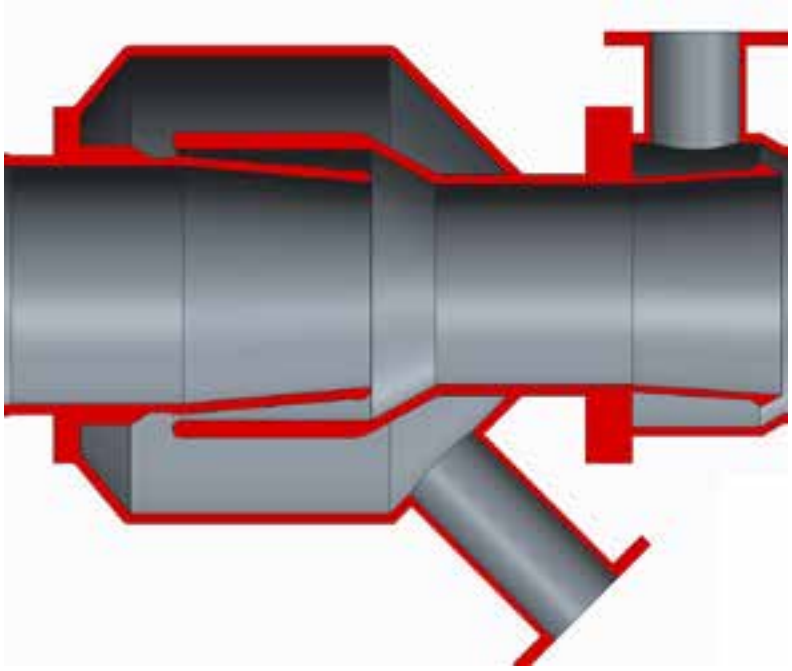

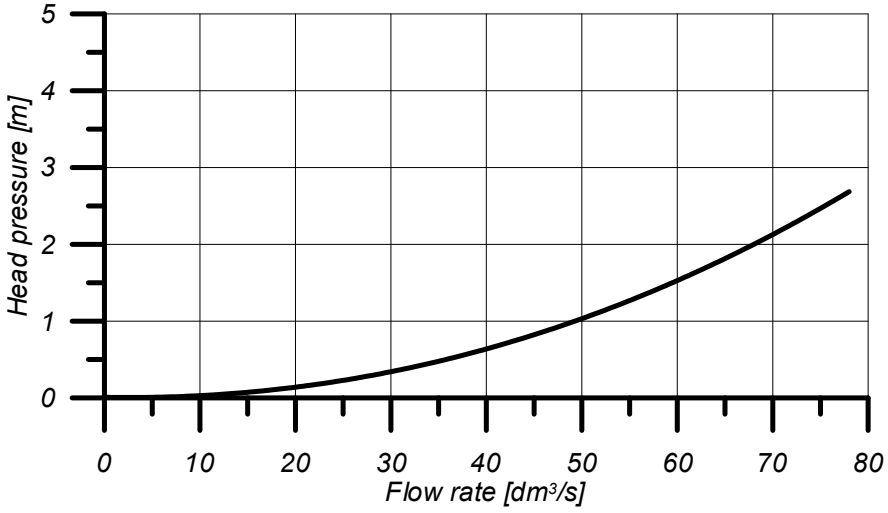

Fig. 2.31. Pump parameters: α=30°, β=0, n=0, r=0, a=0 and pumping height

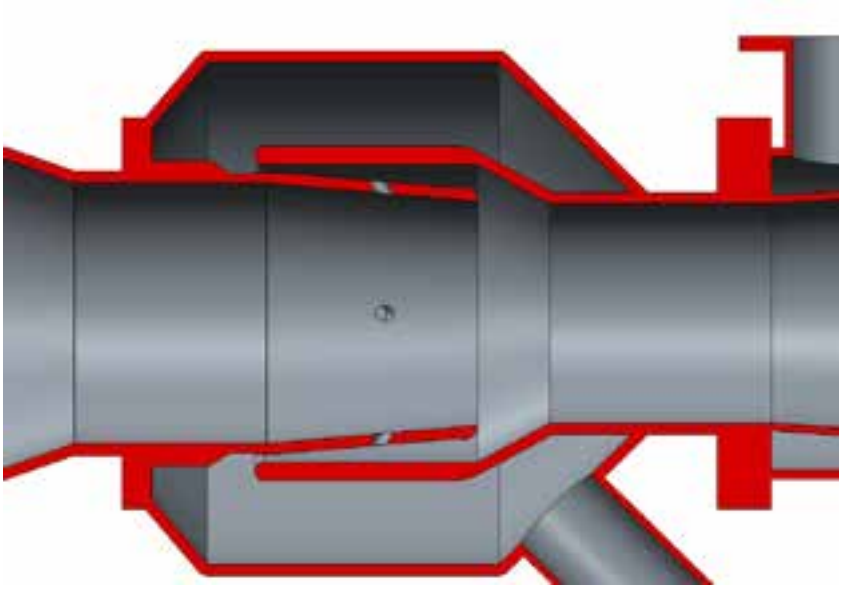

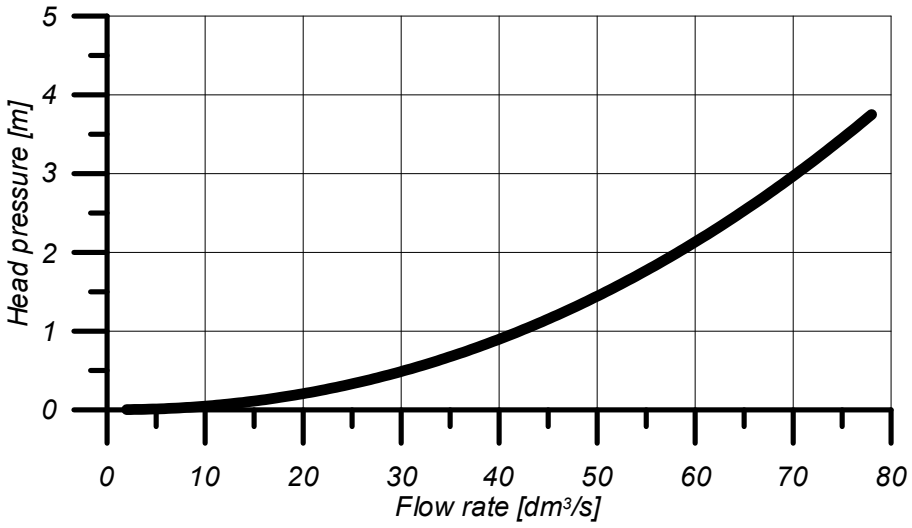

Fig. 2.32. Pump parameters: α=30°, β=30°, n=4, r=1, a=1/2 and pumping height

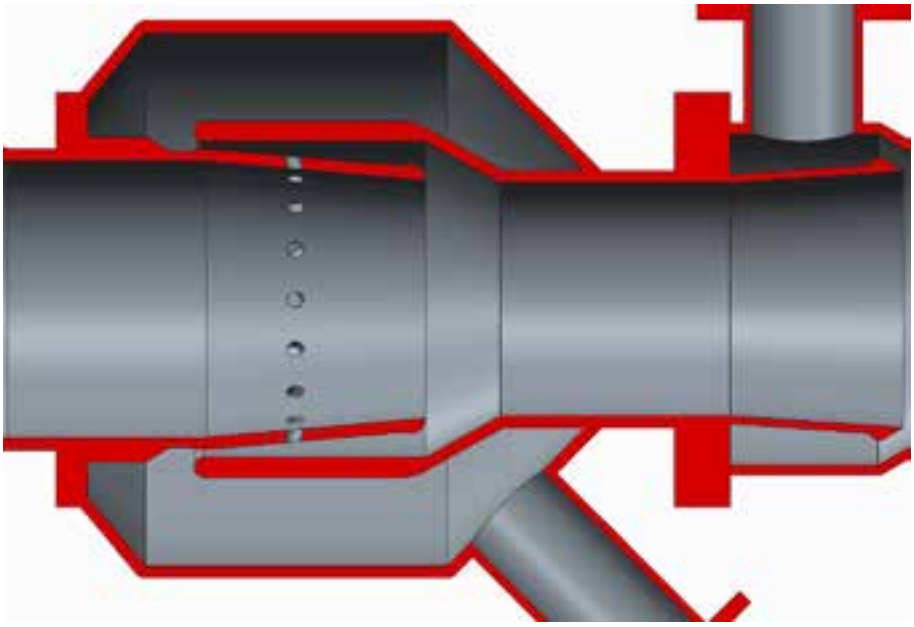

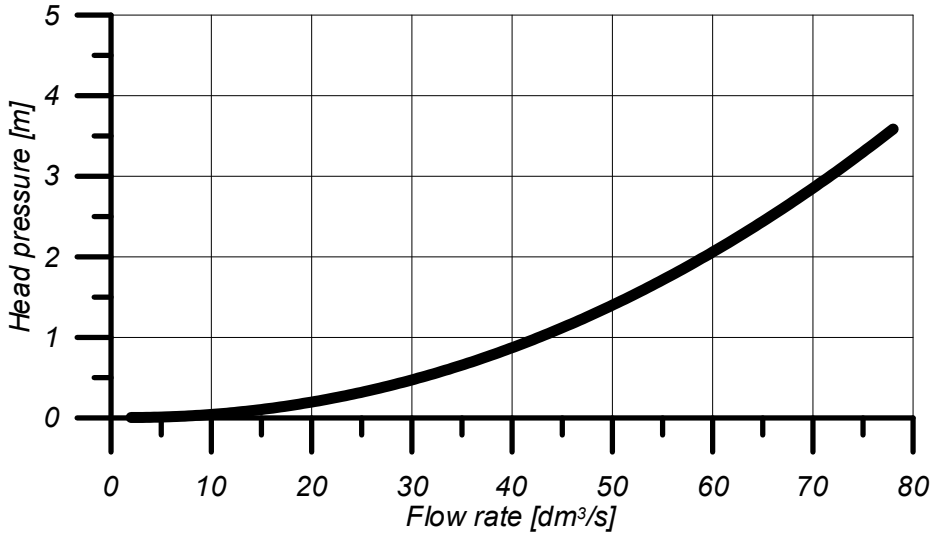

Fig. 2.33. Pump parameters: α=30°, β=30°, n=16, r=1, a=1/2 and pumping height

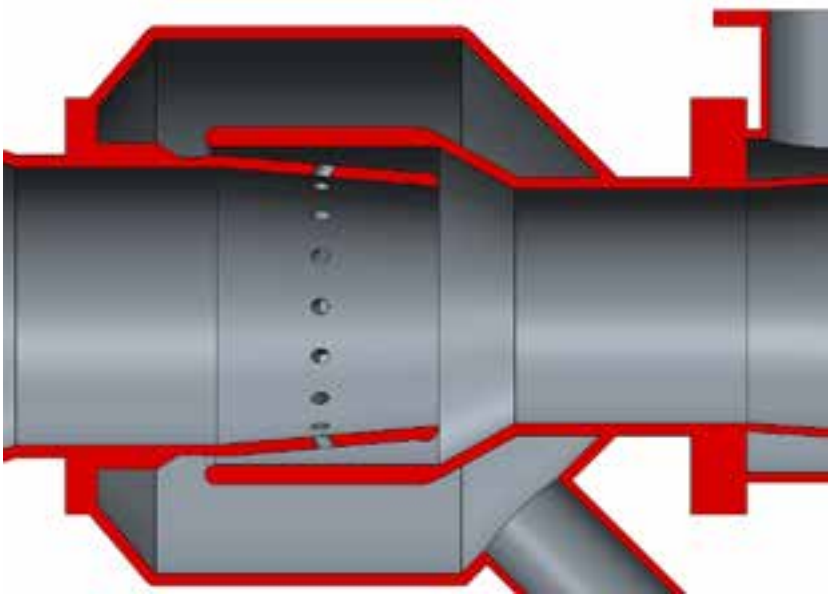

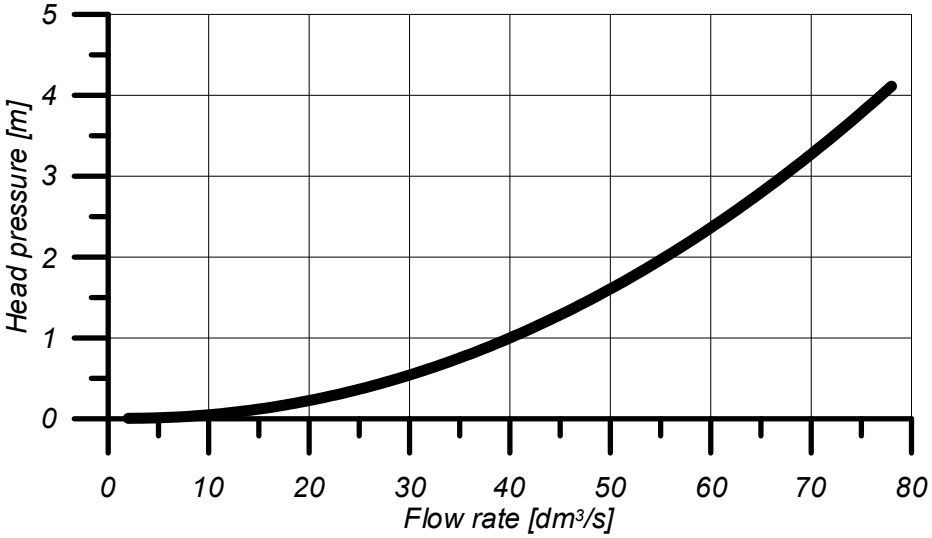

Fig. 2.34. Pump parameters: α=30°, β=-30°, n=16, r=1, a=1/2 and pumping height

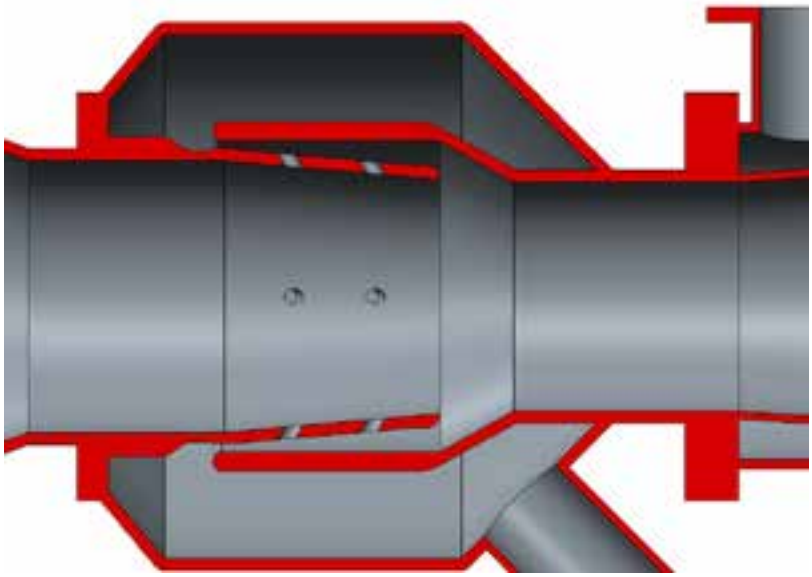

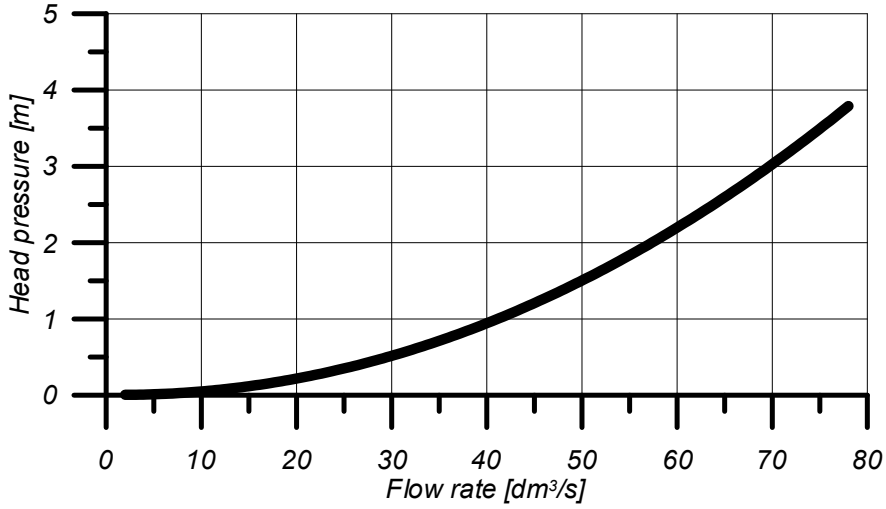

Fig. 2.35. Pump parameters: α=30°, β=30°, n=8, r=2, a=1/2 and pumping height

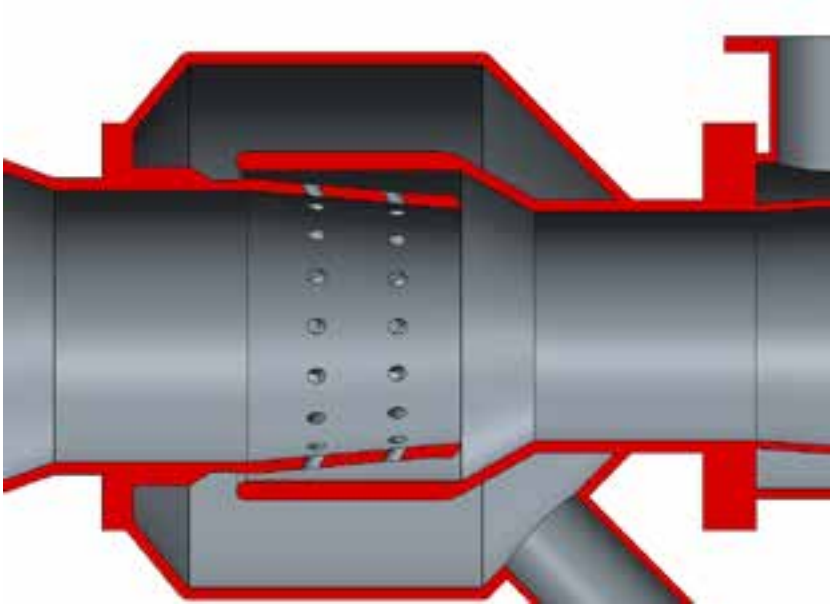

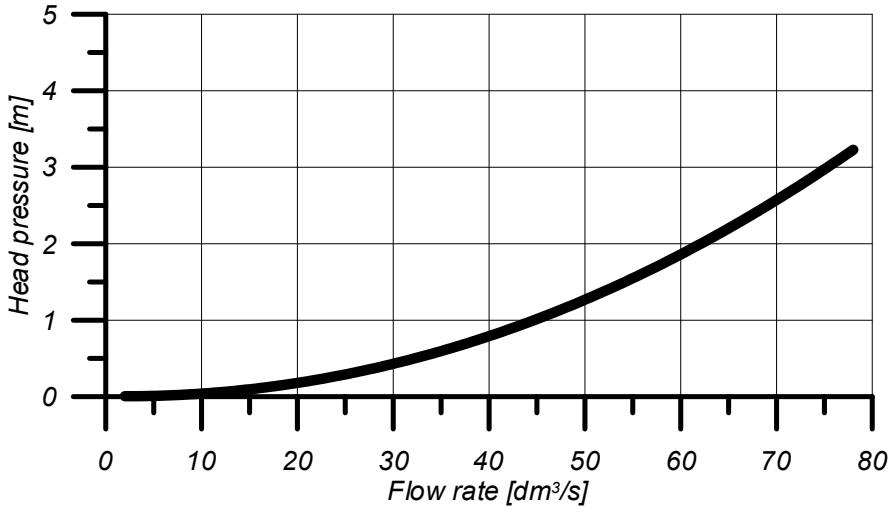

Fig. 2.36. Pump parameters: α=30°, β=30°, n=16, r=2, a=1/2 and pumping height

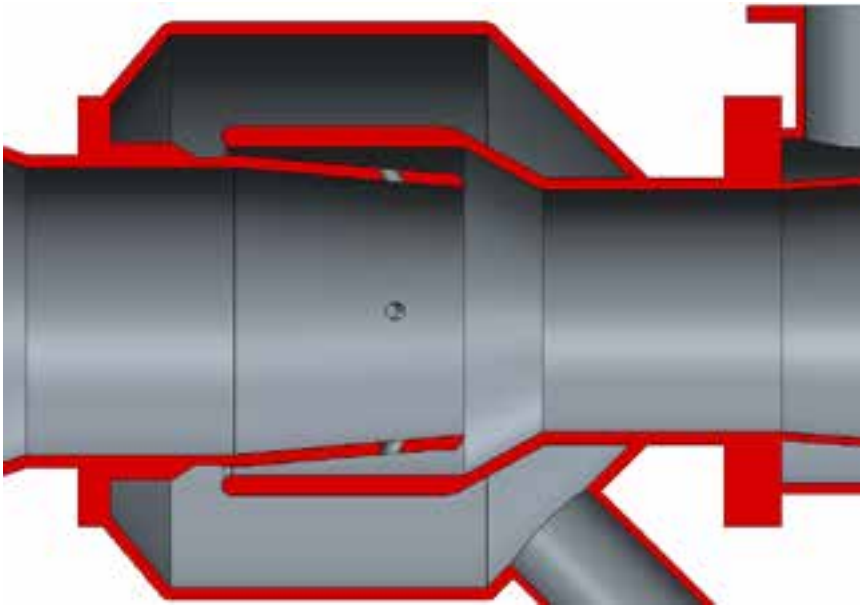

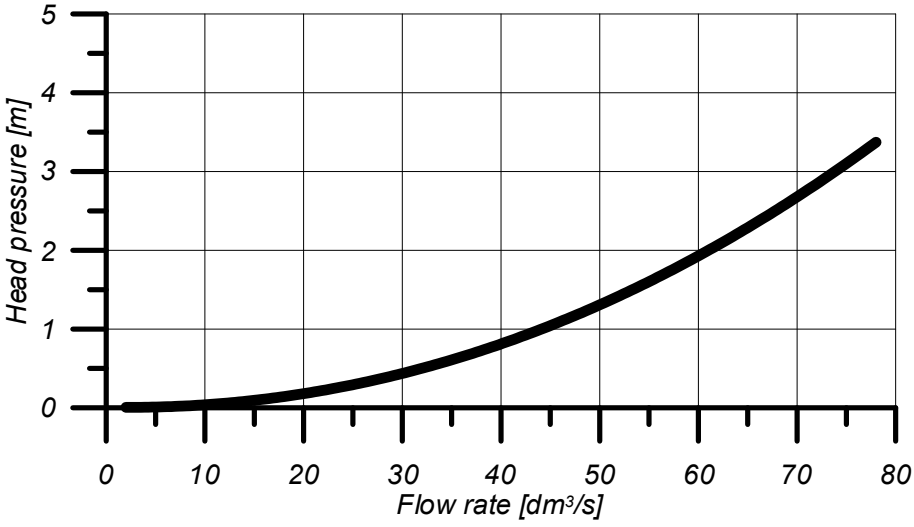

Fig. 2.37. Pump parameters: α=30°, β=-30°, n=4, r=1, a=1/3 and pumping height

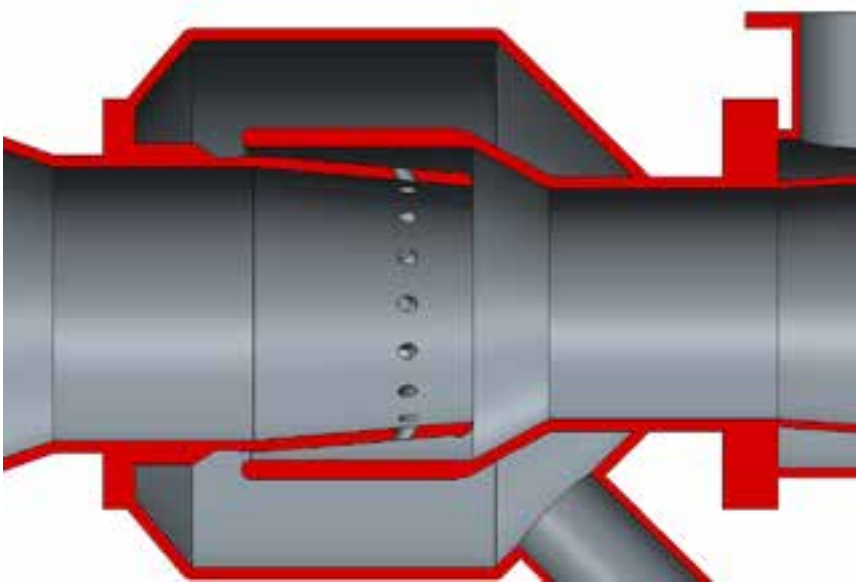

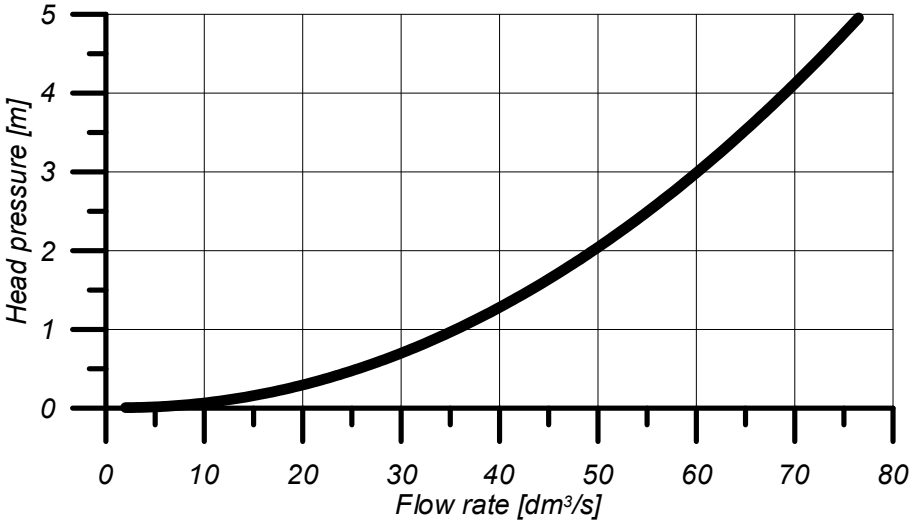

Fig. 2.38. Pump parameters: α=30°, β=-30°, n=16, r=1, a=1/3 and pumping height

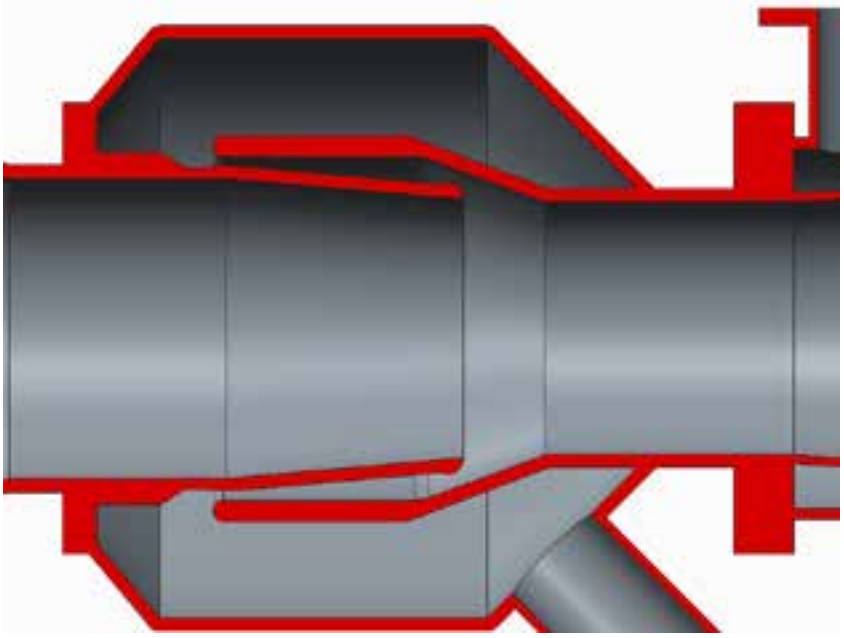

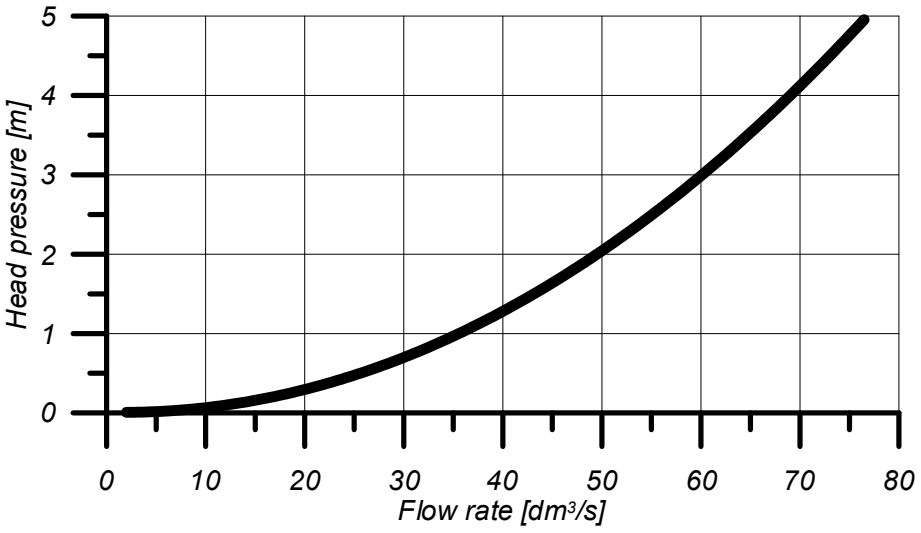

Fig. 2.39. Pump parameters: α=20°, β=0, n=0, r=0, a=0 and pumping height

Presented above results shows that the significant influence on pump flow characteristics is position of discharge holes as well as the inclination angle of motive nozzle. Adequate position of discharge holes allows to reach almost double head pressure in comparison to original design. Similar results might be achieved by changing nozzle inclination angle from 30° to 20°. For both cases we are able to increase almost twice head pressure in comparison to standard nozzle. These investigation shown possible modification of eliminating one of the biggest disadvantageous which is relatively low head pressure.

2.4.9 SIMULATION OF CAVITATION IN JET PUMP

The key issue, particularly in liquid-jet-liquid pumps is cavitation, which may appear during pump operation and in the consequences to pump failure. The conversion of velocity energy into pressure energy may led to drop of pressure of working fluid below saturation pressure at given temperature and formation of vapor bubbles. This parameters (cavitation) limits the usage of LJL pumps and have strong influence on pump wear and noise, and particularly in case of transport of food or live animal has significant meaning. Cavitation is well known engineering problem which is met in many applications. There are available at the literature a rich description of this phenomena, however it is still difficult for modeling. One of the best way for simulation of cavitation in LJL pump is using CFD method. Models of cavitation which are applied in CFD codes are presented below. The tendency a flow to cavity may be defined as the cavitation number:

$$c_a = \frac{p - p_v}{0.5\rho U^2} \tag{2.19}$$

One of the common approach to describe bubble dynamics is the Rayleigh Plesset equation:

$$R_b \frac{d^2 R_b}{dt^2} + \frac{3}{2}\left(\frac{dR_b}{dt}\right)^2 + \frac{2\sigma}{\rho R_b} = \frac{p_v - p}{\rho} \tag{2.20}$$

After deriving this equation, and neglecting second order terms and surface tension the equation is reduced to the following:

$$\frac{dR_b}{dt} = \sqrt{\frac{2}{3}\left(\frac{p_v - p}{\rho}\right)} \tag{2.21}$$

The rate of bubble volume changes is as follow:

$$\frac{dV_b}{dt} = 4\pi {R_b}^2 \sqrt{\frac{2}{3}\left(\frac{p_v - p}{\rho}\right)} \tag{2.22}$$

The rate of change bubble mass is:

$$\frac{dm_g}{dt} = 4\pi {R_b}^2 \rho_g \sqrt{\frac{2}{3}\left(\frac{p_v - p}{\rho}\right)} \tag{2.23}$$

The N_b bubbles per unit volume the volume fraction r_g is expressed by:

$$r_g = \frac{4}{3}\pi R_b^2 N_b \tag{2.24}$$

The total interphase mass transfer per unit volume is:

$$\dot{m}_{fg} = 3\frac{r_g \rho_g}{R_b}\sqrt{\frac{2}{3}\frac{p_v - p}{p_f}} \tag{2.25}$$

When including condensation this expression is as follows:

$$\dot{m}_{fg} = 3F\frac{r_g \rho_g}{R_b}\sqrt{\frac{2}{3}\frac{|p_v - p|}{p_f}\mathrm{sgn}(p_v - p)} \tag{2.26}$$

Vapor transport equation has the following form:

$$\frac{\partial}{\partial t}(\alpha \rho_v) + \nabla \cdot \left(\alpha \rho_v \overrightarrow{V_v}\right) = R_e - R_c \tag{2.27}$$

CFD simulations were conducted for two stage LJL presented before pump with the use of full cavitation simulation using Rayleigh Plesset

model. Some selected results of simulation for both stages are presented in below figures. There are presented distribution of vapor fraction and isosurface of vapor.

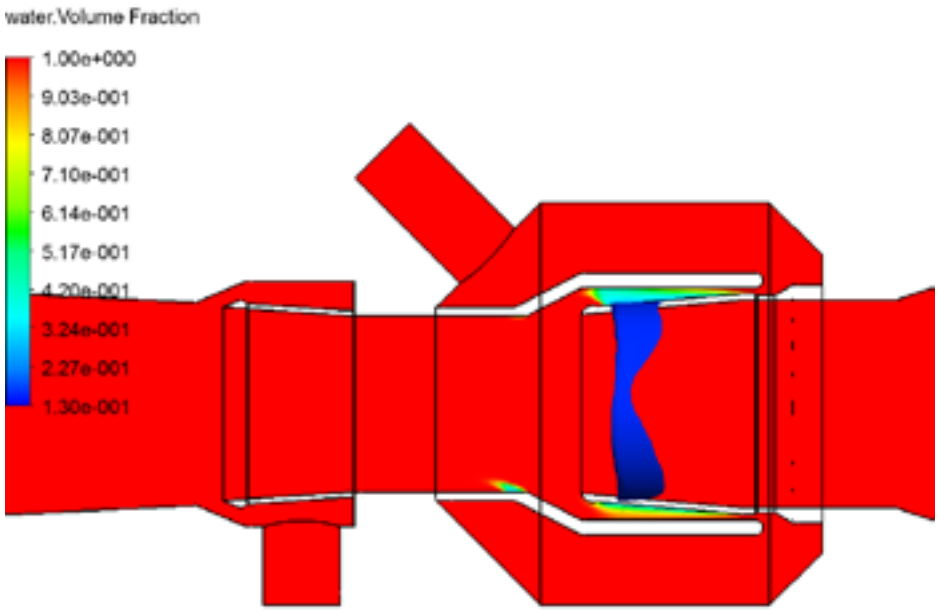

Fig. 2.40. Distribution of vapor pressure

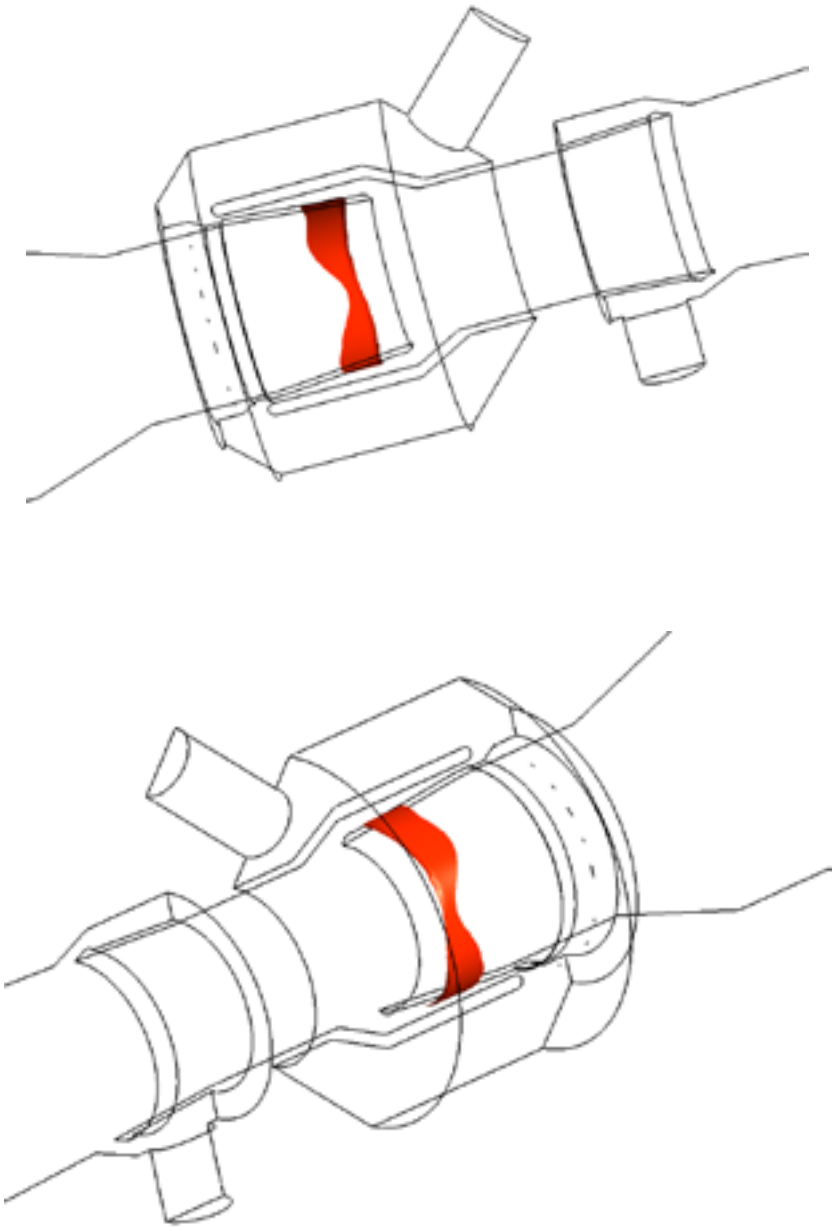

Fig. 2.41. Vapor surface

2.4.10 SIMULATION OFTRANSPORT THICK LIQUID

One of the jet pump application which was mentioned at previous sections was transport extremely hazardous liquids. This section shows results of CFD simulation for transport liquids which density is almost twice bigger than water, which in this case is working liquid. The simulation model consists of LJL pump with tank with thick liquid and LJL pump what was presented on figure below.

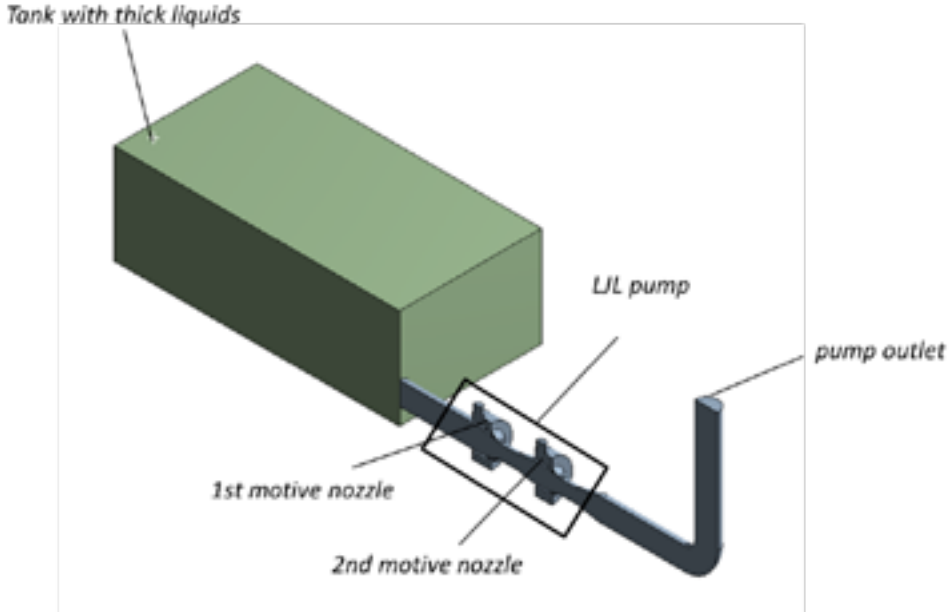

Fig. 2.42. Simulation model

CFD simulations were conducted for various flow rate at motive nozzles and the following assumptions were set:

- both liquids are homogenous with constant properties,
- flow is turbulent,
- body forces are included in the pump, but not in the tank,

- others assumptions are the same as in chapter 2.4.4.

Two motive nozzles allowed not only for increasing head pressure as it was presented in previous chapters but also increase the amount of thicker liquid that is taken away by the pump. Presented below results shows both fraction: water and thick liquid depending on working conditions. Below result shows both liquid distribution when only first stage operates.

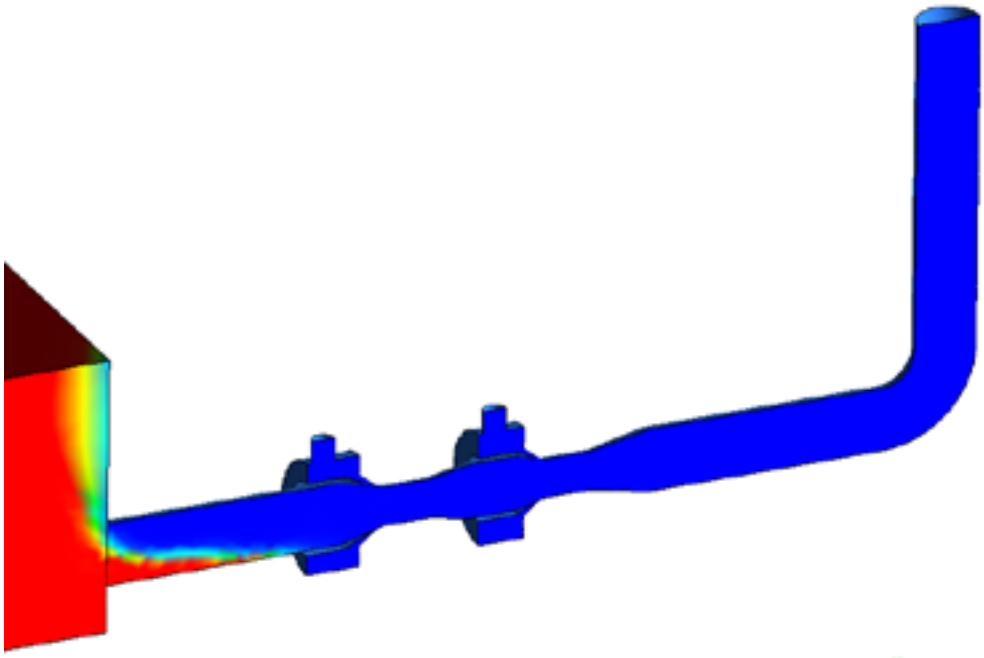

Fig. 2.43. Fractions distribution during operation of only 1st stage

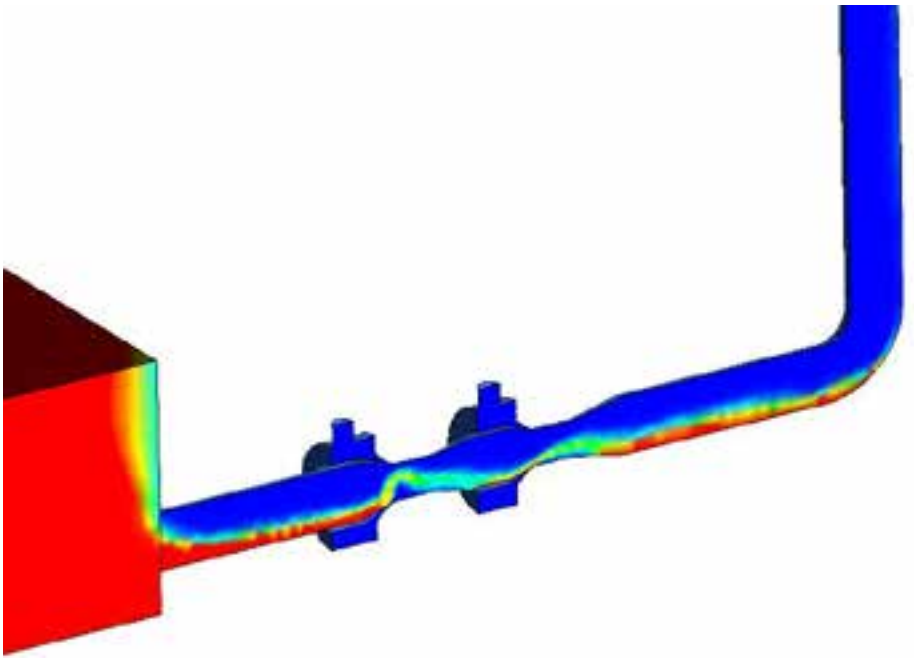

Fig. 2.44. Fractions distribution during operation of both stages

For given working conditions motive liquid gained not enough energy to take thick liquid more than on a little distance from the tank. Increasing twice mass flow rate of motive liquid allows to transport more thick liquid from the tank. What can be found is that energy of motive liquid now is sufficient to transport thicker liquid. When increasing mass flow rate allows to transport more and more thick liquid.

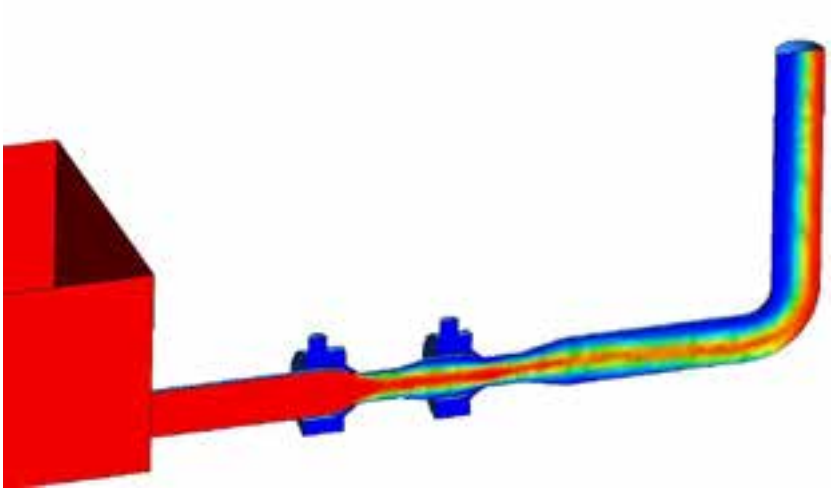

Fig. 2.45. Fractions distribution during operation of both stages with twice increase of motive liquid flow rate

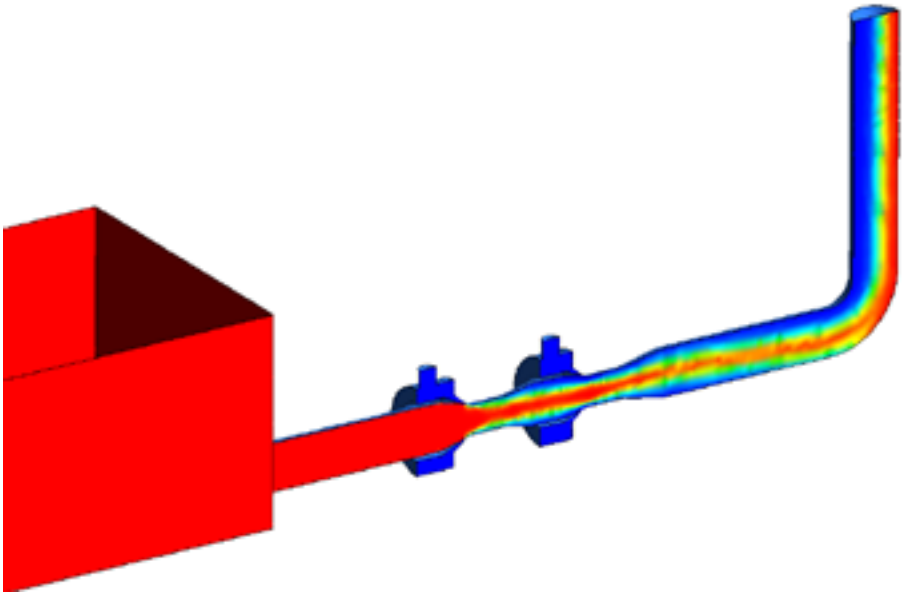

Fig. 2.46. Fraction distribution during operation of both stages with triple increase of motive liquid flow rate

2.4.11 SIMULATION OF TRANSPORT OF SOLIDS

One of the capabilities of jet pump, particularly pumps with annular nozzles is availability of transport solids. This chapter presents few approaches of CFD simulations in case of transport solids. The first approach is to investigate pressure distribution at the throat with solid with fixed position inside. The investigated solid is a ball with a smaller diameter than the throat. LJL pumps with annular nozzles might be used for transportation food and in such case too high pressure drop may destroy object flowing through the pump. Therefore, the aim of CFD simulation was focused on investigation of pressure distribution at the vicinity of object at the throat.

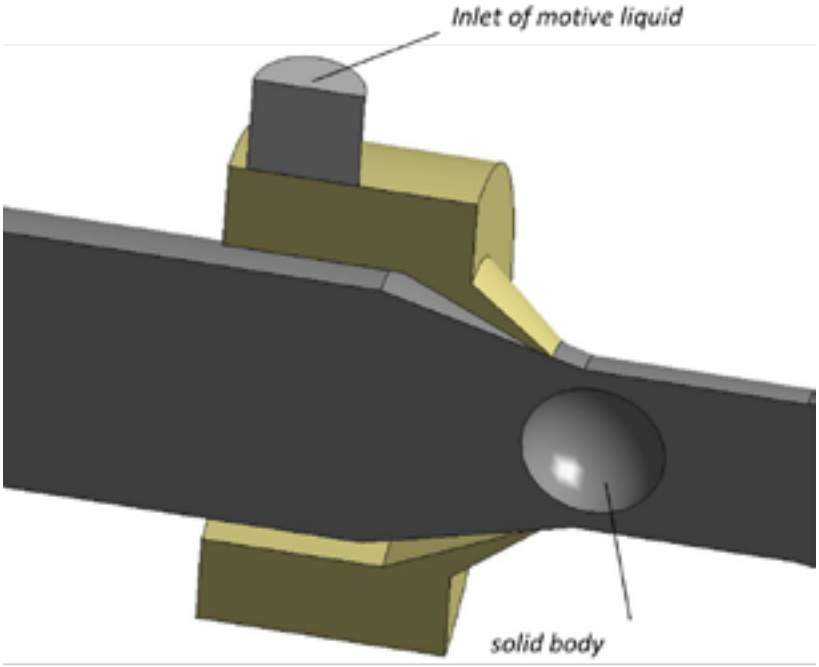

Fig. 2.47.Simulation model

CFD simulations were conducted in steady state conditions, and such approach may be an introduction for further simulation which might be fluid solid interaction simulation at transient conditions.

Below figures presents CFD results as a pressure distribution on object surface as well as a path lines of flowing liquid at the throat. Pressure distribution was investigated when flow rate of motive liquid increase.

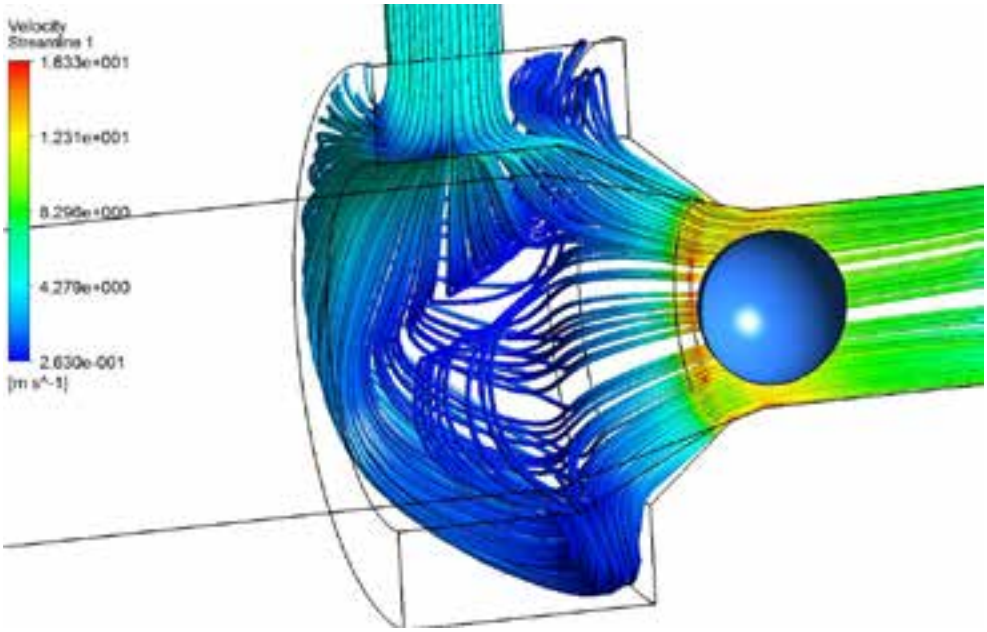

Fig. 2.48. Path lines around solid body

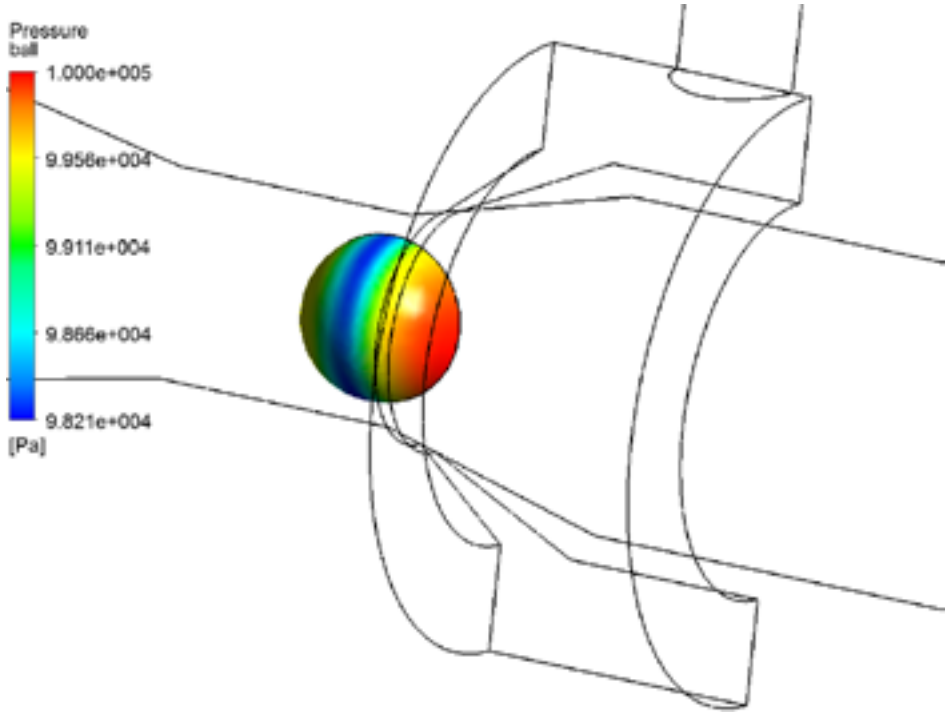

Fig. 2.49. Pressure distribution at the object inside the throat

The next stage of simulation was increasing flow rate of motive liquid double. The influence of increasing flow rate of motive liquid is shown on below figures. What might be found is that the liquid velocity increase close to the object and in the consequences vacuum pressure at the throat also drops.

Below figures presents CFD results as a pressure distribution on object surface as well as a path lines of flowing liquid at the throat.

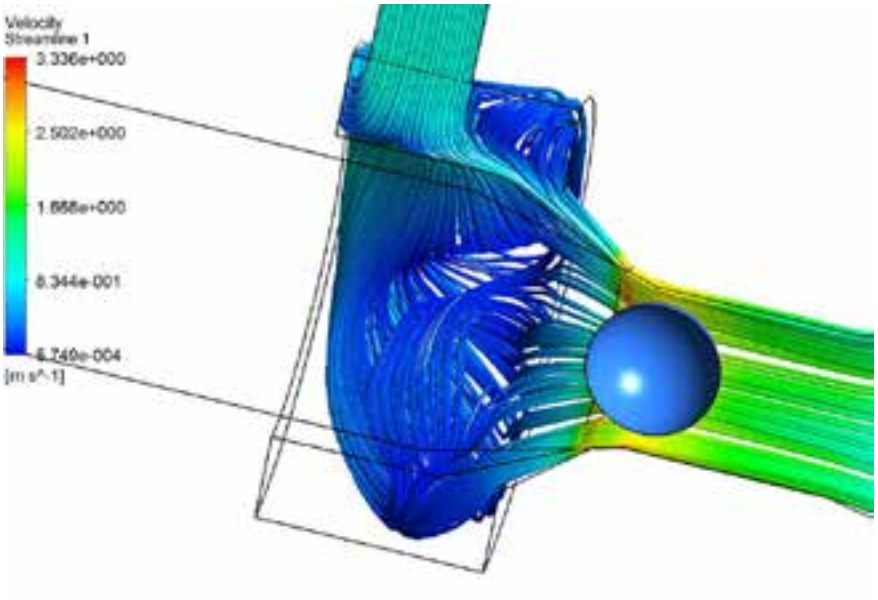

Fig. 2.50. Path lines

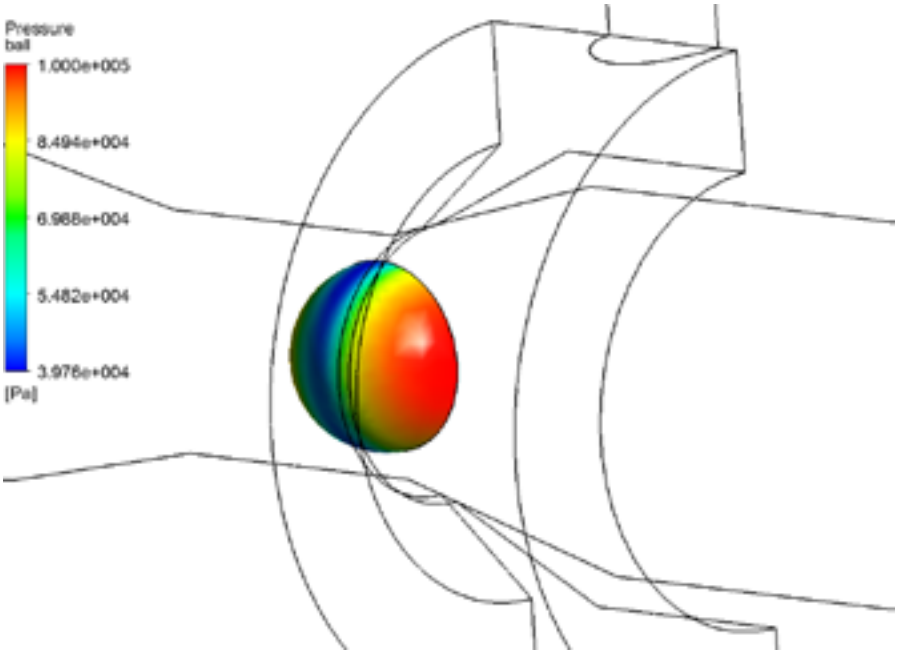

Fig. 2.51. Pressure distribution at the object surface

One of the aim of the previous shown CFD simulation was to investigate the influence of additional holes at the motive nozzle. Already presented results at the chapter 2.4.8 shown that such parameters have influence on head pressure. The following CFD simulation was focused on investigation of pressure distribution and flow inside the throat when 16 additional holes are applied to the motive nozzle. The results of this simulations are presented on below figures. It may be noticed that in comparison to original solution maximal velocity of motive fluid is lower, what also leads to the smaller pressure drop.

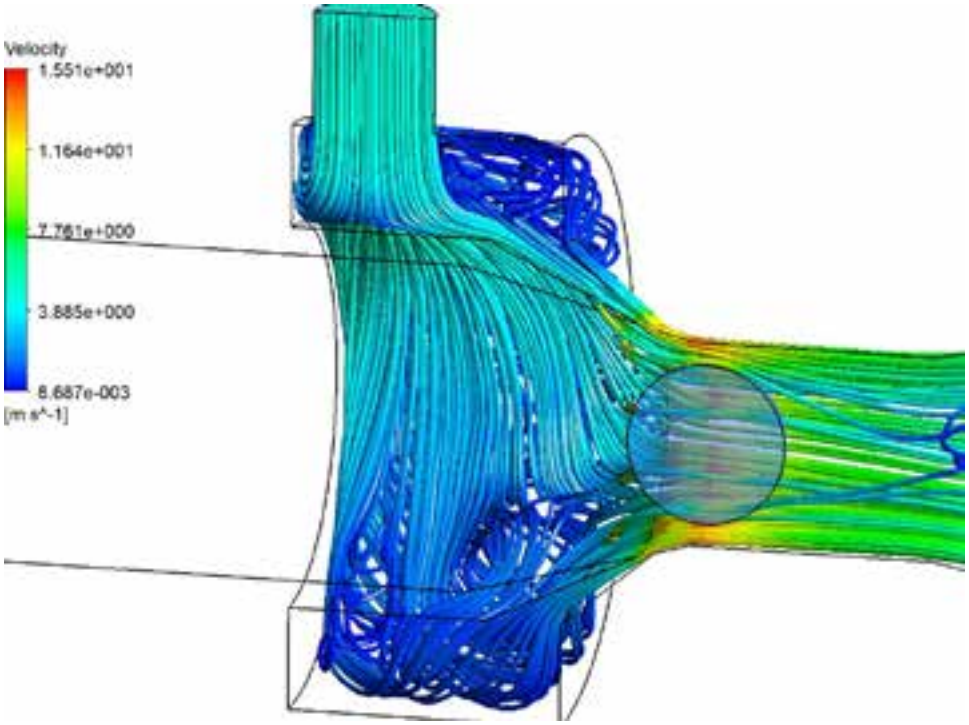

Fig. 2.52.Path lines for motive nozzle with additional holes

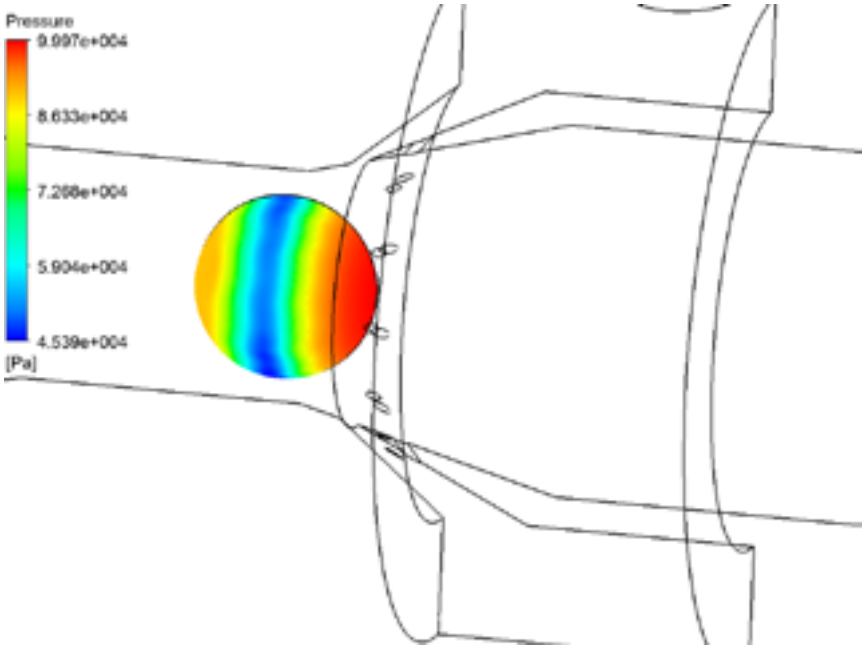

Fig. 2.53. Pressure distribution at the object surface for nozzle with additional holes

Presented above results shown that the modification of motive nozzle parameters have significant influence on pump operational features like head pressure or pressure distribution inside the throat. As it was mentioned before, one of the important parameters for transport food or fragile object is pressure distribution when object flowing through the throat. Therefore for selected flow conditions a static pressure at the symmetry plane on the surface object was presented on the below figure.

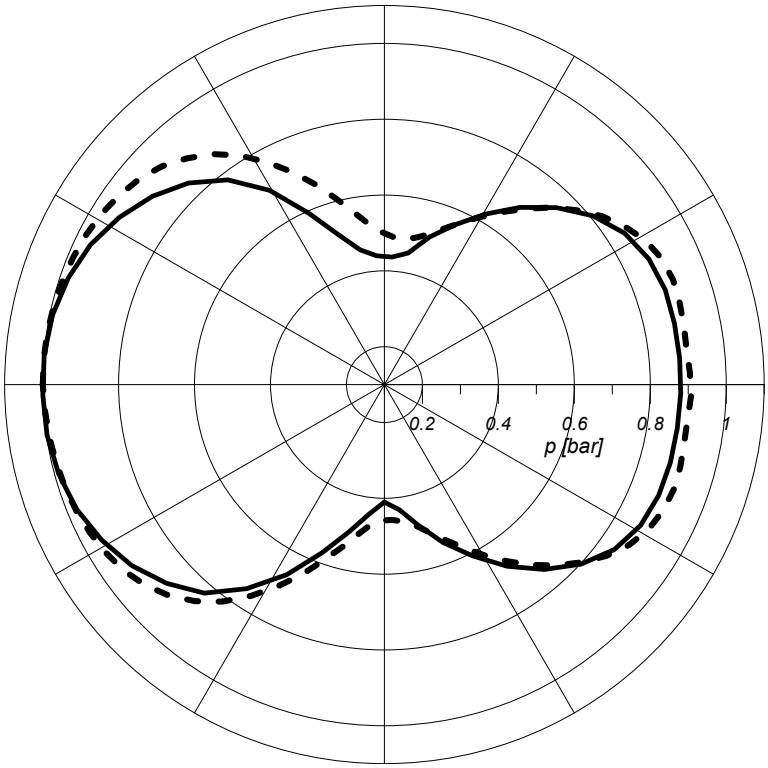

Fig. 2.54. Pressure at the symmetry plane on the object surface

CFD simulations shown that motive nozzle parameters have a significant influence on pressure distribution at the pump throat. At the next stage, there was investigated the influence of the angle of motive nozzle (see Fig. 2.26) and throat on the pressure distribution inside the pump. There was also investigated the influence of shape of the motive nozzle entry to the throat. Below figures presents CFD simulation for the same flow conditions.

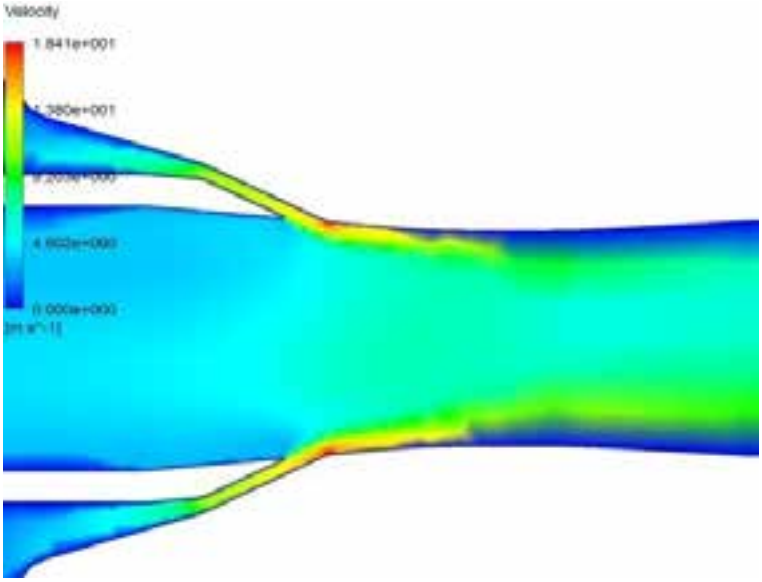

Fig. 2.55. Velocity distribution of the liquid at the symmetry plane for initial geometry

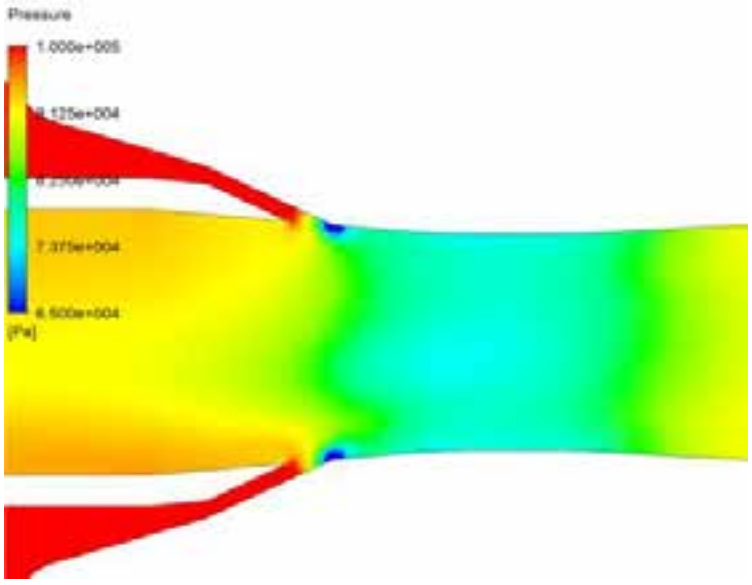

Fig. 2.56. Pressure distribution of the liquid at the symmetry plane for initial geometry

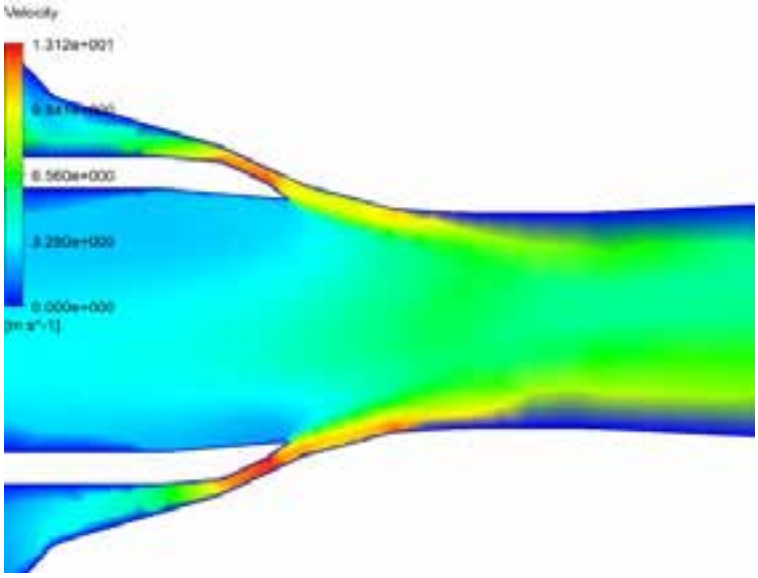

Fig. 2.57. Velocity distribution of the liquid at the symmetry plane for modified geometry (version 1)

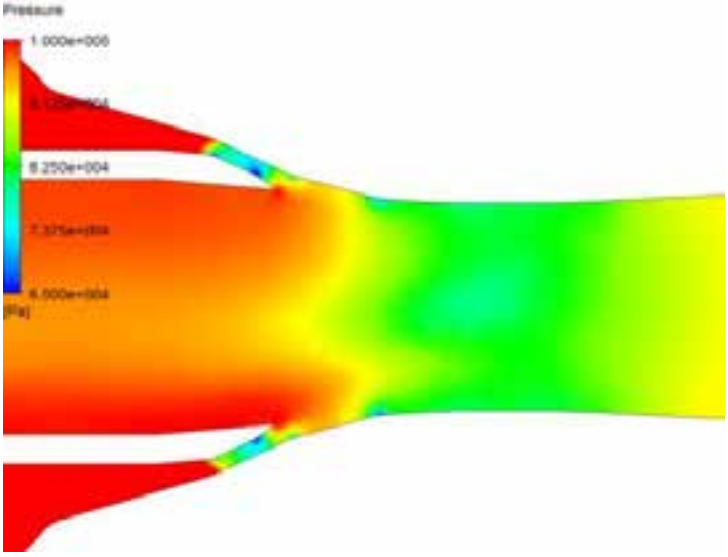

Fig. 2.58. Pressure distribution of the liquid at the symmetry plane for modified geometry (version 1)

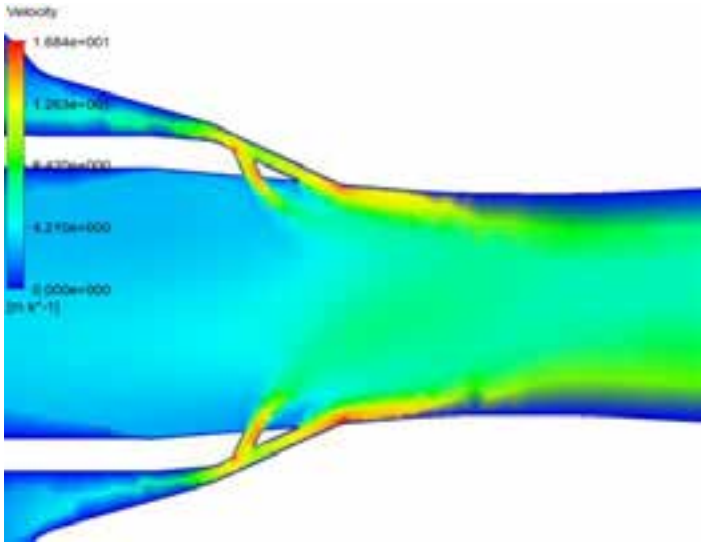

Fig. 2.59. Velocity distribution of the liquid at the symmetry plane for modified geometry (version 2)

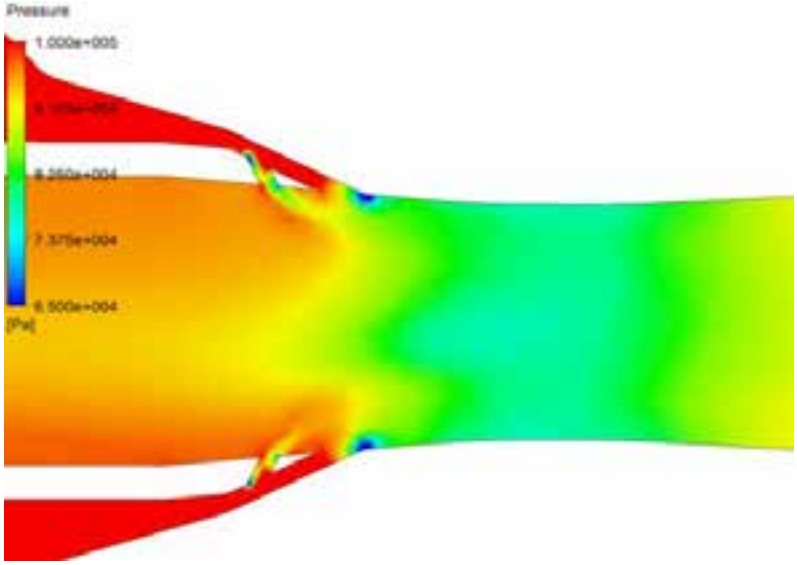

Fig. 2.60. Pressure distribution of the liquid at the symmetry plane for modified geometry (version 2)

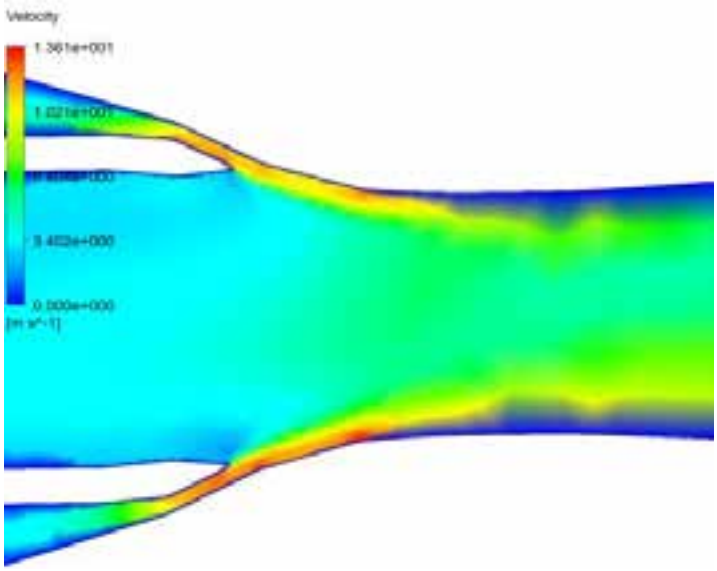

Fig. 2.61. Velocity distribution of the liquid at the symmetry plane for modified geometry (version 3)

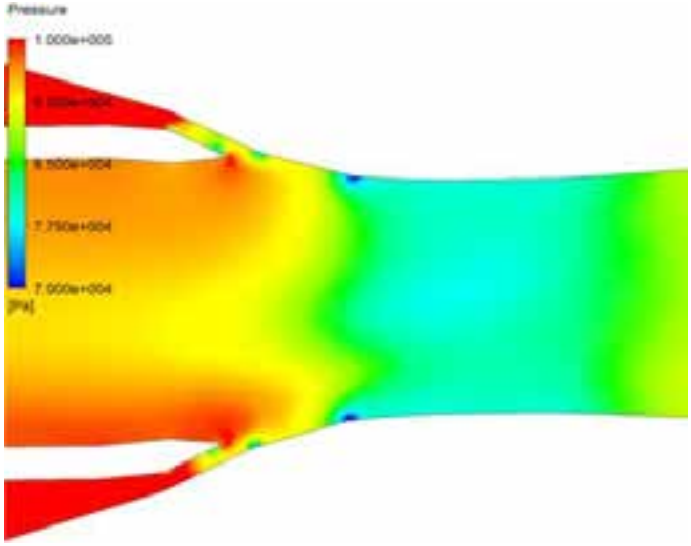

Fig. 2.62. Pressure distribution of the liquid at the symmetry plane for modified geometry (version 3)

Above figures shows that the geometry of motive nozzle and entrance to the throat have influence on pressure distribution inside the pump. For better understanding the influence of motive nozzle parameter on pressure distribution below figures shows region in which vacuum pressure is lower than 0.7 bar.

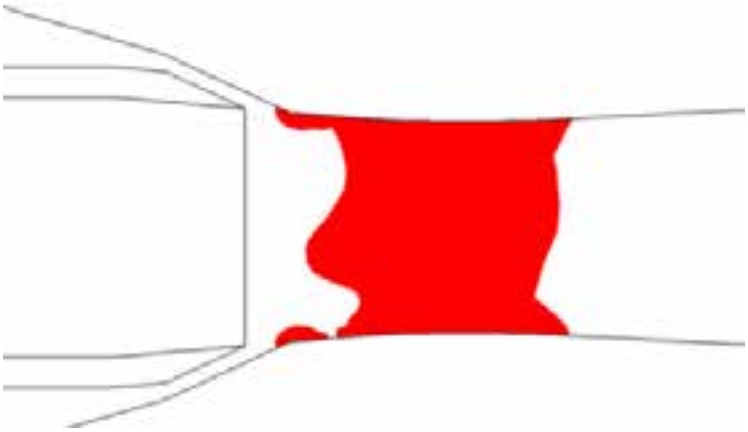

Fig. 2.63. Region with vacuum pressure below 0.7 bar for initial nozzle geometry

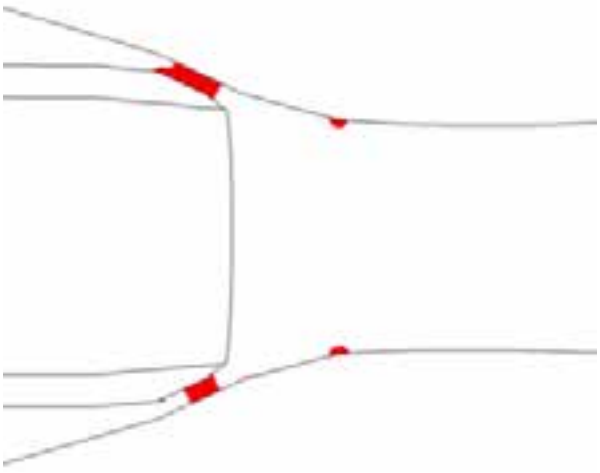

Fig. 2.64. Region with vacuum pressure below 0.7 bar for modified nozzle geometry (version 1)

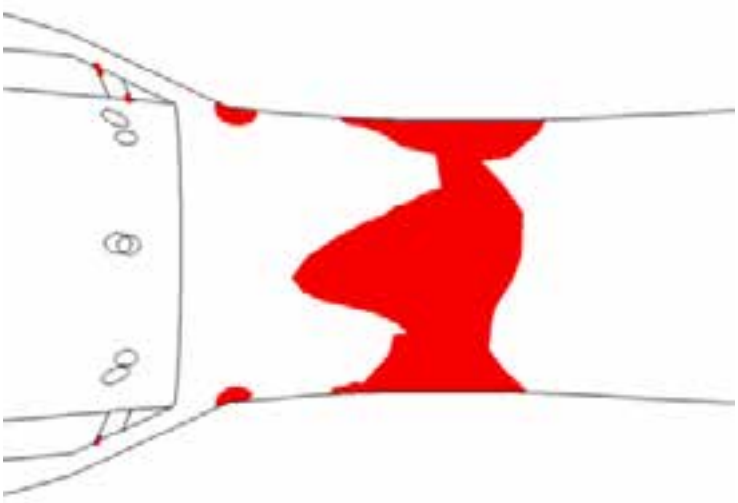

Fig. 2.65. Region with vacuum pressure below 0.7 bar for modified nozzle geometry (version 2)

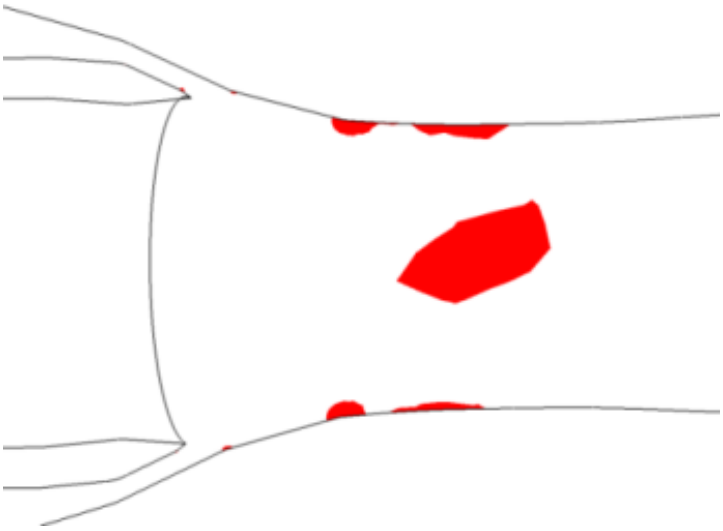

Fig. 2.66. Region with vacuum pressure below 0.7 bar for modified nozzle geometry (version 3)

Presented vacuum pressure region shown that the nozzle geometry have strong influence on this parameter. Presented results shown that the lowest pressure at the throat is achieved for version 1.

2.4.12 SIMULATION OF TRANSPORT OF SOLID PARTICELS

Despite the case presented in previous section this one presents simulation of transport of solid particles with specified dimension. The particles material is rock, with the mean diameter of 1/100 of pump inlet diameter. As in previous simulations jet pump with two motive stages was used. For this kind of simulations was assumed that particles may interact not only with motive liquid (water) but also with pump walls as well as with one another. The results of simulation are presented on results below as a trajectory of each particles.

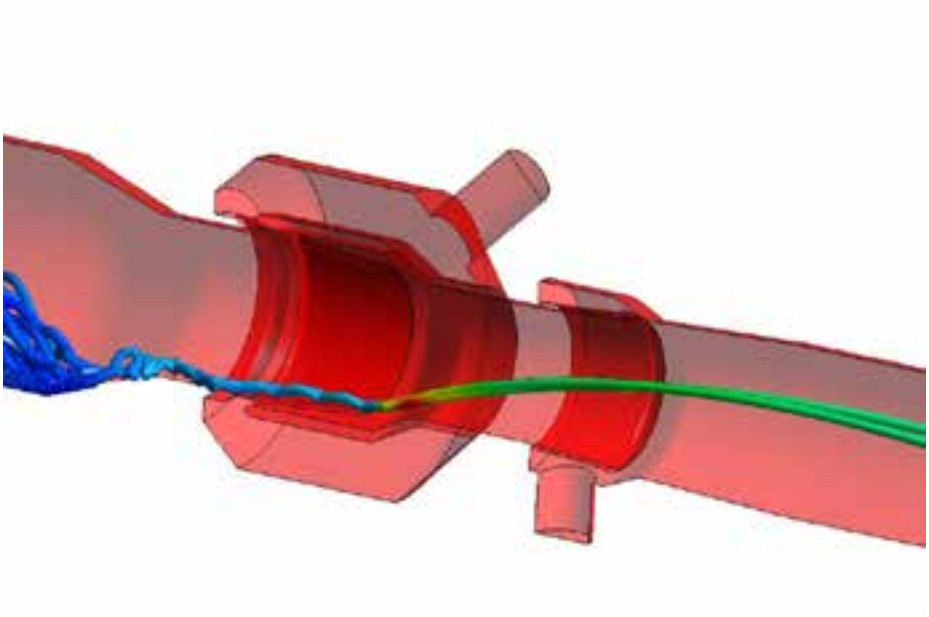

Fig. 2.67. Trajectory of solid particles (initial flow condition of motive liquid)

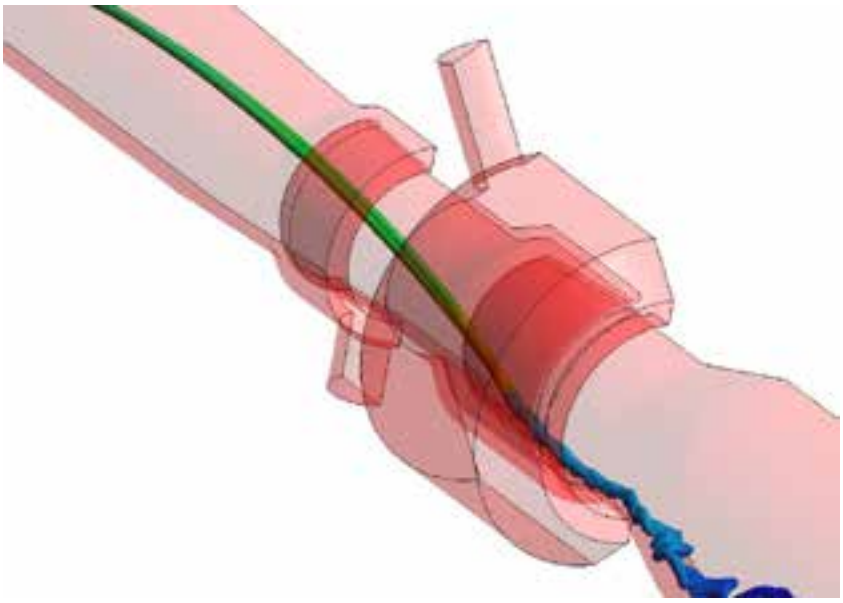

Fig. 2.68. Trajectory of solid particles (initial flow condition of motive liquid)

When the energy of motive liquid rising the number of solid particles which are able to be transported also increase. Figures below shows trajectory of solid particles with double flow rates of motive liquid than initial results.

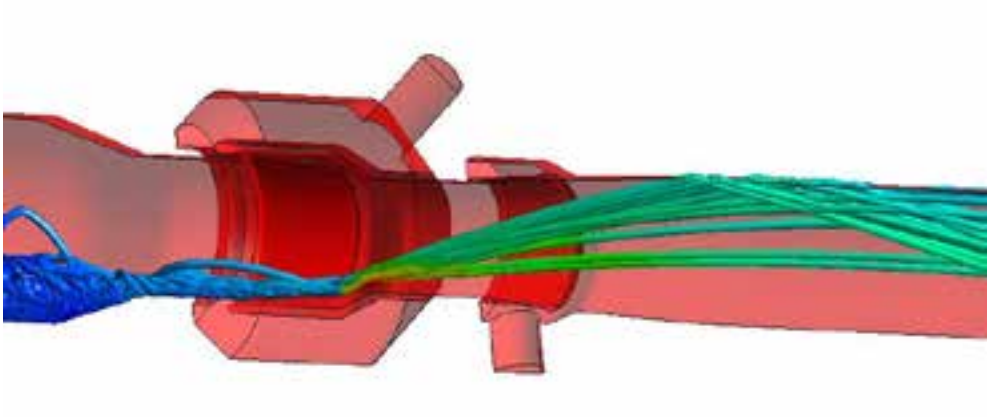

Fig. 2.69. Trajectory of solid particles (mass flow rate of motive liquid twice higher than initial)

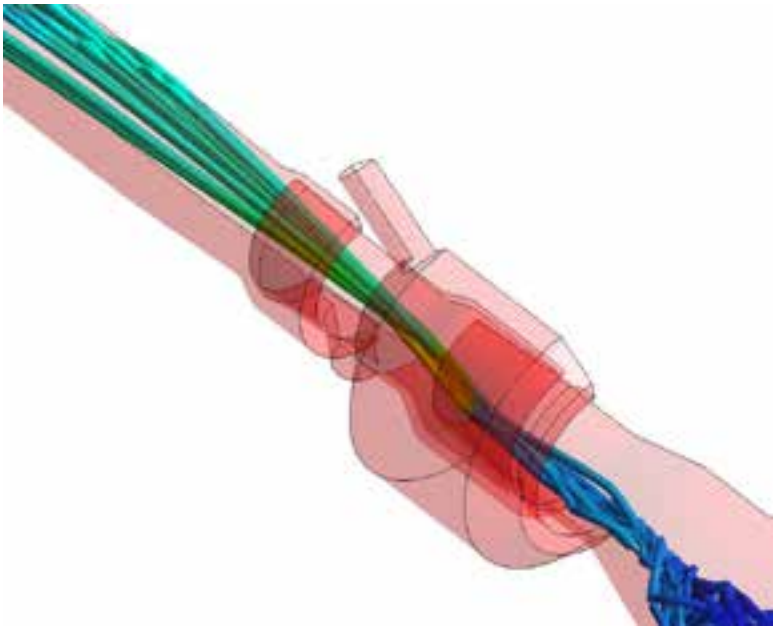

Fig. 2.70. Trajectory of solid particles (mass flow rate of motive liquid twice higher than initial)

Presented results may lead to conclusion that more energy of motive liquid is the amount of solid particles which is transported is bigger.

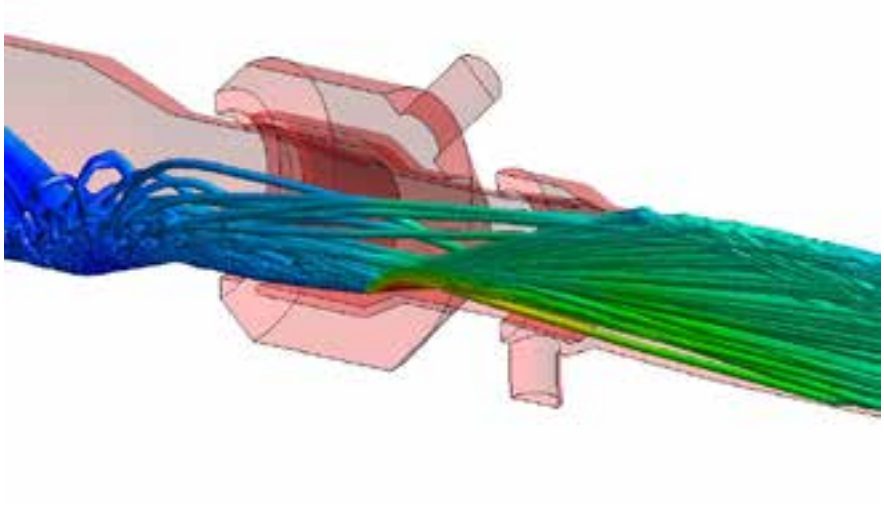

Fig. 2.71. Trajectory of solid particles (mass flow rate of motive liquid three times higher than initial)

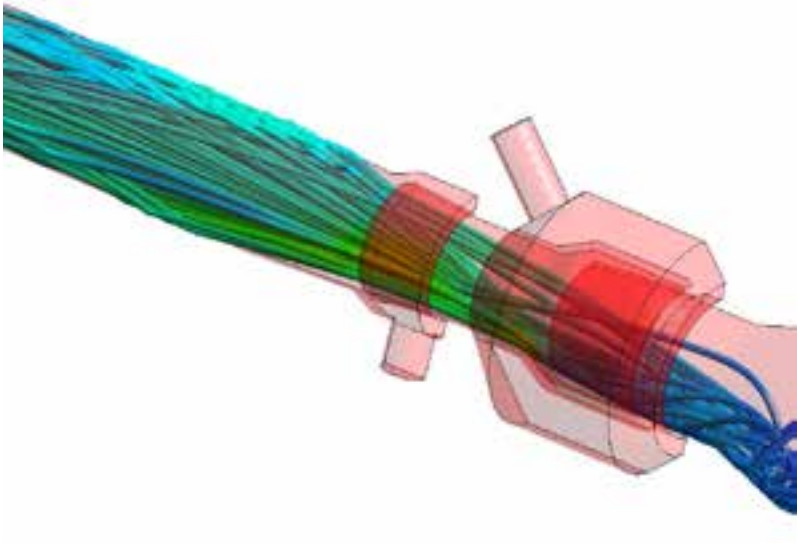

Fig. 2.72. Trajectory of solid particles (mass flow rate of motive liquid three times higher than initial)

Such simulations like presented in this chapter allows to define relation between the energy of motive liquid and amount of solid particles which

may be transported by jet pump. It has to be added that such relation is valid only for defined physical properties (material and dimensions). What is obvious when these properties change, the amount of solid particles also changes. Below figures shows trajectory of solid particles for similar conditions like presented before, however with particles diameter twice bigger. The particles material is still the same. In case of simulation, when motive liquid is twice more than initial the number of particles which transported drops. Similar situations is observed for the case when the motive liquid is three times more than initial.

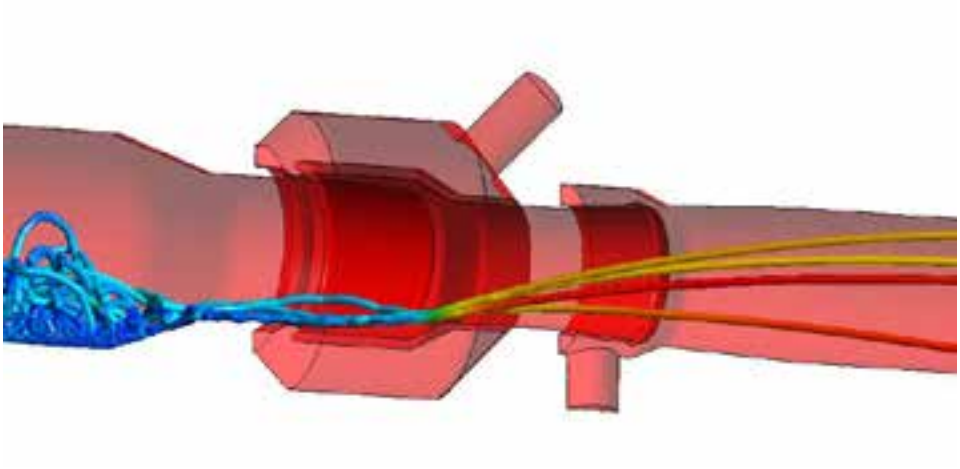

Fig. 2.73. Trajectory of solid particles (mass flow rate of motive liquid twice more than initial, solid particles diameter twice bigger)

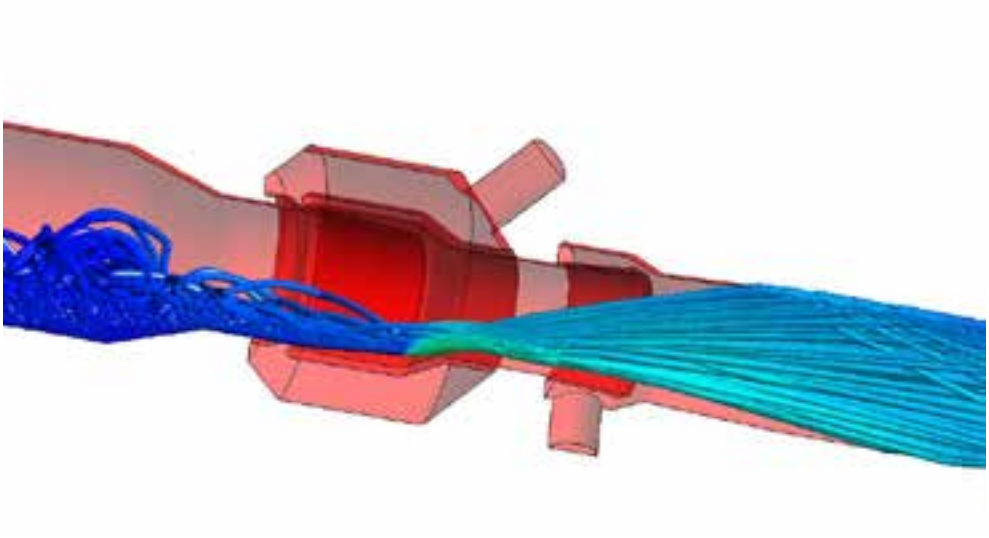

Fig. 2.74. Trajectory of solid particles (mass flow rate of motive liquid three times higher than initial, solid particles diameter twice bigger)

2.4.13 SIMULATION OF GAS-LIQUID JET PUMP

This chapter presents CFD simulation of gas-liquid jet pump. In this case the jet pump is a pump with central nozzle in which gas (air) is a motive fluid, while water is working fluid. Simulation model is presented in Fig. 2.75. CFD simulations includes two phase flow with assumptions that both fluids are homogenous and with constant properties and without thermal energy transfer from one fluid to another. To reduce the simulation model only a half was used, the rest was replaced by symmetry boundary conditions.

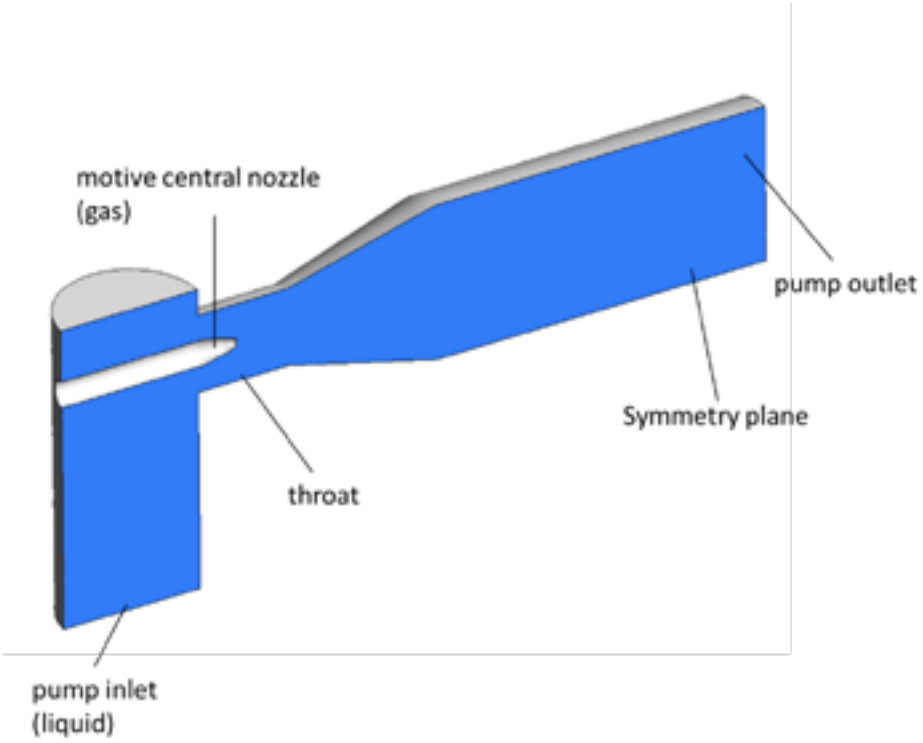

Fig. 2.75. Simulation model for Gas-Liquid Jet pump

Numerical simulations allowed to obtain information about air and liquid velocity which is presented on figures below as well as to investigate the of surface which forms motive fluid (air) inside the driven fluid (water).

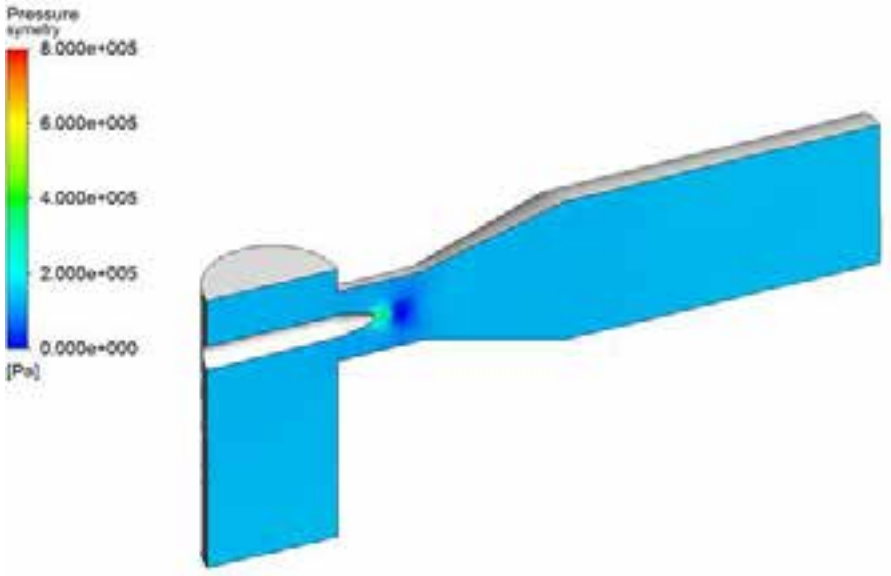

Fig. 2.76. Pressure distribution of Gas-Liquid Jet pump

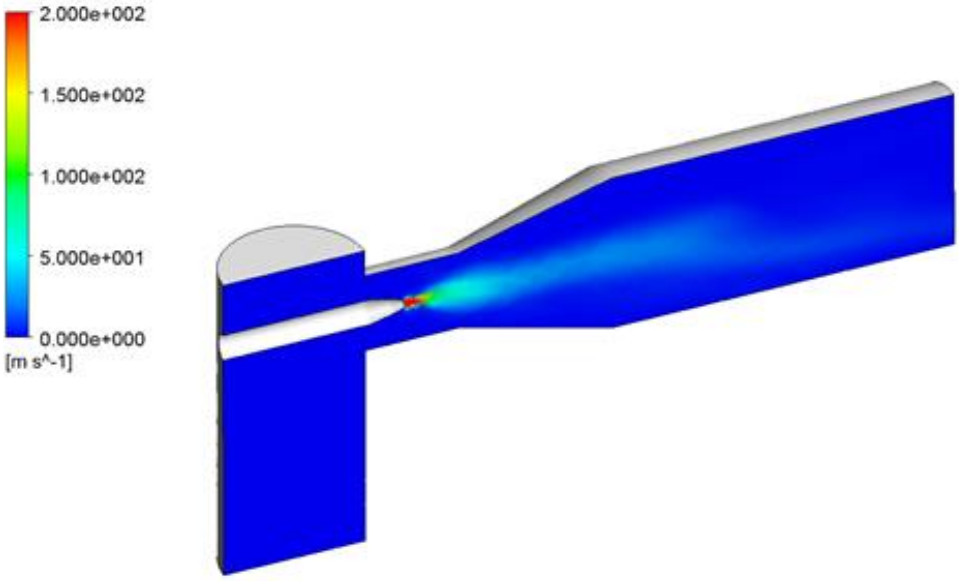

Fig. 2.77. Velocity distribution of Gas-Liquid Jet pump

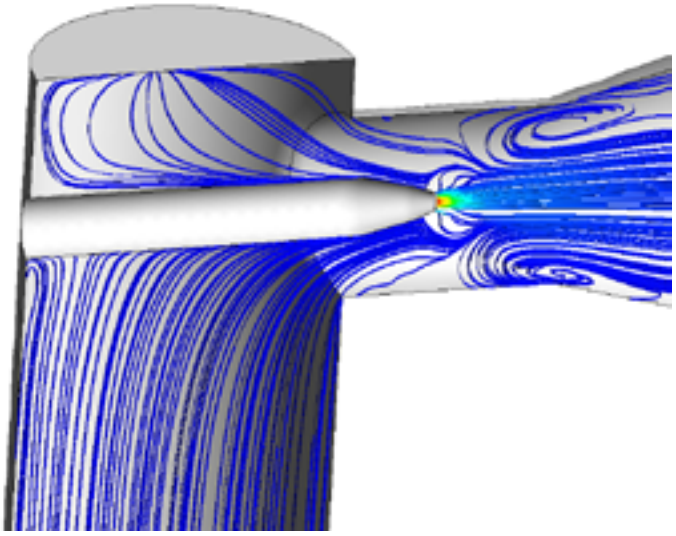

Fig. 2.78. Pathlines at the symmetry plane

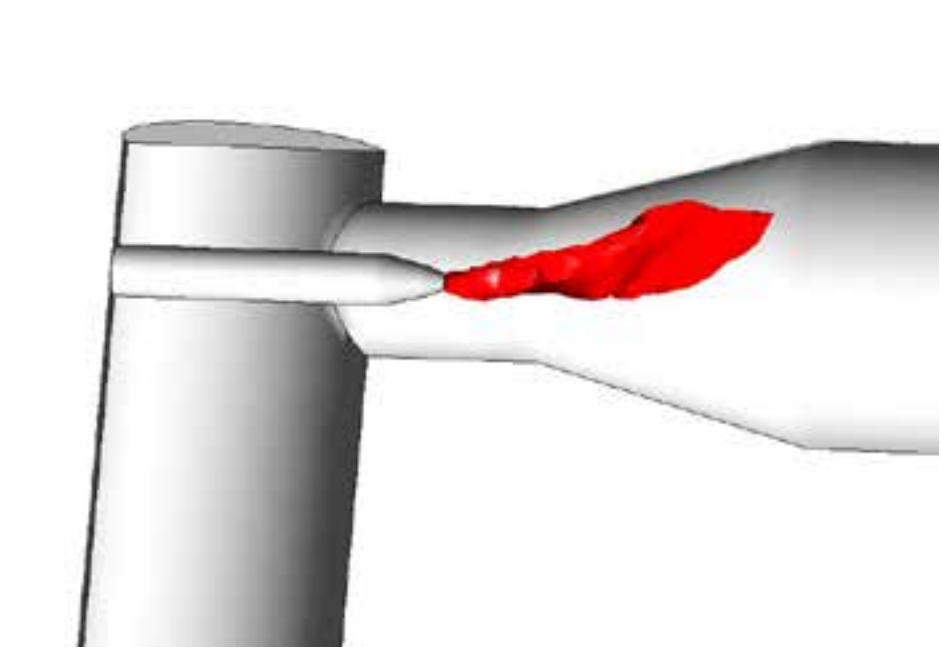

Fig. 2.79. Air fraction distribution

2.5 PROTOTYPING OF JET PUMPS

Results from CFD simulation may be verified on test stand presented in following sections, however, this requires to making pump prototype which may be prepared by using Rapid Prototyping Technology. One of Rapid Prototyping method is Fused Deposition Modeling technology in which presented model of Jet pump has been prepared. Presented in fig. 2.80 model is a two stages Liquid Jet Liquid pump with annular nozzles. It consist of three main components: A – with suction port (1), B – with circumferential drive nozzle of first stage and C – with second stage and pump outlet (4). All components are connected with bolted flanges. As was mentioned before measuring pressure or velocity distribution is difficult therefore prepared model was equipped with ports for installing pressure transducers (p1-p6). The cross section of pump model is presented in fig. 2.81. Prepared model with ABS is presented in fig. 2.82.

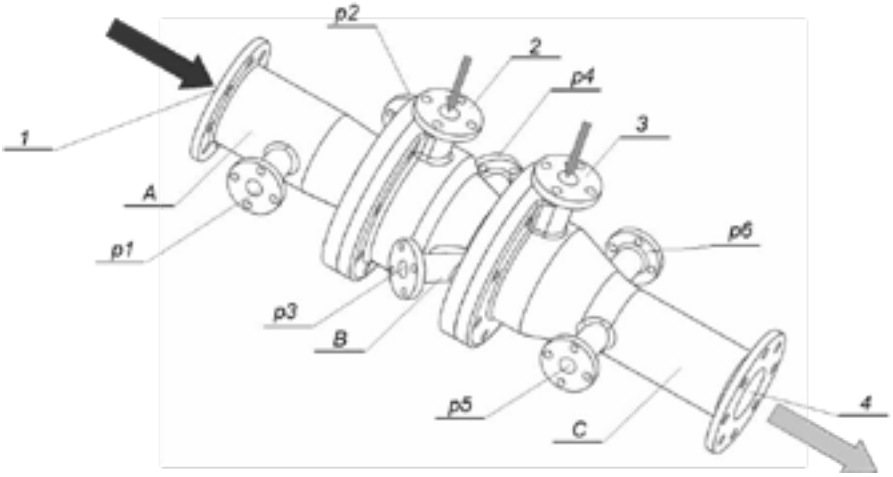

Fig. 2.80. A,B,C – pump components, 1 – pump suction port, 2 – inlet to 1st motive nozzle, 3 – inlet to 2nd motive nozzle, 4 – pump outlet, p1,p2,p3,p4,p5,p6 – ports for pressure transducers

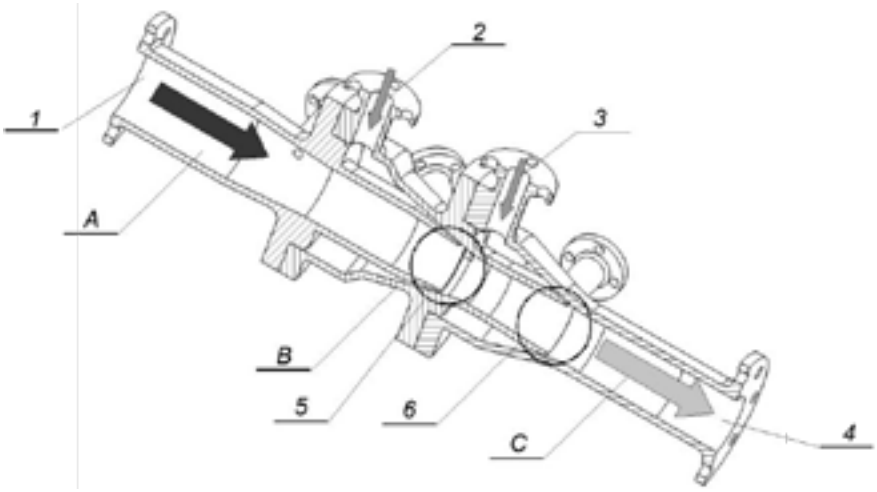

Fig. 2.81. Jet pump cross section: A,B,C – pump components, 1 – pump suction port, 2 – inlet to 1st motive nozzle, 3 – inlet to 2nd motive nozzle, 4 – pump outlet, p1,p2,p3,p4,p5,p6 – ports for pressure transducers, 5,6 – motive nozzles

Fig. 2.82.FDM prototype of jet pump

2.6 TESTING OF JET PUMPS

Within the cooperation between Bergen University College and Cracow University of Technology a test stand for testing jet pumps was built. A schematic diagram of this stand is presented on figure below. Due to difficulties in testing velocity and pressure distribution inside the jet pump an indirect test are provided which allows to measure volumetric flow rate as well as static pressure inside the pump in selected points. The presented test stand is ready for testing two stages LJL jet pumps.

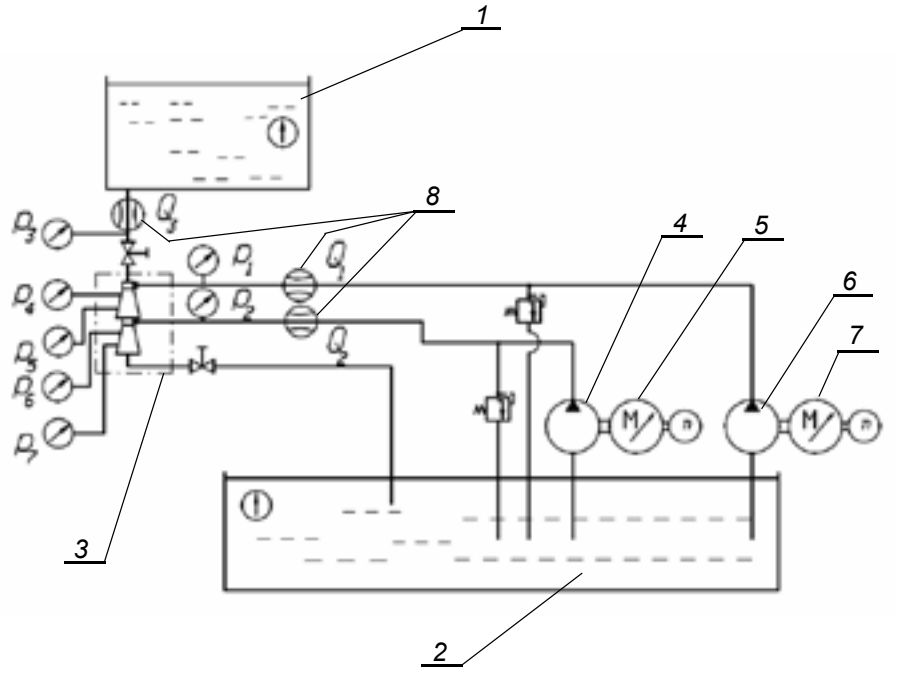

Fig. 2.83. Test stand diagram Test rig for testing jet pumps, 1,2 water tanks, 3 – tested pump, 4,6 – high pressure supply pumps, 5,7 – electric motors, 8-flow meters, Q1 – flow rate of first stage jet pump, Q2 – flow rate of second stage jet pump, Q3 – flow rate on jet pump outlet, p1, p2 – pressures on supply lines, respectively on first and second stage, p3 – pressure at pump outlet, p4, p5, p6, p7

Two supply unit (water pump 4,6 with electric motor 5, 7) with flow delivery up to 50 dm^3/min and maximal pressure head 8 bar are controlled by frequency inverter (one for each) what allows to change flow delivery at each stage separately. The jet pump which is tested might be equipped with pressure transducers (p_1-p_7), with analogue output. At motive liquid lines and at pump outlet was installed electromagnetic flow meters (8) MIK-5NA65AF300 and MIK-5NA35AF300 with frequency counters SPI-94-1433300. Data acquisition system was A/C and C/A PCI DAQ 12bit card Advantech PCI1711-A2 and prepared computer software. By controlling revolutions of electric motors with the use of frequency inverter was possible to change flow rate at motive nozzles. The tested pump has to provide the installation of pressure transducers in investigated cross sections as it was presented in previous section. Figure 2.84 presents photo of the test stand. At presented test stand only one tank was used due to the fact the both, motive and secondary liquids are water. Water in the stand circulates along the arrows marked on the photo. Presented test stand allows to investigate pumps design parameters on its operational features as well as validate CFD model.

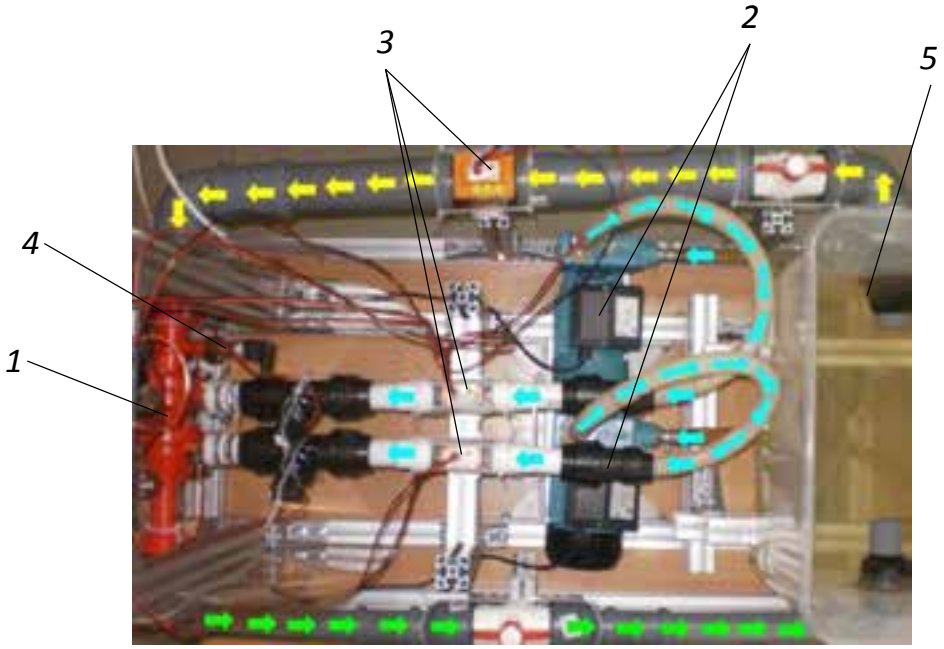

Fig. 2.84. Test rig for testing jet pumps, 1 – tested jet pump, 2 – supply pumps, 3 – flow meters, 4 – pressure transducers, 5 – tank

Figures 2.85 and 2.86 shows selected test results, which were conducted for steady state conditions. Experimental tests were conducted for various working conditions. Fig. 2.85 shows head pressure when only one stage operate, while the next figure shows results for the case when both motive stage operates. These results confirmed what was presented in previous CFD simulations of similar, but much bigger jet pumps.

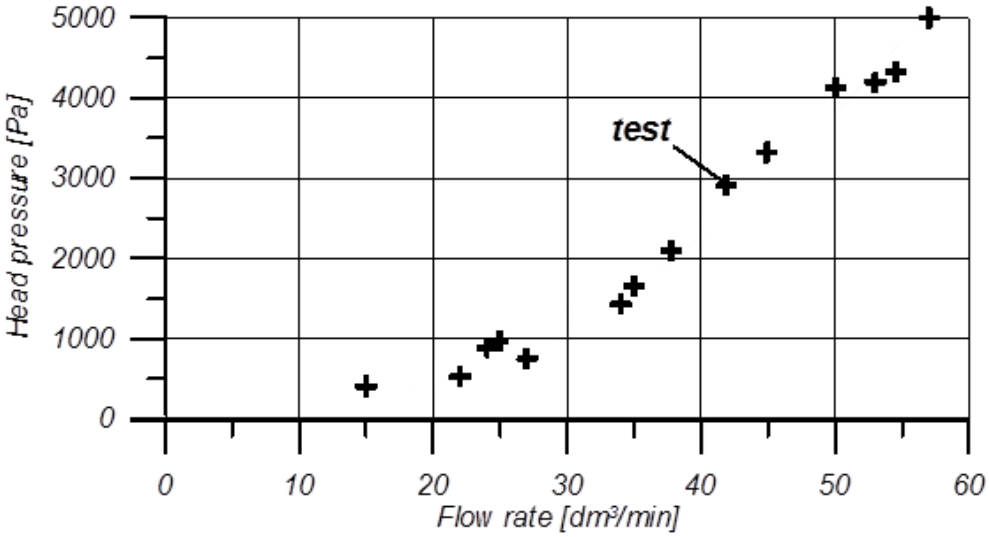

Fig. 2.85. Head pressure for pump prototype when one stage operate

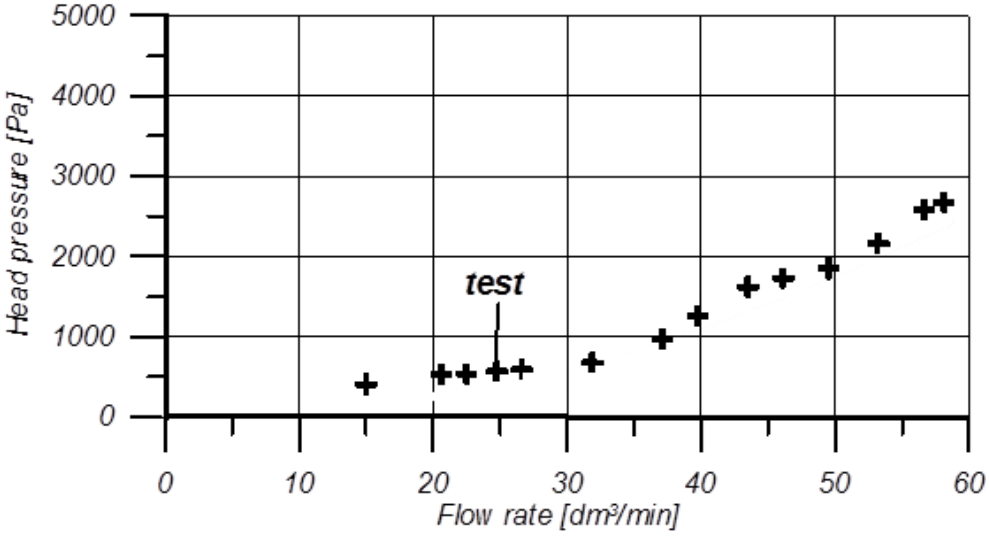

Fig. 2.86. Head pressure for pump prototype when both stages operate

2.7 REFERENCES

[1] Karassik I. J., Messina J.P., Cooper P., Heald Ch.C., Pump Handbook, Third Edition, McGraw Hill, 2001.

[2] Douglas M. Gluntz, Steam assisted Jet pump, Patent no 4,487,043 B2, Pub. date 11.06.1989

[3] Bonnington, S. T., and King, A. L. Jet Pumps and Ejectors: A State of the Art Review and Bibliography, Published by BHRA Fluid Engineering, Cranfield, Bedfordshire MK43 OAJ, United Kingdom, 1976.

[4] Ferziger J. H., Peric M., Computational Methods for Fluid Dynamics, 3rd Edition, Springer Verlag, 2002.

[5] Wilcox D. C., Turbulence modeling for CFD (Second Edition), DCN Industries, 2000.

[6] Hirsch, Ch., Numerical Computation of Internal and External Flows (Second Edition), Elsevier Ltd., 2007.

[7] J. Fan, J. Eves, H.M. Thompson, V.V. Toropov, N. Kapur, D. Copley, A. Mincher, Computational fluid dynamic analysis and design optimization of jet pumps,Original Research Article Computers & Fluids, Volume 46, Issue 1, July 2011, Pages 212-217

[8] Mulley R., Flow of Industrial Fluids - Theory and Equations, ISA/CRC Press, 2004.

[9] Principles of Computational Fluid Dynamics, Springer-Verlag Berlin Heidelberg New York, 2000

[10] Computational Fluid Dynamics: The Basics with Applications McGraw Hill 1995.

[11] Thompson J. F., Warsi Z. U. A., Mastin C. W., Numerical Grid Generation, Foundations and Applications, North Holland, 1985

[12] Lisowski E., Domagała M., Modelling of hydrodynamic interaction forces in direct relief valve by the use of CFD method, The 18th

International Conference on Hydraulics and Pneumatics, Prague, Czech Republic, 2003

[13] Lisowski E., Domagała M., CFD methods in experimental studies on flow phenomena in hydraulic valves, Fluid Power a Technology for the Future 5th Bergen International Workshop on Advances Technology, Bergen, Norway, 2004

[14] Lisowski E., Domagała M., Determination of flow forces in hydraulic valves, 3rd FPNI-PHD Symposium on Fluid Power, Barcelona – Terrassa, Spain, June 2004

[15] Momeni H.,CFD analysis of water jet pump, Technical Transactions, Krakow 2010.

[16] Momeni H., Lisowski E., CFD modelling and rapid prototyping of Liquid Jet Liquid pump, Technical Transactions, Krakow 2011.

[17] Trela M, Kwidzyński R., Burtymowicz D., Karwacki, Exergy analysis of two phase steam—water injector, Applied Thermal Engineering, 2009.

[18] Momeni H., Praca Doktorska, Politechnika Krakowska, Kraków 2011

3 SEQUENCE EXPERIMENT USED TO FLOW STRUCTURE STUDY AND PERFORMANCE INVESTIGATIONS OF CROSS FLOW FAN

3.1 THE MAIN IDEA OF A SEQUENT EXPERIMENT METHOD (SEM)

The dynamic development of electronic technology as well as ventilating and air conditioning systems caused that the cross flow fans known since nineteenth century have found wide application at various industrial branches. The structure of flow inside of the CFF is very complex and differs from radial or centrifugal fans. The lack of accurate mathematical model describing the real flow conditions and analytical methods for velocity and pressure fields estimation caused to use some rather expensive experimental methods based on the functional model tests. An identification and better understanding of some flow phenomena lead from one side to reduction or even elimination of some negative effects in constructional adaptation to concrete application but from the other it is not enough to form a universal designing theory.

In order to improve the CFF performances the sequent experiment method has been proposed [1]. It gives possibility of the complex investigation beginning from identification of flow structure with use of three different experimental methods (part one) and ending on calculation of performance curves (part two) verified by numerical computations. The first element of sequent experiment method (shown in fig. 3.1) is a water visualization of flow fields inside of model designed basing on the optimal shape parameters of components of CFF presented in literature. The analysis of flow pattern shows that the flow field changes in time by formation of so-called “dead” zones , reversing flows and vortices with the main eccentric

vortex. In the case of such sensitive flow machine as CFF where even a small changes of geometric parameters have the main influence on its performance a method of flow visualization, seems to be very helpful in design process.

The direct measurements of velocity and pressure fields in the same CFF model carried out in the air with use of three hole cylindrical probes are the second element of sequent experiment method. The probes are located in flow field at the points exactly determined by the holes made in the transparent plastic frontal wall of test chamber, so it gives possibility to detect very precisely velocity vectors.

Because the measurements of velocity fields are carried out in two different media: air and water, the operating conditions have to be determined from fulfilling the dynamic similarity assuming equality of Reynolds number. The existence of the fluid flow analogy [1] between flow in two different media shows that the method of water flow visualization could be a very useful tool for the CFF design procedure, giving possibility of velocity field estimation in such regions of CFF interior where the direct measurements couldn't be made.

Qualitative analysis resulted from water visualization and quantitative obtained from the measurements in air analysis as well as and the back couplings between data obtained from both methods are very useful method of designing procedure. It is not necessary on this step to construct rather expensive functional CFF models and made investigations using equipped channel or chamber test rig. The experimental results were verified by numerical simulations and some flow phenomena observed earlier could be confirmed using finite element and finite volume methods.

The second part of sequent experiment method is devoted to the CFF performance curves obtained as result of experimental studies of functional

models made from different materials [2] as well as some different constructional parameters, fig.3.2.

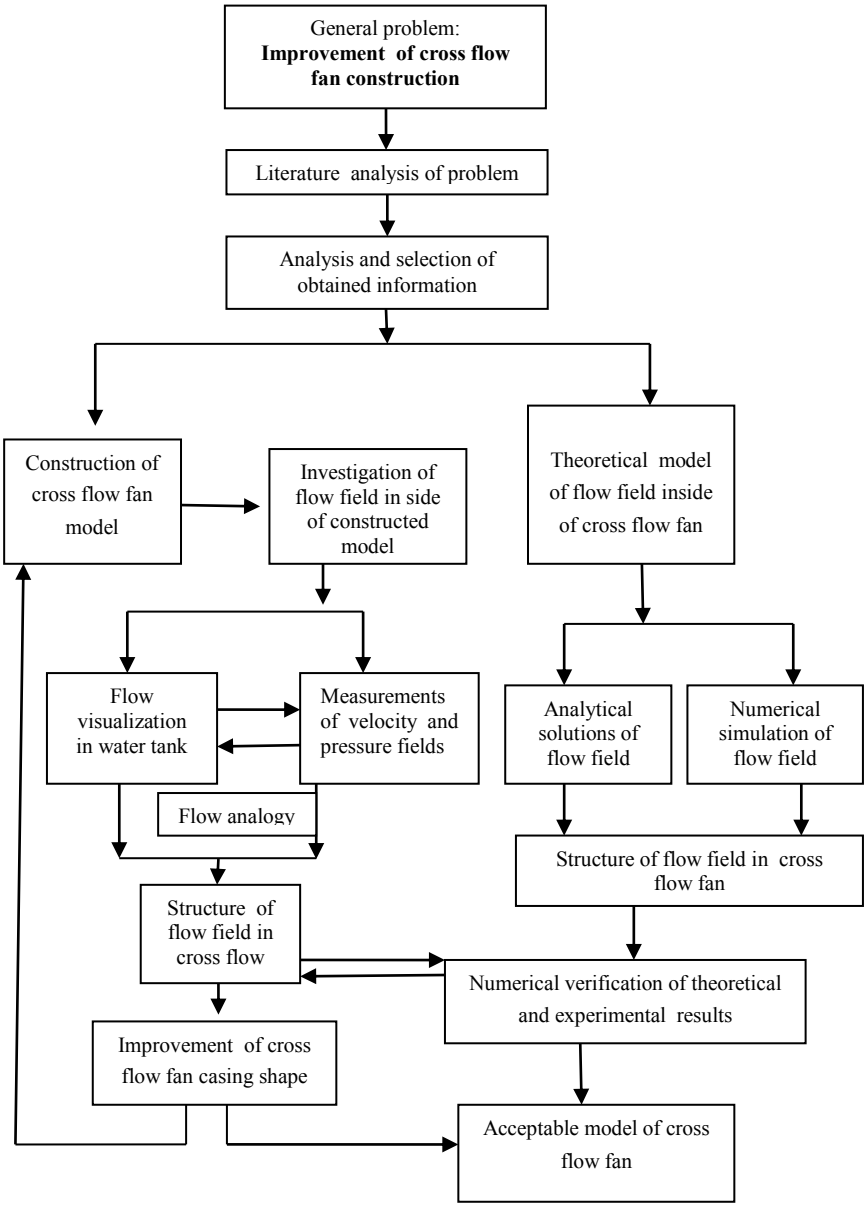

Fig. 3.1. Process of a flow structure determination (part I of SEM)

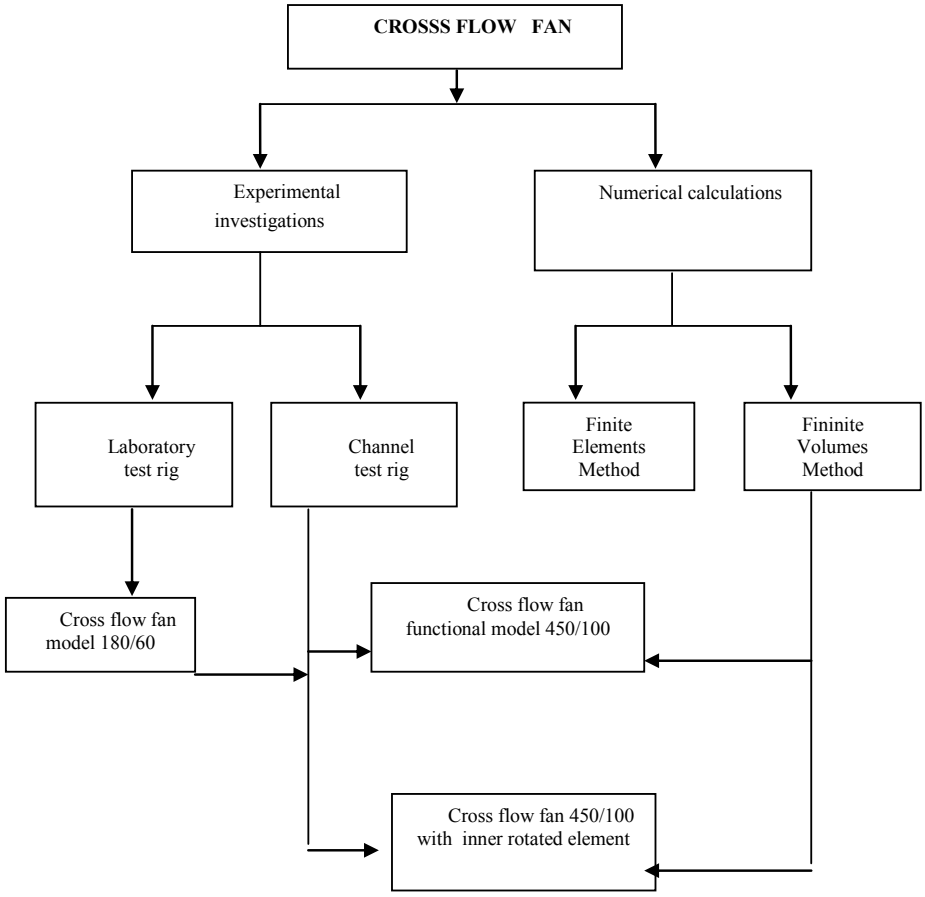

Fig. 3.2. Process of CFF performance curves determination (part II of SEM)

3.2 FLOW STRUCTURE INSIDE OF A CROSS FLOW FAN

The CFF is a unique type of turbo-machine which operates fundamentally in a different way from axial or centrifugal fans. It consists of a cylindrical impeller with forward curved blades, closed at the ends and placed in a casing extending the full length of impeller (fig. 3.3).

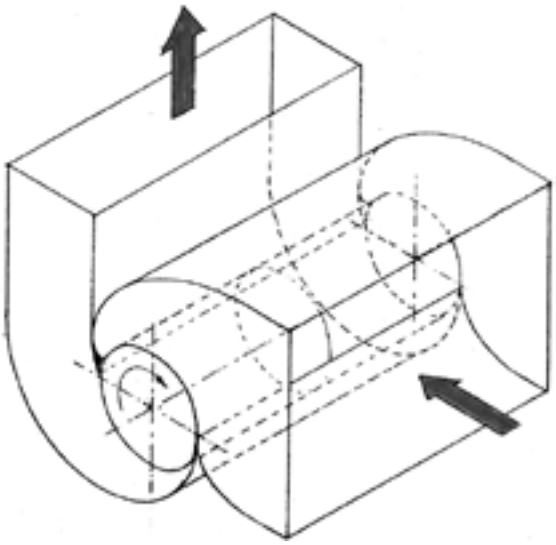

Fig. 3.3. Cross flow fan

The fluid stream flows perpendicularly to the impeller axis crossing twice the blade ring and generates two steps of compression - so CFF is treated as two-steps flow machine. Because of the forward curved blades the impeller has a large absolute flow velocity and equal pressure difference may be achieved at the same flow rate but at the mainly reduced rotational speed.

Usually the flow structure inside of CFF is divided into three different regions: fan inlet, impeller with blading and fan outlet. The most interesting region but very difficult for a mathematical description is an area inside of an impeller with blading, fig.3.4. The velocity distribution changes around an impeller periphery and two main characteristic zones are observed: throughflow perpendicular to an axis of rotation and an eccentric vortex located near to the blading.

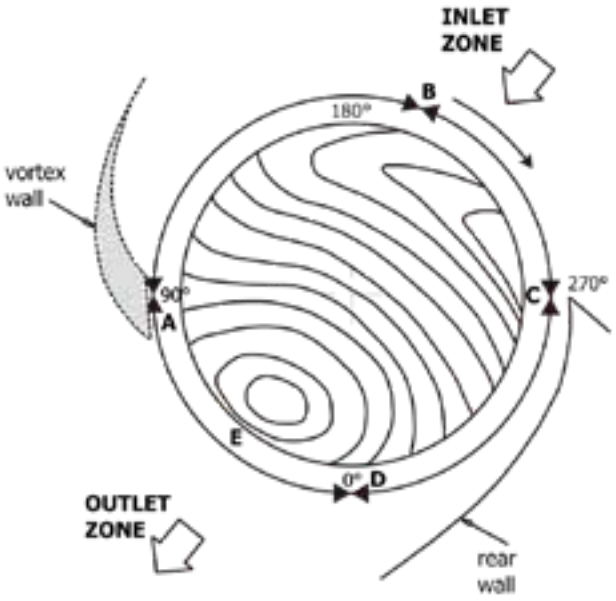

impeller inflow arc		impeller ouflow arc	
AB 0°-190°	main flow - throughflow	CD 270° – 0°	main flow- throughflow
BC 190° – 270°	recirculation area	E ~ 40°	vortex centre localization

Fig. 3.4. Flow pattern in CFF impeller

The magnitude and localization of an eccentric vortex depend on a fan geometry as well as on the operating conditions.

3.3 SELECTED RESULTS OF WATER VISUALIZATION

Flow visualization, carried out in water tank, with the tracers in form of 2 mm diameter polystyrene spheres allows for a quantitative estimation of some flow phenomena effects on flow structure inside the cross flow fan.

The local velocity is estimated from the camera between-lens shutter speed. Recording the photographic streaks is possible by choosing a suitable shutter speed. The streak length representing the displacement of the

polystyrene bead is equal to a local velocity vector and its position corresponds to the direction of motion [3].

Rotation of an impeller causes the movement of water with tracers hanging in a whole volume in the direction of rotation. At constant rotational speed an eccentric vortex moves at two directions: radial and circumferential and its center changes its localization (fig. 3.5).

3.3.1 PROCESS OF FLOW STRUCTURE FORMINING

The problem of phase flow structure sequence: throughflow or eccentric vortex can be solved analyzing the pictures with several phases of flow made at following time. When the impeller starts to rotate a stream containing the fluid drifting from blading into the interior of impeller perpendicularly to axis is formed and flows out at opposite part of impeller.

So at first a throughflow is observed. As result of throughflow an eccentric vortex arises as the second form of flow structure and an average time of vortex forming depends on rotational speed of impeller (Reynolds number). The vortex changes its localization at radial and circumferential directions. Stabilization of a moving vortex can be obtained by introducing one or two flat plates into flow field near to blade ring (fig.3.6).

The observed effect of a gap width (clearance) between a plate and a blading indicates the great importance of this constructional parameter. In a case of wider gap it is impossible to stop the disordered moving vortex and only the reduction of gap width can cause the vortex “bounding”.

Analyzing the pictures of flow pattern obtained during water visualization one can notice that the vortex center located within the blading or very close to the inner periphery of the impeller depends on the operating point. An assumption of vortex center localization at the radius lower than

inner radius of impeller (often used by CFF investigators) is not valid in every cases and depends on flow conditions as well as on a casing shape.

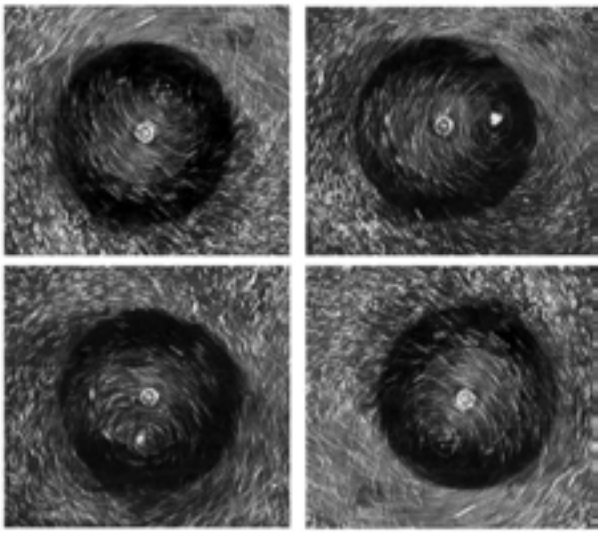

Fig. 3.5. Localization of eccentric main vortex at constant rotational speed

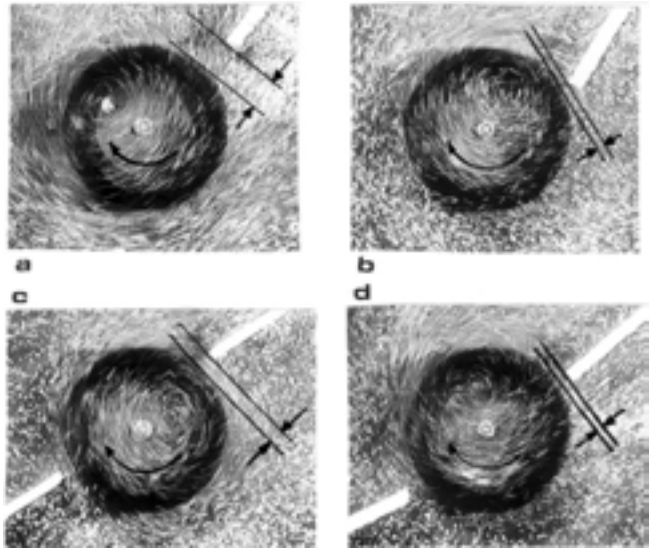

Fig. 3.6. Stabilization of vortex

3.3.2 INFLUENCE OF THROTTLING ON FLOW STRUCTURE

Water flow visualization has confirmed a significant influence of rear wall shape as well as of the flow conditions (throttling) on localization of eccentric vortex center. The rear wall profiled almost parallel along great arc of the impeller and relatively close to it effects on a vortex center locating it near an internal edge of blades during free blowing (great volumetric flow rate). Several throttling influences on the main vortex movement in direction of the impeller center as well as on the reduction of rotational speed of fluid. Full throttling (zero flow) causes the stabilization of vortex with center localized in a place resulting from the vortex wall and the rear wall shapes but fluid rotates in a way characteristic for a forced vortex with a speed equal to rotational speed of impeller [4].

An enlarging of a space at outlet of cross flow fan by change of rear wall shape profiled as a part of an integral spiral positions the main vortex freely near blading. During throttling the vortex center has tendency to move along the runner periphery toward the rear wall (measured by angle φ) and the increase of flow recirculation without a visible decries in speed of rotation (as it was in the case of rear wall profiled partially parallel to outer ring of impeller) is observed, fig. 3.7.

It's worth to notice that throttling of flow has an important influence on a pressure increase till a moment when it reaches the maximal value at relatively small volumetric flow rate. Decrease of the volumetric flow rate affected on flow continuity and instability of fan operation (pumping), loss and recovery of static pressure at random time ranges (pulsation).

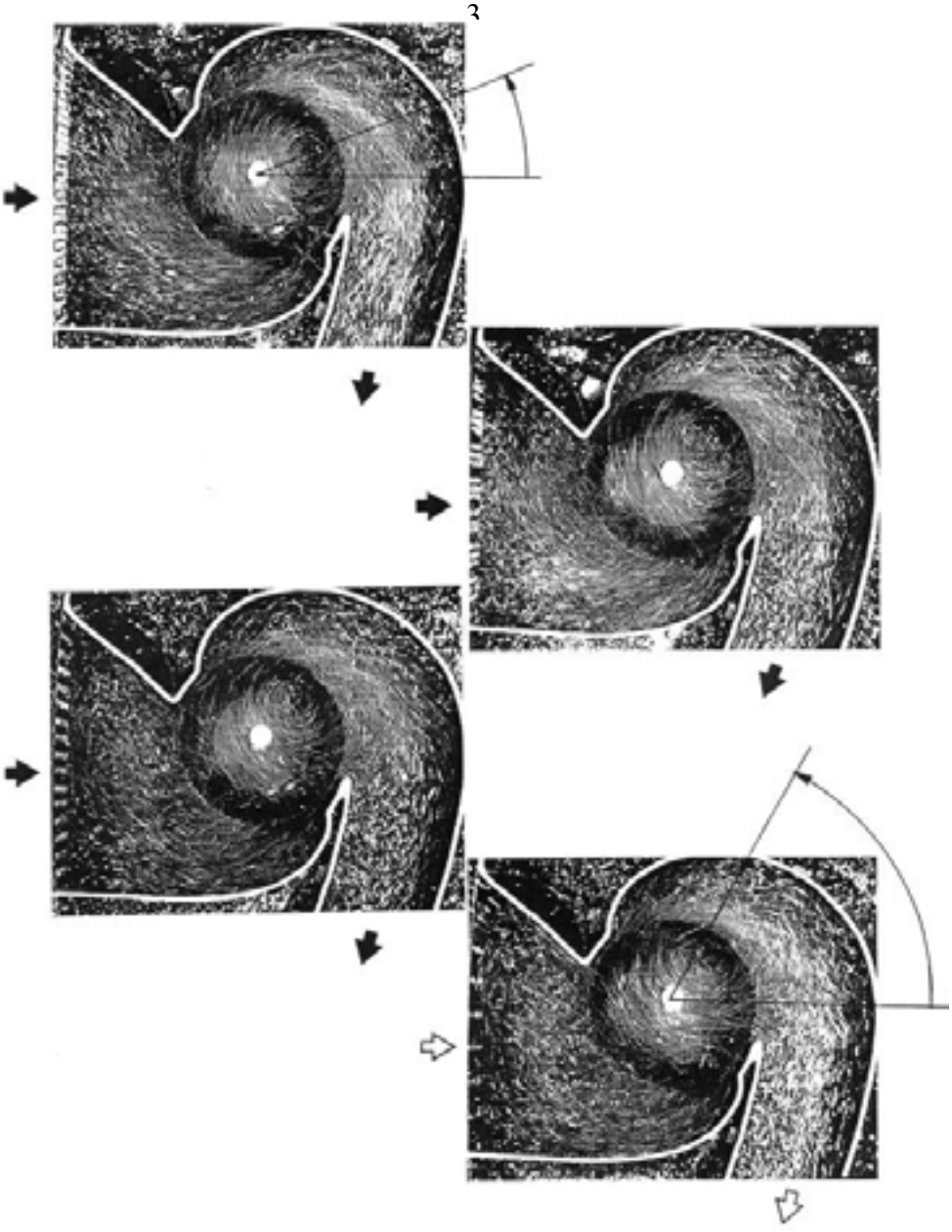

Fig. 3.7. The changes of vortex center localization at different throttle conditions

3.3.3 FLOW STRUCTURE IN CFF WITH INNER VANE

Visual experiments carried out with use of different profiled elements , located inside of the CFF have shown their important influence on the flow structure. Especially, the investigations of CFF with an internal vane mounted axially inside of the impeller gives possibility to observe flow phenomena depending as well on the shape (different shapes shown in fig. 3.8) as on its angular position determined by angle α.

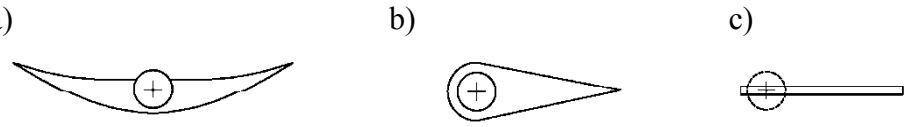

Fig. 3.8. Different shapes of internal vane: (a) moon-like, (b) drop-like, (c) flat plate

For example in the case of use “moonlike” vane mounted inside of the CFF having the symmetric shapes of inflow and outflow parts of spiral casing, the water stream changes the flow direction about 180° without changing the value and direction of the impeller rotation, fig. 3.9. It means, that the phenomena of reverse flow created by special shape of casing and internal vane can find application in ventilating systems where CFF is used as flow machine operating in two directions. It gives possibility for very quick change of air in a room without variation of the direction of impeller rotation or using another type of fan.

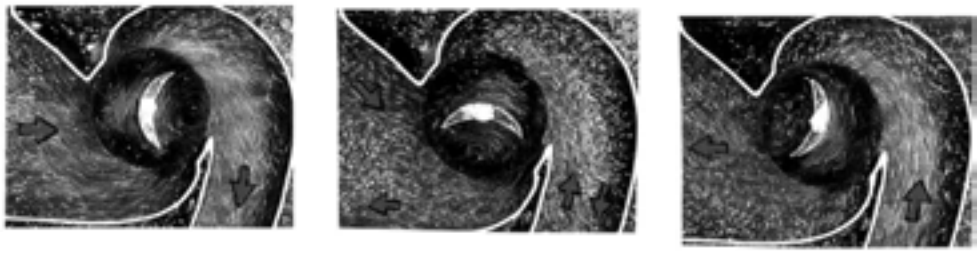

Fig. 3.9. Effect of reverse flow in cross flow fan with symmetric inlet and outlet part of spiral casing generated by moon-like internal vane

The control of volumetric flow rate can be realized applying an internal vane what is observed analyzing the flow structures obtained for the different angular positions of "drop-like" element. Selected from many others two characteristic angular positions of internal vane show the flow phenomena arising in three regions of CFF: inlet, outlet and interior of impeller, fig. 3.10. The arrows show the direction of the stream flow.

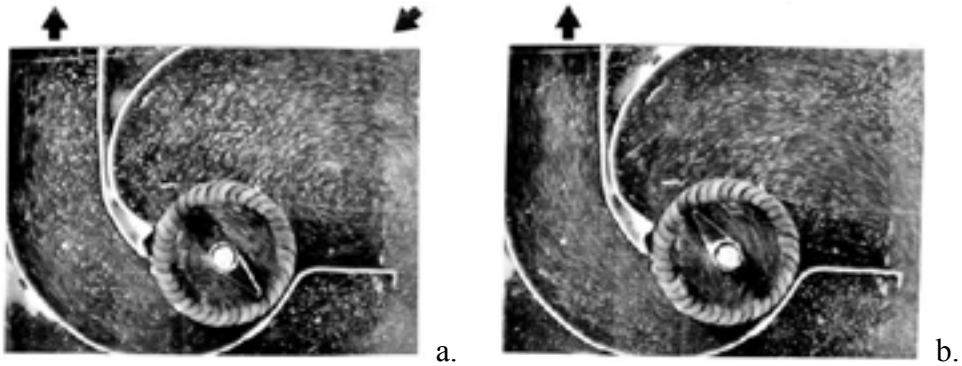

Fig. 3.10. Flow structure inside cross flow fan obtained for different angular position of "drop-like" vane

The throughflow divides into two streams (fig. 3.10 a) and one of them (on left side of vane) returns to inflow region creating there circular vortex occupying almost half of the suction arc. The second stream slipping along

the right side of vane flows in the direction of cross flow fan outlet creating an unordered flow with rather low volumetric flow rate. The angular position of vane shown in fig. 3.10 b ordering the inflow on blading in suction region, creates two streams on both sides of vane forming the throughflow, which takes full advantage of length of discharge arc flowing into the outlet region of cross flow fan. In this region the flow velocity has the highest values in comparison to other angular vane positions (detected by the length of flow lines of tracers) synonymous with the greatest volumetric flow rate [3].

3.4 QUANTITATIVE ANALYSIS OF FLOW PHENOMENA

The changes of flow pattern in the region of impeller interior, observed previously during water flow visualization have found a quantitative confirmation in the velocity and pressure measurements carried out in the air with use of three whole probes. Volumetric flow rate at channel has been estimated using Borda's mouthpiece [5].

3.4.1 ANALYSIS OF VELOCITY DISTRIBUTION

The absolute velocity distribution defined :

$$\vec{c}^{*} = \frac{\vec{c}}{u_2}\,, \tag{3.1}$$

where $\vec{c} = \sqrt{\frac{2p_d}{\rho}}$, $u_2 = \pi \cdot n \cdot D_2$,

measured for a free flow ($\varphi = 0.9$) and for zero flow ($\varphi = 0$) is presented in fig. 3.11.

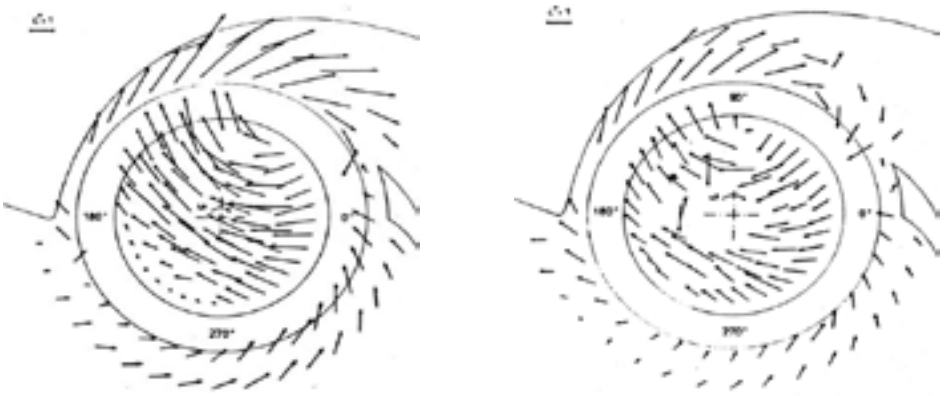

a. b.

Fig. 3.11. Absolute velocity distribution for different flow conditions:
(a) free flow; (b) zero flow, n = 16.6 s^{-1}

Comparison of the velocity distributions achieved for the flow without throttling (free flow) and with strong throttling (zero flow) leads to the following conclusions:

- in the case of zero flow the vortex center moves towards the rear wall;
- at throttle condition a significant decrease of absolute velocity vector values at the outlet duct of impeller is observed;
- at both studied cases the maximal values of absolute velocity vector occur just outside of the impeller exit (outlet arc) approximately at the boundary between the throughflow and the vortex.

3.4.2 ANALYSIS OF PRESSURE DISTRIBUTION

The reduction in total pressure values measured at the outlet region of impeller in condition of several throttle is significant. The explanation of

this phenomenon is rather simple considering the comparison of pressure and velocity distributions at the same regions of flow field. Especially it is seen at zone determined by angle $\theta \approx 70° - 160°$, where the values of absolute velocity are lower under throttling than at free flow. The magnitude of velocity has an important influence on the values of dynamic pressure being one of two components of total pressure.

Analyzing the graph of static pressure distribution around the impeller blading (fig.3.12) it is worth to notice that there exist:

- the great gradient of total pressure in the region of vortex (minimum value at vortex center),
- the lower gradient through the inlet part of blading (inlet arc),
- almost constant pressure in the rest of region inside of the impeller.

Moreover, curves $p_s = f(\theta)$ showing the changes of static pressure along the circumferential direction at the dimensionless radius equal to 0.65 for two different flow conditions: free flow and strong throttle (zero flow) show the same tendency in both cases [3].

The displacement of vortex center towards the rear wall observed earlier during flow visualization and analysis of the absolute velocity vector distributions obtained at different flow conditions find the quantitative confirmation now.

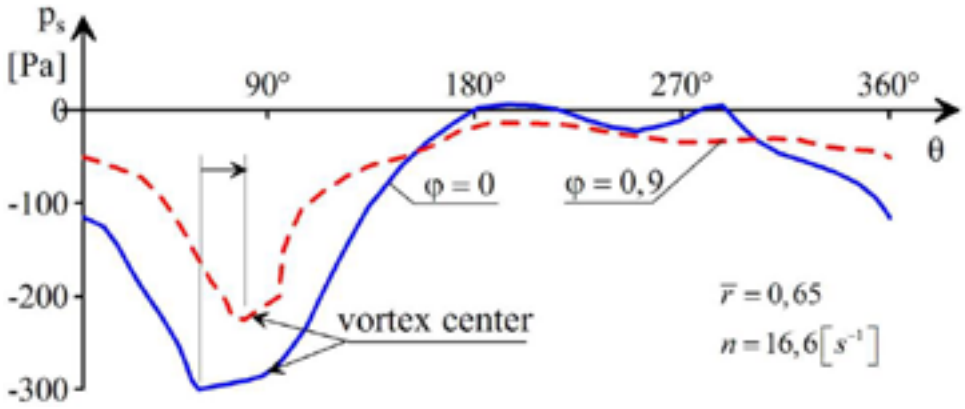

Fig. 3.12. Static pressure distribution at two different flow conditions

The vortex center placed at angle θ = 70° during free flow changes its angle localization at zero flow and moves to the position determined by angle θ = 90°.

The flow analogy presented in literature give possibility for quantitative identification of some phenomena visible during water visualization using measurements carried out in the air. Seems to be useful a very simple formula [6] :

$$c_r = 10 \cdot c_m \tag{3.2}$$

(where: c_r , c_m are the velocities in the air and in water respectively), for a velocity vector calculation in the regions where the direct measurements are impossible or difficult to carry out for example inside of the rotating impeller blade passages.

3.5 NUMERICAL VERIFICATION OF THE EXPERIMENTAL RESULTS

Program Flo++ based on Finite Volume Method (FVM) is used to numerical calculations of the flow in CFF having the same geometry as one

experimentally tested earlier [7]. The computational area is divided into eighteen casing blocks and one impeller block fig.3.13a. The geometry of tested CFF is drawn in Microstation/J with accuracy to million part of main unit. The grid is built from tetrahedral volume elements (cells), with different density concentration fig.3.13b. At the outlet area of fan the blocks with the greatest number of cells are located because of the necessity of high accurate readability of calculated values of pressure and velocity.

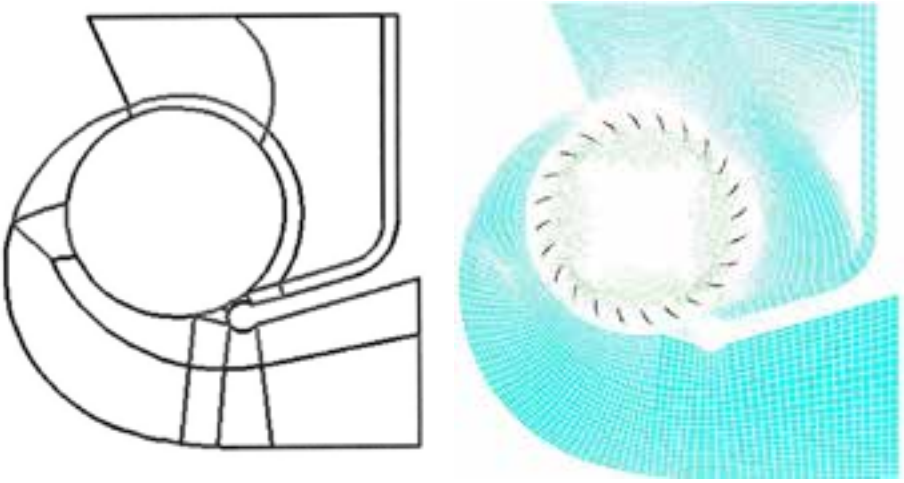

a. b.

Fig. 3.13. Grid for the complex geometry

The unsteady, two-dimensional flow with small velocities (Ma< 0.3) and incompressible flow (small changes of pressure gradients caused little changes of density gradients [8]) are taken into account to numerical simulation. The continuity and momentum equations have the following forms, respectively:

$$\text{div } v = \tag{3.3}$$

$$\frac{\partial u_i}{\partial t} + div(u_i v) = div(\nu \, gradu_i) - \frac{1}{\rho} div(pi_i) + b_i \tag{3.4}$$

The assumption of following constant values: density ρ =1.207 kg m^{-3}, dynamic viscosity η= $1.787 \cdot 10^{-5}$ Nsm^{-2}, atmospheric pressure p_b=101325 Pa and temperature T = 293.15 K, as well as the standard Reynolds k-ε high turbulence model implemented in Flo++ program are employed. Moreover, at the inlet and the outlet regions of cross flow fan the static pressure is assumed as constant and equal to the atmospheric pressure. It means that the cross flow fan is considered without suction and discharge zones [9].

The sliding mesh technique for moving impeller and unmoving casing interaction relying upon the interpolation of the calculated values at contact cells in following time step is used [10]. Because after full five revolutions of the impeller the flow pattern did not change (constant pressure and velocity fields) so the flow as quasi-steady could be assumed in the later considerations. The procedure of numerical calculation with use of two different methods: finite elements and finite volumes is described with details in [10], [11].

Some selected results of flow structure calculated numerically with use of finite volumes method are presented below. Two graphs of vector velocity obtained for different rotational speeds of the impeller: n = 12.5 s^{-1}, n = 41.67 s^{-1} presented in fig. 3.14, show the influence of rotational speed or Reynolds number [$Re = (\rho \, u_2 \, c)/\eta$, where c – is a blade chord] on the flow structure.

Character of flow is similar in both considered cases but differences in velocity fields are observed. It is worth to notice that similarity is in the main eccentric vortex centre location almost at the same place of blading

and having almost the same magnitude independently of the different rotational speed.

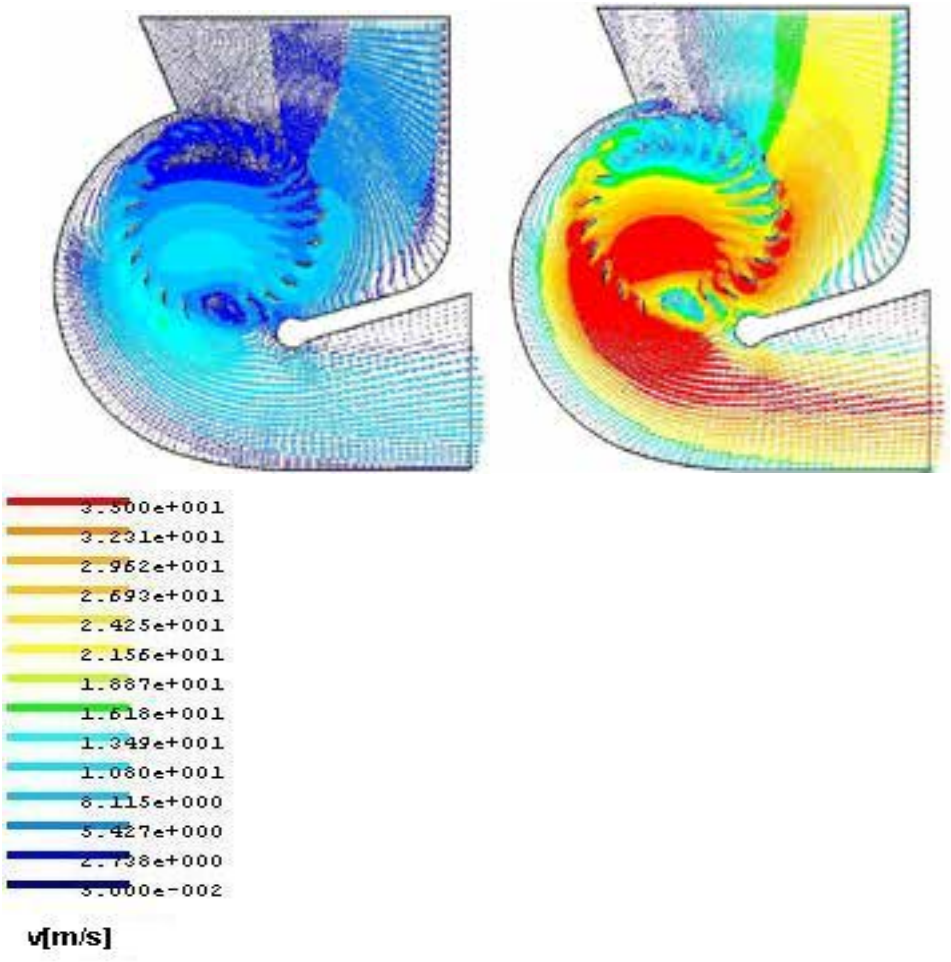

(a) (b)

Dark blue colour means the lowest values and red the highest values of velocity

Fig. 3.14.Vector velocity field for n = 12.5 s^{-1} (a) and n = 41.67 s^{-1} (b)

The analysis of vector velocity fields shows that the velocity distribution at outlet cross section of CFF is not uniform in both cases. The higher values of volume flow rate existed at the higher rotational speeds are unseasonable in the ventilating systems and particularly in the air conditional devices, which require rather lower outlet velocities generated by fan, with regard to maintain the thermal comfort conditions (average flow velocity in the range of $v_{av} = 0.3 - 0.5$ m s^{-1}).

For elimination of CFF dimensions and different methods of testing as well as for more exact comparison several studies of CFF performance, present the results of investigations in dimensionless form of aerodynamic curves as : $\psi_s = f(\varphi)$ and $\psi_t = f(\varphi)$ where the static pressure coefficient ψ_s, total pressure coefficient ψ_t and flow coefficient φ are defined following:

$$\psi_s = \frac{2\Delta p_s}{\rho u_2^2} \tag{3.5}$$

$$\psi_t = \frac{2\Delta p_t}{\rho\, u_2^2} \tag{3.6}$$

$$\varphi = \frac{\dot{V}}{D_2 L\, u_2} \tag{3.7}$$

The results of numerical simulation of flow inside the CFF incorporating a rotated flat vane have been verified by experimental data obtained for model of fan having the same geometry (shape of casing) and basic impeller dimension: outer diameter $D_2 = 100$ mm, length L = 450 mm, shown in fig.3.15 [12].

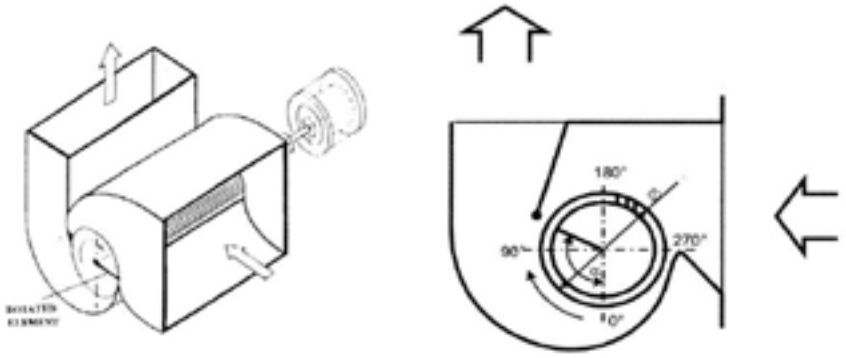

a. b.

Fig. 3.15. Cross flow fan with rotated internal vane (a) and procedure of vane angular position α measurements (b)

In fig.1.16 some selected numerical results in form of the vector velocity graphs for different angular positions of internal vane: α = 0º; 120º; 250º; 350º at constant impeller rotational speed n = 24.16 s-1 are presented [13]. An analysis of graphs shows that in the range of $\alpha = 0^{o} \div 250^{o}$ the maximal velocity increases from v_{max} = 18.1 ms^{-1} to 38.2 ms^{-1} what is synonymous with more than twofold increase of flow rate. At angular position of internal vane $\alpha = 350^{o}$ (Fig 3.16d) the maximal velocity decreases to v_{max} = 22.6 $ms^{-1,}$ what means that the flow rate reduces about 60% from the highest value.

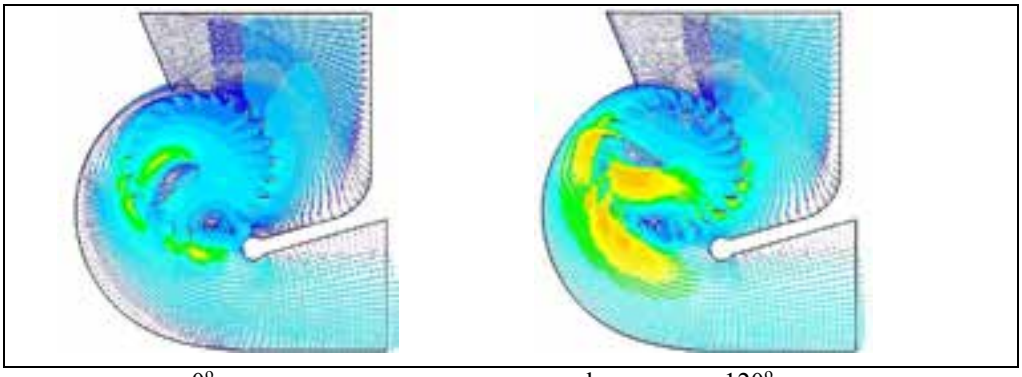

a. $\alpha = 0^{o}$ b. $\alpha = 120^{o}$

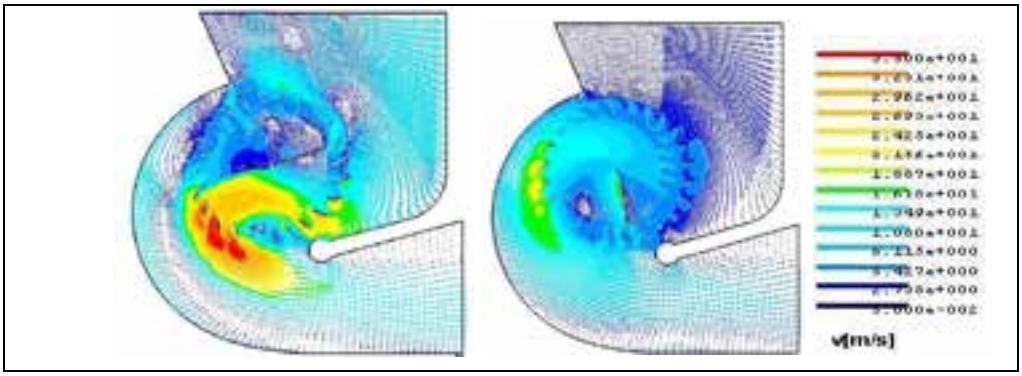

c. $\alpha = 250^{o}$ d. $\alpha = 350^{o}$

Fig. 3.16. Vector velocity graphs for different angular position of internal vane

This phenomenon is probably caused from one side by the displacement of eccentric main vortex center towards the leading casing and from the other its occupation of the greater part of blading do not let impeller for effective operation.

Analyzing the flow structures created at varying angular positions of flat vane one can see that localization of a main eccentric vortex near blading, an increase of its magnitude (occupied field of flow) as well as additional vortices and recirculation zones have a great influence on losses of power flow connected with disordered stream. Therefore a fluid flow requires to supply more electric power but very less than tenfold.

Numerical simulation of flow in the CFF allows to calculate some quantities characterizing the fan operation: the difference of static and total pressure measured at inlet and outlet cross sections of fan and volumetric flow rate for various but constant rotational speed [14]. The selected dimensionless performance curves for two different rotational speeds numerically calculated and measured are shown in fig.3.17.

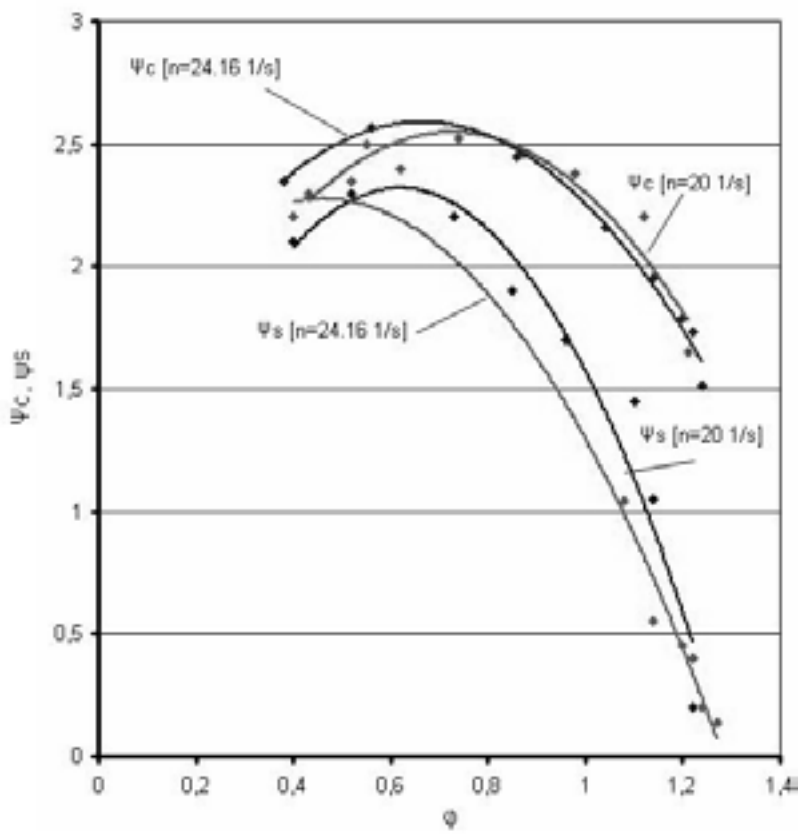

Fig. 3.17. Dimensionless performance curves $\psi_s = f(\phi)$ and $\psi_c = f(\phi)$

On the base of the contour static and total pressure plots, the values of pressure are red off at the determined points and then averaged at the inlet and outlet cross sections, respectively. The values of volumetric flow rate are estimated from the mass flow rate calculated in Flo++ program and density of the air .

As mentioned above the proposal of using internal rotated vane mounted axially inside the impeller of CFF to control its operation seems to be advantageous in some applications. It gives possibility to obtain several different shapes of aerodynamic curves and ranges of dimensionless flow

parameters at the same rotational speed, what means that one CFF can behave as a few fans. The change of internal vane angular position in range $\alpha = 0^o \div 120^o$ shows the threefold increase of flow rate, fig.3.18.

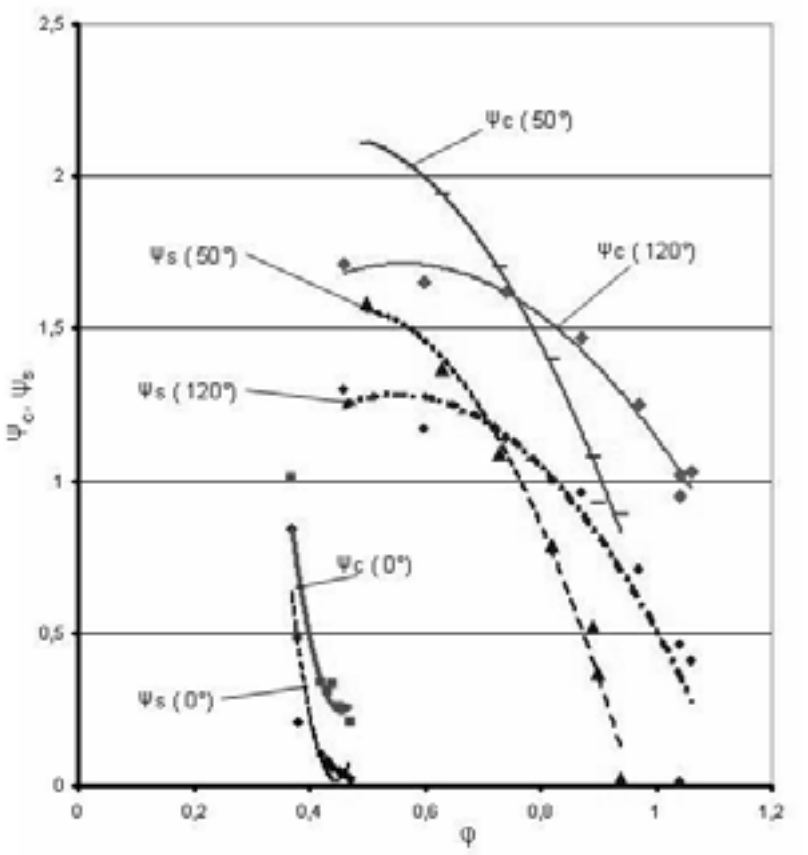

Fig. 3.18. Total ψ_c and static ψ_s pressure coefficient versus flow coefficient ϕ for different angular position of internal vane: $\alpha = 0^o$, 50^o, 120^o at rotational speed n= 37.5 s^{-1}

3.6 Estimation of the compatibility of numerical and experimental results

The compatibility of the results obtained with use of two different methods: numerical calculations (finite volume method) and experimental measurements has been estimated basing on some selected performance curves: $\psi_s=f(\varphi)$ and $\psi_c=f(\varphi)$. There are taken into consideration two aerodynamic performances obtained for CFF without internal vane (results in fig. 3.19) , and for CFF with internal vane at angular position of internal vane $\alpha = 50^o$ (fig.3.20) tested at the same rotational speed n =24.16 s^{-1} [14].

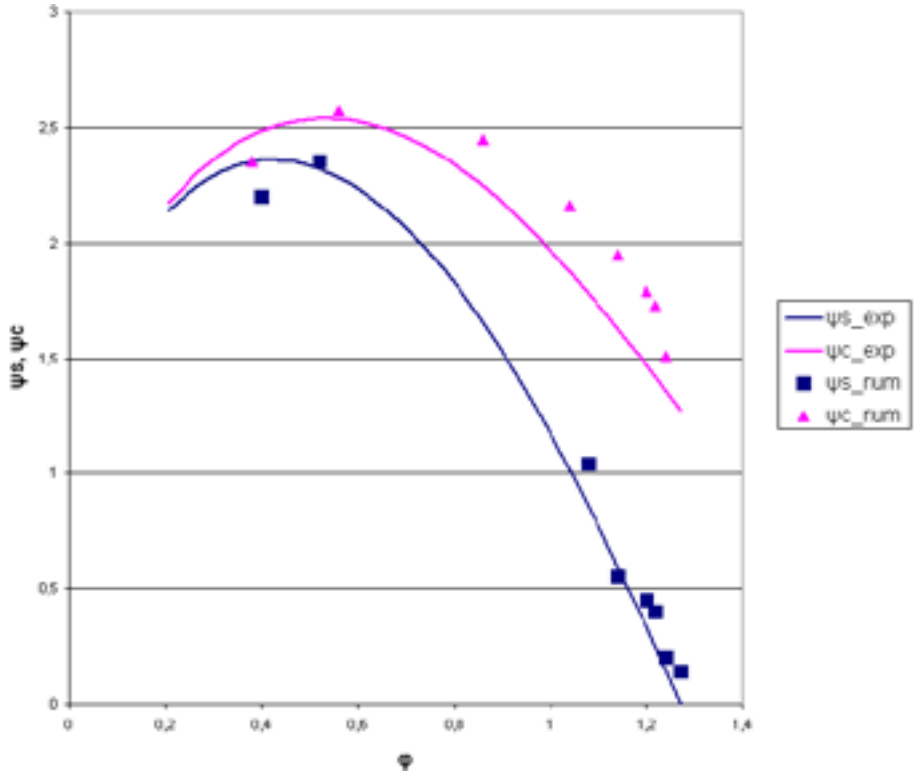

Fig. 3.19. Comparison of experimental and numerical results for WPU 450/100

In the whole range of flow coefficient changes the character of performance curves is similar but the differences between values of static and total coefficients calculated numerically and obtained experimentally are visible. One can see that the values of the dimensionless coefficients ψ_s and ψ_c calculated numerically are higher than those obtained experimentally.

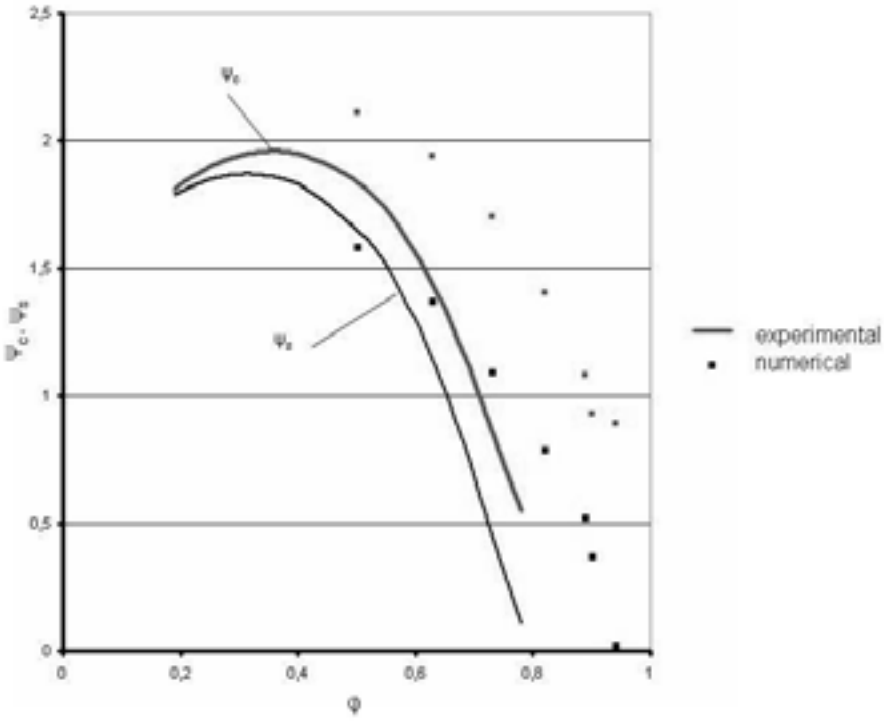

Fig. 3.20. The comparison of numerical and experimental results for $\alpha = 50^{o}$, n = 24.16 s^{-1}

The estimation of compatibility of the obtained results is made using the test of goodness of fit test - chi-square test. Chi-square is calculated by

finding the difference between each observed O_i (experimentally measured) and theoretical E_i (numerically calculated) frequency for each possible outcome, squaring them, dividing each by the theoretical frequency, and taking the sum of the results [15]:

$$\chi^2 = \sum_{i=1}^{n} \frac{(O_i - E_i)^2}{E_i} \tag{3.8}$$

In agreement with the rule assumed in chi square test the discrepancy between the results is rejected if the calculated quantity χ^2 is bigger than adequate value read out from the table $\chi^2_{K-1,\alpha}$ determined by assumed step of probability α which in our case is equal to 0.995 and the step of freedom (K-1) which for the eight frequencies is equal to 7.

Comparison of calculated value of χ^2 = 0.02 with the read out $\chi^2_{7,0.995}$ = 0.989 for the assumed step of probability leads to the following inequality:

$$0.02 < 0.989 \tag{3.9}$$

From the inequality (3.9) results that the goodness-of-fit of numerical and experimental values is very high because for the assumed step of probability the numerical and experimental results have been covered. Compatibility of the obtained results is higher than the ones presented in publications of the other authors.

3.7 REFERENCES

[1] Stacharska-Targosz J., *Identyfikacja przepływów w wentylatorach poprzecznych metodą eksperymentu sekwencyjnego*, Monografia 117, Kraków 1991

[2] Stacharska-Targosz J., Płachetko A., *Analiza wpływu wybranych tworzyw sztucznych na charakterystyki wentylatora poprzecznego*, Prace Naukowe, Monografie, Konferencje, Z.1 , Gliwice , 275-282

[3] Stacharska-Targosz J., *Wentylatory poprzeczne*, Kraków 2006

[4] Stacharska-Targosz J., *Studies on flow pattern under different throttle conditions in a cross flow fan,* Zeszyty Naukowe Politechniki Łódzkiej , Nr 674, 1993, 43-50

[5] JaumotteA, Onockx L., *Mesure du d'ebit d'air a l'aspiration d'un circuit par ajutage de Borda*, Institut de Mecanique Appliquee, NT 54, 1985

[6] Stacharska-Targosz J., *Flow analogy applied to the velocity fields determination in cross flow fans,* Cieplne Maszyny Przepływowe, Z.108., 315-322

[7] Sowa A., *Flow simulation in cross flow fans using finite element and finite volume methods*, TASK Quartyerly,1/2004

[8] Ferziger J.H., Peric M.: *Computational Methods for Fluid Dynamics*, Springer 2002

[9] Stacharska-Targosz J., Sowa A., *Flow simulation in cross flow fans using finite methods*, Turbomachinery, 122, Łódź 2002

[10] Sowa A., *Symulacje numeryczne przepływów w wentylatorach poprzecznych*, Rozprawa doktorska, Politechnika Krakowska, Kraków 2004

[11] Chmielowiec-Jabłczyk M., *Wyznaczanie charakterystyk aerodynamicznych wentylatorów poprzecznych za pomocą numerycznej symulacji przepływu*, Rozprawa doktorska, Politechnika Krakowska, Kraków 2008

[12] Stacharska-Targosz J. Gołogórski J., *Badania eksperymentalne wentylatora poprzecznego WPU 450/100,* Czasopismo Techniczne Mechanika,Z.1-M/1995, 157-166

[13] Stacharska-Targosz J., Chmielowiec M., *The influence of internal vane on uniform velocity distribution in the cross flow fan*, The Archive of Mechanical Engineering, Vol. LVI, No. 1, 2009 61-72

[14] Stacharska-Targosz J., Chmielowiec M., *Application of finite volume method for numerical calculations of the cross flow fan performance curves*, Archives of Thermodynamics, Vol.29(2008) No. 2, 3-20

[15] Newbold P., Carlson L., Thorne B.: Statistics for business and Economics, Prentice Hall 2003